8-1-2012

Evaluation of possible source rocks in northern Nye County, Nevada: implications for hydrocarbon exploration

Inessa Yurchenko
University of Nevada, Las Vegas, inessayurchenko@gmail.com

EVALUATION OF POSSIBLE SOURCE ROCKS IN NORTHERN NYE COUNTY, NEVADA: IMPLICATIONS FOR HYDROCARBON EXPLORATION

by

Inessa Yurchenko

Bachelor of Science in Geology
Moscow State University
2009

A thesis submitted in partial fulfillment
of the requirements for the

Master of Science in Geoscience

Department of Geoscience
College of Science
The Graduate College

University of Nevada, Las Vegas
August 2012

THE GRADUATE COLLEGE

We recommend the thesis prepared under our supervision by

Inessa Yurchenko

entitled

Evaluation of Possible Source Rocks in Northern Nye County, Nevada: Implications for Hydrocarbon Exploration

be accepted in partial fulfillment of the requirements for the degree of

Master of Science in Geoscience
Department of Geoscience

Andrew Hanson, Committee Chair

Ganqing Jiang, Committee Member

Wanda Taylor, Committee Member

Sean Clark, Graduate College Representative

Thomas Piechota, Ph. D., Interim Vice President for Research and Graduate Studies and Dean of the Graduate College

August 2012

ABSTRACT

Evaluation of Possible Source Rocks in Northern Nye County, Nevada: Implications for Hydrocarbon Exploration

by

Inessa Yurchenko

Dr. Andrew Hanson, Examination Committee Chair
Associate Professor of Geology
University of Nevada, Las Vegas

The presence of oil outside of Railroad Valley, northern Nye County has sparked the interest of exploration companies in Nevada. The geology in this region is very complex and the level of petroleum exploration is low. In order to understand the distribution of oil, a complete petroleum systems analysis is required. Previous studies confirmed that the Mississippian Chainman Shale and Cretaceous to Paleocene Sheep Pass Formation, Member B are source rocks. However, a number of other possible source rocks exist in northern Nye County, but they are not confirmed because of incomplete datasets. The goal of this thesis project is to determine if effective source rocks other than the Chainman Shale and Sheep Pass Formation exist in northern Nye County. I obtained samples from outcrops and used organic geochemistry to test the hypothesis that different strata, including Paleozoic Vinini, Pogonip, Woodruff, Guilmette Formations, Pilot Shale, Ely Limestone, and Cretaceous Newark Canyon Formation have the necessary qualities to be petroleum source rocks.

This evaluation revealed source rock potential for Woodruff Formation, but none of the other analyzed candidate units met the requirements for organic matter quantity, quality, and thermal maturity in order to be called source rocks. The Devonian Woodruff Formation displayed excellent organic matter quantity, and oil-prone kerogen type,

however samples appeared to be thermally immature. Additional oil – source rock correlation suggested genetic relationship between the Woodruff Formation and Chainman-derived oils from Railroad Valley. This knowledge will help to estimate the petroleum potential of northern Nye County for future exploration and development in Nevada.

ACKNOWLEDGEMENTS

It is without a doubt that there are many people who supported and encouraged me along the way of completing my MS degree. I am grateful to ExxonMobil Geoscience Scholarship Program for giving me this amazing opportunity and sponsoring my degree here at UNLV under the advisement of Dr. Andrew Hanson. I want to thank Dr. Hanson for tremendous guidance throughout my research process and writing. I admire his incredible knowledge and academic wisdom. Each meeting, each draft revision were a reflection of his unending dedication. Thank you for sharing your experience and knowledge with me, I will be forever grateful. I am also grateful to my other committee members, Dr. Wanda Taylor, Dr. Ganqing Jiang, and Sean Clark for their constructive comments, guidance, and support throughout my graduate years. I also appreciate the support and encouragement of all my American friends. I feel so lucky to have met each of you and will always be grateful for all of the time we spent together. I am especially thankful for my boyfriend and best friend Brett Perry, for intellectual and mental support, encouragement, and inspiration. Thank you for keeping life normal and reminding me of the important things in life. I express my deepest gratitude to my parents, Lubov and Alexander Yurchenko, and my brother Igor. Thank you for loving me unconditionally and supporting me from afar. With a family like you, every goal is within reach, and no dream is too big. Thank you all.

TABLE OF CONTENTS

CHAPTER 1

INTRODUCTION

Petroleum production in Nevada is concentrated in sixteen small oil fields in three main areas of the state: Pine Valley in northern Eureka County, Railroad Valley in northeastern Nye County, and Deadman Creek in Elko County (Fig. 1).

The first well drilled for oil in Nevada was back in 1907, and it was dry (Garside et al., 1988). The first successful discovery of oil was in 1954 in Railroad Valley (Eagle Springs No. 1-35). The second oil discovery did not occur until 1976 (Trap Spring No. 1; Garside et al., 1988). New oil field was discovered every two to three years between 1976 and 1998. Overall, since the first well was drilled in 1907, about 750 wells have been drilled (Garside et al., 1988). Today, the density of drilled wells ranges from one per square mile to one per 30 square miles in the state of Nevada (LaPointe et al., 2007).

According to Davis (2007), total oil production for Nevada in 2006 was over 425,000 barrels and was produced from nine fields located in Railroad Valley, Nye County, and from two fields in Pine Valley, Eureka County. Based on the oil records of 2006, Nevada occupied 26th position out of the 31 oil producing states in the United States (Davis, 2007). Almost 90% of Nevada's oil has been produced from fields in Railroad Valley (Davis, 2007). Although the total oil production for all commercial oil fields in Nevada (from 1954 through 2009) reached a peak of 50 million barrels, the annual production has declined since 1992 (Fig. 2). The details of the oil field and total production for each oil field during 1954-2009 are presented in Table 1.

Recent discovery of an oil field outside Railroad Valley (Toana Draw, Elko County, 2007) has sparked the interest of exploration companies in Nevada. The

commercial prices for oil produced in the state ranged from $8 to $20/barrel during the 1990's, exceeded $50/barrel in 2006 (Fig. 2), to its maximum today at $83/barrel. The currently high prices of oil may attract more petroleum development.

The geology of the northern Nye County is very complex and the level of petroleum investigation is low. The structural and thermal complexity of the area and poor quality seals have limited the success of exploration wells. In order to understand the distribution of oil, a complex petroleum systems analysis is required, including study of source rocks, reservoirs and seals, together with understanding of processes of petroleum generation, migration, accumulation and preservation. This study of northern Nye County focuses on the investigation of one of the essential elements of the petroleum system - source rocks, which play the main role in hydrocarbon generation. I collected samples of potential source rock units and used organic geochemistry to test organic matter quantity, quality and thermal maturity of candidate rocks in order to determine which stratigraphic intervals have the necessary qualities to be petroleum source rocks.

I hypothesized that different strata claimed as possible source rocks have the necessary qualities to be able to generate oil in northern Nye County. The candidate rocks include Ordovician Pogonip Group and Vinini Formation, Devonian Slaven Chert, Guilmette Formation and Woodruff Formation, Devonian and Mississippian Pilot Shale, Joana Limestone and Eleana Formation, Pennsylvanian Ely Limestone and Cretaceous Newark Canyon Formation.

The objectives of this thesis project were to use organic geochemistry and vitrinite reflectance to examine the quantity, quality and thermal maturity of possible source

rocks. As a result, this study determined whether different analyzed strata have the necessary qualities to be petroleum source rocks.

CHAPTER 2

GEOLOGICAL FRAMEWORK

Regional Geology

The project area is situated in the Basin and Range geomorphic province. According to Peterson (1994), generation, migration, accumulation and preservation of hydrocarbons in Railroad Valley are related to the tectonic and burial history of the eastern Great Basin. Moreover, tectonic events influenced the regional distribution of reservoir and source rocks, which are important for the petroleum history of the study area (Peterson, 1994).

The Great Basin has a wide variety of lithologies, which include, but are not limited to platform carbonates, marine and non-marine siliciclastics, and volcanic rocks. Together, the lithologies represent a variety of depositional environments and they have been influenced by multiple stages of tectonic activity, sea level change and/or climate changes. During its extensive tectonic history the study region experienced the Antler, Sonoma, and Sevier contractional orogenies, and Cenozoic Basin and Range extension (Dickinson, 2006). The main stages of tectonic activity and the depositional environments from Paleozoic to recent are summarized below (Figs. 3 and 4).

Strata exposed in the study area include Paleozoic sediments, which are usually unconformably overlain by Cenozoic units, however in some places the Mesozoic (Cretaceous) Newark Canyon Formation is present. From the early Paleozoic Era until the late Devonian, sediments were deposited in passive margin environments, influenced by sea level fluctuations (Dickinson, 2006). At the passive margin setting, carbonates were deposited along a platform in eastern Nevada with associated deep ocean sediments

to the west. The primary lithologies were shales and limestones (Peterson, 1994). Early Paleozoic potential source rocks located in the study area include the Cambrian Dunderberg Formation; the Ordovician Pogonip Group and Vinini Formation (Anna et al., 2007).

In the late Devonian, the Antler orogeny occurred as a result of collision between a volcanic arc and the western North American craton (Burchfiel et al., 1992) (Fig. 5a), thus the region started to experience a contractional event. This event resulted in a subduction zone, associated with a volcanic island arc (Dickinson, 2006) (Fig. 5a). The collision resulted in east-vergent thrusting that formed an eastward-migrating system consisting of the Roberts Mountain allochthon, foreland basin, forebulge, and back-bulge (Morrow and Sandberg, 2008) (Fig. 5b). During this time, mixed siliciclastic (sand and silt) and carbonate sediments, derived from both the east and west margins of the basin, were deposited in the basin. The Devonian and Mississippian possible source rock units exposed in the proposed study area include the Guilmette Formation, Woodruff Formation, Pilot Shale, Joanna Limestone, and Chainman Shale (Peterson, 1994). Middle and Late Paleozoic tectonostratigraphic units and basins of northeastern east-central Nevada are shown on Figure 4 (by Cashman et al., 2011).

The Sonoma orogeny took place in the late Permian to mid-Early Triassic and resulted in oceanic sediments of the Havallah basin being thrust on top of the Antler orogen along the Golconda thrust west of the Roberts Mountain thrust. In mid-Early Triassic the incipient Cordilleran magmatic was formed followed by the Late Triassic to Early Jurassic back-arc basin development (Burchfiel et al., 1992; Dickinson, 2006). During the Jurassic through the Cenozoic there were several deformational events in the

western North America. Late Jurassic to early Cenozoic contraction in the western United States is known as the Sevier Orogeny. This east-vergent contractional event extended for hundreds of miles from Mexico to southern California and Nevada, through central Utah, northward into southern Canada up to Alaska (Taylor, 2001; Dickinson, 2006). The central Nevada thrust belt (CNTB) was probably a narrow compressional zone, trending from north to south (Taylor, 2001). The age of this event is poorly constrained (Taylor et al., 2000). According to Speed et al. (1988), the Eureka belt is a thin east-vergent contractional zone related to the Sevier belt by a decollement. Timing, location and relationships between the CNTB, Sevier and Eureka belts remain highly controversial and its discussion lies beyond the scope of this research. Modern day east-central Nevada was situated in the Sevier hinterland (Taylor, 2001).

According to Dickinson (2006), the Late Cretaceous to Paleogene magmatism migrated inland from the Sierra Nevada toward the Rocky Mountains, followed by Late Eocene to Early Miocene re-migration from the continental interior back to the continental margin. Neogene extensional deformation resulted in formation of the Basin and Range Province. Development of the San Andreas transform margin began in the Oligocene. During the Eocene-Miocene, southward migrating volcanism passed though Nevada (Best et al., 1993). This mantle derived volcanism resulted in the formation of a series of rhyolitic and andesitic calderas (Best et al., 1993).

In summary, northern Nye County lies within the Great Basin. The region has experienced extensive tectonic activity, which has led to a diversity of depositional environments for potential source rocks. The tectonic evolution also greatly affected the thermal history and hydrocarbon generation.

Previous Work

Previous Nevada oil data reports marine and non-marine petroleum source rocks (Poole et al., 1983). The organic matter appears to be mostly sapropel, ranging from thermally immature to over-mature in the Paleozoic rocks and from mostly immature to mature in the Cretaceous and Tertiary rocks. Previous research indicates at least two episodes of petroleum generation (Poole et al., 1983).

In order to investigate the regional distribution of possible source rocks in the Great Basin, Poole and Claypool (1984) published analytical datasets obtained from marine Paleozoic rocks, lacustrine Cretaceous-Paleogene rocks, and oil samples collected over ten years. Their study revealed the Mississippian Chainman Shale and Cenozoic Sheep Pass Formation Member B as the most likely source rocks in Railroad Valley. Biomarker analysis showed very good correlation between oils from some fields (Trap Springs, Bacon Flat Grant Canyon and Blackburn) and the Chainman Shale (Ahdyar, 2011). However, the correlation between other oils and the Sheep Pass Fm. were problematic. As a result, Poole and Claypool (1984) suggested the presence of several other possible source rocks (Joana Limestone, Eleana Limestone, Newark Canyon Fm., Elko Fm., Slaven, Vinini and Woodruff Fm. etc.) in the Great Basin and indicated the necessity of further geological and geochemical investigation of this problem.

Sandberg and Poole (1975) first described the Pilot Shale as a possible source rock, providing a few total organic carbon (TOC) values and some thermal maturity data. Mullarkey et al. (1991) published geochemical data supporting the petroleum potential of the Newark Canyon Fm. in north-central Nevada.

In 2007, the US Geological Survey published the Geologic Assessment of Undiscovered Oil and Gas Resources of the Eastern Great Basin Province, Nevada, Utah, Idaho, and Arizona (Anna et al., 2007). In this assessment several published geochemical databases of Paleozoic and Tertiary possible source rocks were combined (Fig.6). Formations or groups were ranked by TOC, and those that have mean TOC higher than 0.5 % were described as potential source rocks (Table 2, Anna et al., 2007). This study didn't perform a detailed analysis, but indicated potential for undiscovered oil resources.

To summarize, previous study confirmed Mississippian Chainman Shale and Cretaceous Maastrichtian to Paleocene Sheep Pass Formation, Member B as the two most likely source rocks and described other possible source rocks in northern Nye County (Ahdyar, 2011). The other possible source rocks include the Ordovician Pogonip Group, Vinini Formation; Devonian Woodruff Fm., Slaven Fm. and Guilmette Fm.; Mississippian Pilot Shale and Joana Limestone, Pennsylvanian Ely Limestone, Cretaceous Newark Canyon Fm., and Paleogene Elko Fm. (Fig. 6; Anna et al., 2007). However very little work has been done and there are no published geochemical data that confirm these possible source rocks.

CHAPTER 3

MATERIALS AND METHODS

In order to assess the petroleum potential of the study area, I collected outcrop samples from different parts of northern Nye County. I used organic geochemistry to test the hypothesis whether different strata have the necessary qualities to be petroleum source rocks.

In order to evaluate source rock potential three main geochemical characteristics have to be assessed: quantity of organic matter (OM), quality (or type) of OM and thermal maturity (Peters and Cassa, 1994). Geochemical analyses performed during this study included determination of total organic carbon, Rock-Eval pyrolysis, vitrinite reflectance, and biomarker analysis.

Stratigraphic sections and sampling

Detailed meter-scale stratigraphic sections were measured at Shingle Pass, Fox Mountain, Moody Peak, and Hot Creek Range localities (Fig. 7) in order to construct a sedimentological record for the chemostratigraphic data. Each section was measured using a Jacob staff or tape-compass-clinometer method, as described in Compton (1985). While measuring sections, samples were collected and preliminary lithological descriptions of the strata, sedimentary structures, and contacts were taken. Samples for geochemical analysis were chosen based upon lithology and grain size. Candidate rocks were preferentially sampled from freshly broken surfaces, while rocks showing obvious evidence of alteration (veins, fractures, or surface weathering) were avoided.

Total Organic Carbon measurements and Rock-Eval pyrolysis

Total organic carbon measurements and Rock-Eval pyrolysis of all samples were performed at Weatherford Laboratories, in order to assess organic matter quantity, quality and thermal maturity of candidate rocks. See Appendix 3 for a description of laboratory procedures. Based on the initial results, samples with the best source rock characteristics were selected for further organic geochemistry analysis (biomarker analysis).

Vitrinite reflectance and visual kerogen analysis

Several samples were submitted for whole rock vitrinite reflectance (% R_o) determination in order to provide alternative thermal maturity data. Samples older than Devonian in age were submitted for visual kerogen and thermal alteration index for thermal maturity indication. The EGS-ploration Company performed both analyses. See Appendix 4 for a full description of the laboratory procedures.

Petrographic analysis

In addition to geochemical analysis, nine samples were submitted to Quality Thin Section for standard thin-section preparation.

Molecular organic geochemistry

Two source rock extracts from the Woodruff Formation were analyzed in this study. Geochemical analyses consisted of normal alkane analysis using gas chromatogaphy (GC), diamondoid analysis on gas chromatography–mass selective detector (GC-MSD), biomarker analysis using gas chromatography–mass selective

detector (GC-MSD), and metastable reaction monitoring GC–mass spectrometry (MRM-GCMS). All biomarker analyses were performed at the Molecular Organic Geochemistry Laboratory at Stanford University.

Preparation for molecular geochemical analysis included crushing samples and bitumen extraction. Samples were crushed using mortar and pestle and a mechanized crushing tool. Soluble bitumen was extracted from approximately one hundred grams of rock powder from each sample using a mixture of solvents, consisting of methanol (50%) and dichloromethane (50%). Each sample was run for a total of 60 minutes with a sonic extractor.

Source rock extracts were diluted with solvent (pentane) to 1.5 ml and were analyzed using an Agilent Technologies 6890N Gas Chromatograph (GC) equipped with Flame Ion Detector (FID). Approximately 1 microliter of each sample was auto-injected to the 30 m DB-1 long column GC with an internal diameter of 0.25 mm, 25 micron phase thickness, and hydrogen carrier gas. The temperature program begins at 50°C for 1 minute, then 10 °C /min up to 320°C where it is held for 15 minutes. The injector and detector are held at 325°C. A portion of the source rock extract underwent hydrous pyrolysis at 340°C for 72 hours. Pyrolyzed samples were run on GC with an identical set-up.

Another portion of each source rock extract was separated into saturate and aromatic fractions. The saturate/aromatic separation was done using silica gel chromatography, for description of procedure see Ahdyar (2011). Silicalited saturate fractions and aromatic fractions were analyzed for biomarkers using a selected ion monitoring gas chromatography–mass selective detector (SIM GC-MSD). For silicalited

saturate fractions, m/z 191 and 217 were monitored, and m/z 253 and 231were monitored for the aromatic fractions. A Hewlett-Packard 5972 series GC-MSD with a 60 m DB-1 long column, 0.25 mm i.d., 25-micron phase thickness, and helium carrier gas was used to analyze the samples. The GC-MSD program initiated at 140°C for 1 minute, then increased by 2°C /min to 320°C and was held at 320°C for 20 minutes. In addition, silicalited saturate and aromatic fractions were further analyzed using metastable reaction monitoring (MRM-GCMS) Hewlett-Packard 5890 Series II Autospec. Finally, four Woodruff samples were processed for diamondoid analysis. The detailed description of autospec set-up and diamonoid analysis procedures are provided by Ahdyar (2011).

CHAPTER 4

RESULTS

Stratigraphic sections and sampling

A total of 95 rock samples were collected from several outcrops in different parts of northern Nye County. A map of sample locations and geographic coordinates is depicted in Figure 7. The sampled possible source rock intervals included Ordovician Pogonip Group and Vinini Formation, Devonian Slaven Chert, Guilmette Formation and Woodruff Formation, Devonian and Mississippian Pilot Shale, Joana Limestone and Eleana Formation, Pennsylvanian Ely Limestone and Cretaceous Newark Canyon Formation. All samples collected with geographic coordinates are listed in Table 3. As a result, eight sections were measured and are illustrated in Appendix 5.

Total Organic Carbon measurements and Rock-Eval pyrolysis

TOC (wt. %) indicates the quantity of OM, including bitumen and kerogen of a rock sample. Rock-Eval pyrolysis determines OM quality and thermal maturity. This procedure includes measurements of free hydrocarbons (HC) that can be vaporized without cracking kerogen of the rock (peak S_1, mg HC/g rock), hydrocarbons derived from cracking of kerogen (peak S_2, mg HC/g rock), organic carbon dioxide (peak S_3, mg CO_2 /g rock) and a temperature at which the S_2 peak reaches its maximum (T_{max},^oC). Based on these measurements, production index PI = $S_1/(S_1+S_2)$, hydrogen index HI = $(S_2/TOC)*100$ (mg HC/g TOC), S_2/S_3 ratio and oxygen index OI = $(S_3/TOC)*100$ (mg CO_2/g TOC) were calculated. A summary of analytical results from TOC and Rock-Eval pyrolysis is provided in Table 4.

Vitrinite reflectance and visual kerogen analysis

Thirty outcrop samples were submitted for whole rock vitrinite reflectance (R_o, %) determination. Organic petrology results are summarized below. Vitrinite reflectance values are reported in Table 4. Photomicrographs in Plates 1 through 9 show typical views of the organic matter assemblages in incident white light (546 nm). A second series of photomicrographs labeled Plates 1 through 6 shows typical views of the organic matter assemblages in incident blue light (450-490, FT 510, LP 520). All photomicrographs are displayed in Appendix 6.

Four samples were submitted for visual kerogen and thermal alteration index (TAI) analysis, including 10SH7, 1011SH (Pogonip), 10VI43 (Vinini Formation) and 10PO45 (Pogonip Group). Summary of visual kerogen data are listed in Table 4.

Petrographic analysis

One Vinini sample and eight Woodruff samples were selected for thin-section analysis for collection of additional information about candidate rocks. All samples are mudstones with different amounts of disseminated OM. Photomicrographs of all thin-sections and petrographic notes are included in Appendix 7.

Ely Limestone (10SH1-6)

Six samples from Shingle Pass were analyzed and showed a range of TOC values from 0.03% to 0.38%, with average of 0.17%. T_{max} measurements range from 435^{o}C to 449^{o}C (avg. 441^{o}C). PI ranges from 0.05 to 0.13 (avg. 0.1), HI varies from 80 to 290 (avg. 149), while OI spans from 112 to 887 (avg. 403).

Pogonip Group (10SH7-11, 10PO45, 10MD46, 47)

Eight samples from three different locations (see Table 3) were tested. TOC measurements showed a range from 0.03% to 0.77% (avg. 0.28%). T_{max} values range from 342°C to 523°C (avg. 448°C). PI ranges from 0.11 to 0.2 (avg. 0.14), HI ranges from 18 to 233 (avg. 77), while OI varies from 36 to 933 (avg. 303).

Two samples of the Pogonip Group from Monitor Range (10MD46 and 10MD47) were analyzed for vitrinite reflectance, and three samples from Shingle Pass (10SH7, 10SH11and 10PO45) were submitted for visual kerogen analysis.

The following is directly from the report from EGS-ploration:

> "Sample 10MD47 has slightly richer organic matter content. Shale in this sample has low to moderate organic matter content. This is comprised of fairly high maturity vitrinite which occurs as stringers, some of which are very thin and some poor quality. This is followed by minor recycled vitrinite and inertinite. Fluorescence appears to be mineral-derived. Sample 10MD46 is poor. There is a very low organic matter content that is comprised of a few small and sometimes poor quality lenses of vitrinite and minor inertinite. No organic matter fluorescence persists, but there is just a suggestion of a dull mineral fluorescence.
>
> Vitrinite reflectance values are shown in Table 1. These two samples return vitrinite reflectance values of 1.32 % R_o (10MD46) and 1.30 % R_o (10MD47). These data indicate thermal maturity is early wet gas/condensate zone mature.

Histogram populations were determined from notes taken for each measurement, and the level of confidence in the thermal maturity determinations is poor to fair.

These kerogens are characterized by a dominance of poor quality non-fluorescing granular amorphous matter. Coaly matter is present in moderate amounts in most samples except 10SH11. Woody material is minor to moderate in abundance and present with smaller amounts of solid bitumen. Kerogen in sample 10SH11 indicates a possible marine-derived origin and is at a slightly lower level of thermal maturity relative to other samples in this series. This kerogen is comprised mostly of non-fluorescing amorphous matter with very little contribution from coaly or woody particles. Sample 10SH7 was most likely a carbonate with trace organic carbon content. Following acid-digestion, no significant organic matter was recovered to allow for any characterization.

Kerogen in 10SH11 is classed as Type I/II, but has a poor potential for hydrocarbon generation. Kerogen in sample I0PO45 has matured to a level where their components are being, and have been, transformed into non-reactive organic matter. Kerogen in samples I0PO45 will currently plot as Type III/IV on a van Krevelen diagram. This kerogen have poor to no potential for the generation of gaseous hydrocarbons.

TAI is mainly based on red-brown, dark brown and dark grey-black amorphous kerogen color, which is less reliable than spore TAI. TAI (3 to 3+) is lowest in sample 10SH11 increasing 5 in samples

I0PO45. These data indicate kerogen in these samples varies from late oil window maturity through wet gas/condensate mature and into the zone of dry gas zone formation."

Guilmette Formation (10FM12-22)

Ten samples from the Fox Mountain location were analyzed. TOC data vary from 0.03% to 0.07 %, with average of 0.05%. T_{max} measurements range from 431°C to 465°C (avg. 445°C). PI ranges from 0.1 to 0.2 (avg. 0.14), HI varies from 111 to 258 (avg. 180), while OI ranges from 364 to 822 (avg. 580).

Three samples were submitted for vitrinite reflectance.

The following is directly from the report from EGS-ploration:

"In general, these samples are characterized by marl and mudstone lithologies that typically have low organic matter contents and poor quality vitrinite. Indeed, marl lithologies are virtually barren in organic matter. Organic matter fluorescence has extinguished in all samples.

Vitrinite reflectance is recorded in Table 1. This sample series is characterized by vitrinite reflectance values that range 1.14 % R_o to 1.24% R_o (10FM25) reaching a maximum of 1.36 % R_o (10FM22), with one sample yielding no result (10FM23). These data indicate thermal maturity is in the zone of wet gas/condensate.

Histogram populations were determined from notes taken for each measurement, and the level of confidence in the thermal maturity determinations is poor to fair."

Pilot Shale (10FM23-25)

Three samples from Fox Mountain were analyzed and showed a range of TOC values from 0.06% to 0.42%, with average of 0.19%. T_{max} measurements range from 450°C to 494°C (avg. 470°C). PI ranges from 0.11 to 0.27 (avg. 0.16), HI varies from 76 to 131 (avg. 104), while OI ranges from 83 to 770 (avg. 445).

Samples were submitted for vitrinite reflectance. Sample 10FM24 produced a value of 1.24%, while sample 10FM23 yielded no result. The level of confidence in the thermal maturity determinations was poor.

Joana Limestone (10FM26, 27)

Two samples from Fox Mountain were tested and showed similar TOC values of 0.01% and 0.03%. T_{max} measurements also have similar values 443°C and 445°C. PI changes insignificantly from 0.14 to 0.2. However HI varies from 194 to 364, and OI ranges from 452 to 909.

Newark Canyon Formation (10NC28-31)

Four samples from the northern part of Moody Peak were analyzed and showed a range of TOC values from 0.07% to 0.27%, with average of 0.13%. T_{max} measurements range from 433°C to 443°C (avg. 441°C). PI ranges from 0.05 to 0.14 (avg. 0.12), HI varies from 145 to 346 (avg. 234), while OI ranges from 324 to 462 (avg. 374).

Eleana Formation (10HC49-58)

Ten samples were analyzed and showed a range of TOC values from 0.1% to 1.14%, with average of 0.67%. T_{max} measurements range from 344°C to 577°C (avg. 488°C). PI ranges from 0.11 to 0.25 (avg. 0.16). HI varies from 8 to 82 (avg. 19), while OI ranges from 53 to 408 (avg. 113).

Two samples were submitted for vitrinite reflectance. The following is directly from the report from EGS-ploration:

> "Shale and silty shale have moderately abundant organic matter contents. This is typically comprised of terrestrially-derive organic matter particles that are characterized by thin stringers of fair quality primary vitrinite as well as some poor quality lenses. There is a fair contribution from recycled vitrinite, and minor inertinite. Pyrite is abundant, and fluorescence appears to be mineral-derived and/or devoid of liptinite.
>
> Vitrinite reflectance values are shown in Table 4. These two samples return vitrinite reflectance values of 0.95 % R_o (10HC50) and 1.00 % R_o (10HC58). These data indicate thermal maturity is late oil window mature.
>
> Histogram populations were determined from notes taken for each measurement, and the level of confidence in the thermal maturity determinations is poor to fair."

Slaven Chert (10SL72-78)

Seven samples from the Toquima Range were analyzed and showed a range of TOC values from 0.04% to 1.48%, with average of 0.47%. T_{max} measurements range from 349°C to 546°C (avg. 429°C). PI ranges from 0.14 to 0.25 (avg. 0.2), HI varies from 2 to 119 (avg. 36), while OI ranges from 46 to 952 (avg. 247).

Two samples (10SL73 and 10SL78) were submitted for vitrinite reflectance. The following is directly from the report from EGS-ploration:

"These two samples have very low organic matter contents and sample 10SL73 contains scattered particles of poor quality organic matter tend to be difficult to differentiate. Sample 10SL78 contains abundant hematite and a trace-level abundance of organic matter particles. However, three phytoclasts were deemed good enough quality to indicate thermal maturity in this sample. Pyrite is also abundant. Organic matter fluorescence has extinguished.

Vitrinite reflectance data is shown in Table 1. While vitrinite reflectance results in sample 10SL73 must be treated with caution, the data for sample 10SL78 is considered to be more reliable. The latter sample returns a vitrinite reflectance value of 1.79 % R_o and sample 10SL73, 1.35 % R_o. These data indicate thermal maturity is early wet gas/condensate zone to dry gas zone mature.

Histogram populations were determined from notes taken for each measurement, and the level of confidence in the thermal maturity determinations is poor to fair."

Vinini Formation (10VI45, 11MC1-20)

Twenty samples from the Toquima Range and one sample from Horse Heaven were analyzed and showed a range of TOC values from 0.01% to 1.99%, with average of 0.74%. T_{max} measurements were invalid for most of the samples, one sample from the Toquima Range showed 321^{o}C, while the sample from Horse Heaven was 493^{o}C. PI ranges from 0.1 to 0.7 (avg. 0.4), HI varies from 0.5 to 100 (avg. 8), while OI ranges from 12 to 1100 (avg. 128).

Samples 10VI45 was submitted for visual kerogen analysis. The following is directly from the report from EGS-ploration:

> "Kerogen in samples I0VI43 has matured to a level where their components are being, and have been, transformed into non-reactive organic matter. This kerogen is characterized by a dominance of poor quality non-fluorescing granular amorphous matter. Coaly matter is present in moderate amounts. Woody material is minor to moderate in abundance and present with smaller amounts of solid bitumen. It will currently plot as Type II/III on a van Krevelen diagram."

Woodruff Formation (10CW36-41, 79-97)

Twenty-four samples from the Fish Creek Range were analyzed and showed a range of TOC values from 0.01% to 2.31%, with average of 0.32%. T_{max} measurements range from 308^{o}C to 430^{o}C (avg. 405^{o}C). PI ranges from 0.014 to 0.13 (avg. 0.1). HI varies from 4 to 739 (avg. 205), while OI ranges from 9 to 6000 (avg. 608).

Nineteen samples of the Woodruff Formation were analyzed for vitrinite reflectance. The following is directly from the report from EGS-ploration:

> "Mudstone, shale and marl have extremely low to moderately rich organic matter contents in general. However, five samples in this series are virtually barren in organic matter and in two samples it was impossible to make any maturity determination based on vitrinite reflectance. The majority of organic matter assemblages are characterized by contribution from terrestrially-derived organic matter. Vitrinite is typically present as recycled particles but there is often a minor contribution from primary

vitrinite fragments. Differentiation of the two types was often difficult. Primary vitrinite is commonly present as very small lenses and very thin stringers that are difficult to measure accurately. However, there are occasional good quality stringers in some samples. In general, liptinite content is very low and appears to be algal, where present.

These results plot in a fairly tight range of vitrinite reflectance values. The minimum recorded vitrinite reflectance value is 0.76 % R_o for sample 10CW79, increasing to a maximum of 1.02 % R_o in sample 10CW95. However, the majority of values range between 0.80 % R_o and 0.90 %. The histogram populations were determined from notes taken for each measurement, and the level of confidence in the thermal maturity determinations is fair."

Molecular Organic Geochemistry

Based on the results of the initial source rock screening, two samples (10CW79 and 10CW95) of organic-rich Woodruff Formation were selected for biomarker analysis. However, due to insufficient TOC and thermal maturity, none of the other candidate rocks were included in further detailed geochemical analyses. Gas chromatograms illustrate biodegraded and thermally immature OM (Appendix 10). Both samples were pyrolyzed (10CW79p, 10CW95p) in the laboratory and all samples were subjected to GC-MSD (Appendix 9) and GCMS-MRM (Appendix 10) procedures. In addition, four samples (10CW79, 10CW95, 10CW96 and 10CW97) were analyzed for diamondoid analysis (Appendix 11).

As a result, peak heights were measured and different biomarker parameters were calculated. Key for calculated ratios is displayed in Appendix 15. Summary of these analyses can be found in Tables 8-11 and is a subject of discussion of the following chapter.

CHAPTER 5

INTERPRETATION AND DISCUSSION

Source - Rock Screening

Proper interpretation of Rock-Eval pyrolysis, TOC, vitrinite reflectance and TAI data depends on multiple factors such as lithology, relative abundance of OM, level of thermal maturity, sampling, contamination, and measured procedures. Thus, some difficulties and uncertainties are associated with the following interpretations that are discussed in the following chapter.

Prospective source-rock samples in order to be called active (or effective) source rocks must meet certain requirements for quantity, quality, and thermal maturity of the organic matter. For source rocks characterization I used the generally accepted criteria described by Peters and Casa (1994), which are displayed in Table 5.

Quantity of Organic Matter

One method to visualize the quantity of organic matter is to plot TOC versus the Rock-Eval S_2 peak (Peters et al., 2007). This plot displays two useful measurements related to the quantity of OM. Figure 8 is a plot for all of the samples and a separate plot for just Woodruff Formation samples. The Woodruff samples display the best OM quantity among all the samples. Based on TOC data, samples 10CW93-96 have excellent petroleum potential. Samples 10CW79 and 10CW80 demonstrate good and fair quantity of OM respectively. The rest of the Woodruff samples didn't show significant petroleum potential, however most of them had TOC values in the fair to very good range (0.5 to 3%) with poor S_2 characteristics (< 2.5). Samples from other formations reveal TOC

values up to 2%, which is considered good quantity range. However S_2 data are very low for all samples and overall petroleum potential is poor.

Quality of Organic Matter

One of the most common methods of classifying the quality of organic matter is by using a modified van Krevelen, or HI vs. OI, diagram (Tissot et al., 1974). In this plot (Figure 9, 10) three main types of kerogen (insoluble, non-extractable organic matter) are shown (Tissot and Welte, 1984). Type I is a sapropelic (algal) and very oil prone kerogen. It originates mainly from lacustrine algae. Type II kerogens are oil prone and the most common for petroleum source rocks. It is a lipid-rich type of kerogen and its major contributors are phyto- and zooplankton marine organisms. Type III is a humic and gas-prone type of kerogen and represents terrigenous organic matter. Type II/III is transitional between types II and III. Inert kerogen is typically referred to as type IV and would plot near the bottom of a modified van Krevelen diagram (Demaison et al., 1983). Type IV is not on the diagram because it contains insignificant hydrocarbons.

Figure 9 is an HI vs. OI plot for the complete sample set, with an expanded OI axis, whereas Figure 10 shows the standard modified Van Krevelen diagram with kerogen types and thermal maturation path ways (the highest maturation in the lower left corner). The difference lies in the OI axis. A fair number of my samples have elevated OI values (up to 6000 mg CO_2/g TOC). A typical diagram only shows OI data up to 500 mg CO_2/g TOC. The elevated OI values reported may reflect oxidation of organic matter during deposition and/or diagenesis (Peters, 1986). In addition, OI is a function of S_3, and it is quite common for outcrop samples to have low S_1 and S_2 values, and elevated S_3 data because of the weathering effects (Peters, 1986).

The majority of samples showed type II/III (mixed oil and gas prone), type III (gas prone) or even type IV (inert) kerogens. Woodruff samples stand out from other samples, and they are the only ones that show highly oil prone (type I) and oil prone (type II) kerogens.

Thermal maturity of Organic Matter

Rock-Eval Pyrolysis

As mentioned above, an estimation of thermal maturity can be made based on where samples plot on the HI vs. OI diagram. However, the main indices for thermal maturity are T_{max} and production index (PI) (see Table 5). T_{max} is measured at maximum S_2 generation and mostly depends on time/temperature conditions and OM type, while PI = $S_1/(S_1+S_2)$ indicates the volume of hydrocarbons that can be generated from a source rock (Peters et al., 2007). The S_1 peak measures free hydrocarbons that can be vaporized without cracking kerogen of the rock and can be easily affected by weathering and/or diagenetic degradation in outcrop samples. Thus, T_{max} values would be considered more reliable than PI, although samples with S_2 peak less than 0.2 mg HC/g rock T_{max} are reported to be inaccurate and shouldn't be taken into account (Peters, 1986). However, only 18 samples out of total 95 analyzed samples showed S_2 values more than 0.2 mg HC/g rock, including one sample from the Pilot Shale and the Pogonip Group, two samples from the Ely Limestone and Newark Canyon Formation, and twelve samples from the Woodruff Formation (Table 6).

I plotted samples with reliable T_{max} data on a HI vs. T_{max} diagram (Espitalié et al., 1984) and these are shown on Figure 11. All Woodruff samples and one Newark Canyon sample are immature based on this plot ($T_{max} < 435^oC$), while the rest of the samples are

in the early maturation stage (T_{max}= 435 - 445^{o}C). The HI vs. T_{max} plot also shows maturation pathways and types of kerogens, which helps to avoid problems associated with OI on a pseudo van Krevelen diagram. Four Woodruff samples (10CW93-95, 97) have type I kerogens (HI > 600). Two Woodruff samples (10CW79, 80) and one Newark Canyon Formation (10NC31) have type II kerogens (HI = 300 - 600). One Newark Canyon sample (10NC29) and one Woodruff sample (10CW96) have type II/III kerogens (HI = 200 - 300). Both Ely samples, one Pilot Shale sample, and four Woodruff samples (10CW36-39) have type III kerogens (HI = 50 - 200). The Pogonip sample and the Woodruff sample 10CW87 show type IV kerogens (HI < 50).

Vitrinite Reflectance

Vitrinite is one of the common macerals in kerogen that is derived from woody-plant material and typically indicates OM of terrestrial origin. Vitrinite, like T_{max} and TAI, provides a sensitive response to changes in time/temperature conditions by increases in reflectance of vitrinite with thermal maturity (Peters et al., 2007).

Table 5 shows the general correlation between R_o and T_{max} values, and levels of thermal maturation. Figure 12 is the T_{max} vs. R_o plot for my samples that had reliable T_{max} data and measured R_o (modified from Peters, 1986). All R_o data indicate higher maturity stage than the T_{max} measurements. Thus, all Woodruff samples are immature based on $T_{max,}$ while R_o provides values from 0.76 % to 1.02 %, which indicate peak of thermal maturity. The Pogonip sample is in the early maturation stage according to T_{max}, while 1.3 % vitrinite reflectance value supports the end of late mature zone.

The vitrinite reflectance data for these samples are less reliable, due to the lack of autochthonous vitrinite in all samples. According to visual kerogen analysis, vitrinite is

typically present as recycled particles that are very small in size and difficult to accurately measure.

Source - Rock Screening Output

As a result of source rock screening, samples from the Woodruff Formation appeared to have the best petroleum potential (up to excellent). They are also highly oil prone with oil prone kerogens.

I selected samples 10CW79 and 10CW95 as representatives of each kerogen type with the best source rock characteristics for further biomarker investigations. Geochemical parameters describing organic matter quantity, quality and thermal maturity of 10CW79 and 10CW95 samples are summarized in Table 7, photographs of samples are illustrated on Figure 13. Sample location map is included in Appendix 8.

Biomarker Analysis

Gas Chromatography (GC)

Gas chromatographic fingerprints are useful and sensitive tools for preliminary screening of samples before detailed biomarker analysis. Gas chromatograms (GCs) of samples 10CW79 and 10CW95 are displayed in Appendix 9. GCs for both samples have a sharp rising baseline forming a shape of a "hump", that consist of an unresolved complex mixture (UCM) of compounds. This shape and absence of *n*-alkanes are characteristic for biodegraded and low-maturity oils (Peters et al., 2007). Low level of thermal maturity is also supported by the T_{max} results. Pristine (Pr) and phytane (Ph) are distinguished, however their relative abundance could have been lowered, thus Pr/Ph

ratio shouldn't be trusted. Sample 10CW95 appeared to be less biodegraded and/or more mature than 10CW79, since its relative abundance of Pr and Ph is distinguishably higher and nC$_{17}$ and nC$_{18}$ are still identifiable.

Both thermally immature samples underwent hydrous pyrolysis experiments in order to generate products (10CW79p and 10CW95p) chemically and physically similar to natural crude oils (Ruble et al., 2001; Peters et al., 2007). GC chromatograms of source rock pyrolizates are displayed in Appendix 9.

Both pyrolyzates have common geochemical features, such as similar distribution of *n*-alkanes (nC$_{12}$ – nC$_{34}$) with predominance of odd versus even *n*-alkanes, particularly in the nC$_{12}$–nC$_{34}$ range, and they show *n*-alkanes profiles that are fairly typical of mature oil. There is no evidence of β-carotane and botryococcanes, common for saline lacustrine, or highly restricted marine settings.

The Pr/Ph ratios of pyrolyzates are relatively higher than source rock extracts, which provides additional evidence of OM degradation. Interpretation of redox conditions based on Pr/Ph ratio is not very meaningful because samples were pyrolyzed. Low TAR (terrigenous/aquatic ratio) values indicates aquatic sources for both samples, however this parameter is sensitive to thermal maturation and biodegradation. The Carbon preference index (CPI) values are around 1, which suggests a predominance of marine input and/or thermal maturation. The odd-to-even preference (OEP) ratio also equals 1, which suggests, but does not prove, that the samples are thermally mature. Implications from the above mentioned ratios should be supported by other biomarker parameters due to interference by thermal maturity, source rock input, biodegradation and pyrolysis.

Gas Chromatography/ Mass Spectrometry (GCMS)

GCMS is a more sensitive tool to analyze biomarkers, allowing detection of peaks too small to be seen on GC (Figure 14).

Mass/charge (m/z) 191 Terpanes

Mass chromatograms showing C_{19}-C_{30} tricyclic terpanes and C_{29}-C_{35} hopanes in the saturated hydrocarbon fraction of source rock extracts and pyrolyzates are displayed in Appendix 10. In addition to the four samples discussed above, samples 10CW96 and 10CW97 were submitted for diamondoid analysis. As a result they were run on GS-MSD and their terpane fingerprints (*m/z* 191) were analyzed together with 10CW79 and 10CW95 samples (see Appendix 10).

C_{30} hopane is a widespread higher homolog in the majority of samples. However, C_{23} tricyclic is higher in 10CW79 and 10CW79p samples. C_{31} tricyclic is the highest peak in 10CW97 trace sample.

Tricyclic/17α-hopane ratio is an important source and maturity parameter. All samples showed low values. However, sample 10CW79 has the highest value among all the samples, which indicates relatively higher level of thermal maturity for that sample. Tricyclic terpanes and 17α-hopanes originate from different precursors, like bacterial or algal lipids (tricyclics) and prokaryotic species (hopanes). Thus, their ratio can vary considerably depending on OM source. Other ratios of various tricyclic terpanes (C_{22}/C_{21}, C_{24}/C_{23}, C_{26}/C_{25}) can be useful in distinguishing OM source and are widely used for oil-source rock correlation (Figure 15). Figure 15 illustrates that Woodruff samples plot in a different area than carbonate and lacustrine samples. I interpret the Woodruff samples as having been deposited in a marine shale depositional environment. Low

C_{29}/C_{30} hopane ratio (<1) is indicative of shale source. Samples 10CW79 and 10CW79p have relatively higher C_{29}/C_{30} hopane ratio (1.00 and 1.08) that may indicate some input of carbonate material. Tricyclic/17α-hopane vs Ts/(Ts+Tm) plot on Figure 16 suggests interpretation of Woodruff Formation as algal-rich and clay-rich source-rock and supports oil-source rock correlation.

Gammacerane is present in all samples. Samples 10CW79 and 10CW97 have higher gammacerane index values that suggest water-column stratification, potentially due to hypersalinity. Absence of oleanane in all samples suggests that the source is older than Late Cretaceous in age, which is in agreement with the known Devonian age of the unit.

The C_{31}-C_{35} homohopanes are present in all analyzed samples, indicating a certain degree of anoxia (Figure 17). Sample 10CW79 shows higher relative abundance of C_{35} homohopanes compare to the lower homologs, indicating highly reducing marine source-rock depositional environments (Rullkötter and Philp, 1981).

Moretane/hopane ratios range from 0.13 to 0.27 and suggest that samples underwent catagenesis. Relatively low Ts/(Ts+Tm) values indicate low thermal maturity stage for all samples. C_{29} Ts / (C_{29}Ts + C_{29} Hopane) ratios are comparable, but slightly less than Ts/(Ts+Tm). All three ratios individually suggest change in thermal maturity in the following order 10CW95, 10CW96, 10CW97 and 10CW79, where 10CW79 is the most mature among source rock extracts. Pyrolyzate 10CW95p appears to be more mature than the 10CW79p sample.

GCMS-MRM Steranes

MRM chromatograms of samples 10CW95 and 10CW95p are fairly similar and are considered to be reliable (see Appendix 12). The MRM chromatogram of sample 10CW79 has high signal-to-noise ratio and should be considered with caution, while the 10CW79p chromatogram has a good signal.

Presence of C_{30} 24-*n*-propylcholestanes in all samples is one of the most powerful indicators of marine OM. All samples reveal relatively low diasteranes/steranes ratios, which indicates absence of catalytic clays. This ratio is typically used to distinguish petroleum from carbonate versus clastic source rocks, however it doesn't correlate directly with clay content but depends on quantity of clay relative to TOC (Peters et al., 2007). The ternary diagram on Figure 18 displays distribution of C_{27}, C_{28}, and C_{29} steranes in saturated fractions. The Woodruff samples plotted in the region defined by non-marine shale, marine carbonate organic matter source, or outside of designated environments.

The C_{29} 20S/(20S+20R) and C_{29} αββ/(αββ+ααα) ratios increase with thermal maturity. Based on these data, source rock extract 10CW79 and pyrolyzate 10CW79p appeared to be more mature than source rock extract 10CW95 and pyrolyzate 10CW95p respectively.

m/z 253 Monoaromatic steroids

Monoaromatic steroids provide information about source characteristics. The ternary diagram on Figure 19 shows more variable distribution of C_{27}, C_{28}, and C_{29} monoaromatic steroids in the aromatic fraction than those for steranes and as a result is more useful for describing the depositional environments of source rock. Ratio

MA(I)/MA(I+II) increases with thermal maturity from 0 to 100% (Seifert and Moldowan, 1978). All analyzed samples display relatively low ratios, indicating low level of thermal maturation. GC-MSD traces (*m/z* 253) of analyzed samples are displayed in Appendix 13.

m/z 231 Triaromatic steroids

Triaromatic steroids originate from aromatization of monoaromatic steroids with increasing maturation (Peters et al., 2007). Thus, triaromatic steroids ratios are source and maturation parameters similar to those for monoaromatic steroids. TA(I)/TA(I+II) appeared to be more sensitive at higher levels of maturity than MA(I)/MA(I+II). All samples in this study have low ratios, indicating immature OM. GC-MSD traces (*m/z* 231) of analyzed samples are displayed in Appendix 14.

Diamondoids analysis

Diamonoids are thermally stable and highly bioresistant hydrocarbons in the saturated fraction that remain unaltered even in severely biodegraded oils (Williams et al., 1986). Figure 20 shows the schematic relationship between concentrations of 3- and 4- methyldiamantanes (diamonoids) and stigmastane (biomarker) for 10CW79, 10CW95, and 10CW96 samples. No evidence of significant cracking is observed. The major variation between samples is the abundance of stigmastane (sterane), which is probably related primarily to biodegradation; which removes steranes from the extractable hydrocarbons. Sample 10CW97 has very high stigmastane abundance (6033 ppm) due to very low maturity and plots outside of the scale of the diagram. GC-MSD chromatograms of source rock extracts for diamondoid analysis are displayed in Appendix 11.

Oil-source rock correlation

Samples from the Woodruff Formation displayed very good source rock parameters, including OM quantity and quality, however they are thermally immature. I performed an oil–source rock correlation based on published data on 18 oil samples from several fields in Railroad Valley and one sample from Pine Valley (Ahdyar, 2011).

Figures 15 and 16 show a positive correlation between Woodruff extracts and oils from Railroad Valley. Note that 10CW79 sample plots near Trap Spring oil, while samples 10CW95-97 have parameters similar to the Kate Spring, Ghost Range and Eagle Spring oils. Steranes and monoaromatic steroid ternary diagrams suggest, but don't prove, an oil-source rock correlation (Figure 18, 19). However these parameters are sensitive to biodegradation and thermal maturation. Figures 21-23 display cross-plots with different biomarkers parameters, which suggest a genetic relationship between Woodruff samples and some oils. However, the level of thermal maturity of source-rock extracts is lower than the analyzed oils, which challenge reliable interpretation. In addition, cluster analysis (dendrogram on Figure 24) reveals the genetic relationship between 18 oil samples from Railroad Valley, one oil sample from Pine Valley, two source rock extracts and two pyrolyzates from the Woodruff Formation. This dendrogram is a result of statistical cluster analysis using Ward's method, based on 10 biomarker parameters listed in Appendix 16.

In summary, the Woodruff samples have several biomarkers that point toward a marine carbonate influenced source rock. They cluster more closely with the oils from Railroad Valley that Ahdyar (2011) interpreted as having been derived from the Mississippian Chainman Shale marine mudstones than they do with lacustrine carbonate

mudstones of the Sheep Pass Formation member B rocks. These results are not surprising given the lack of carbonate seen in thin sections or in hand samples, which are dominantly dark marine shales with recrystallized radiolaria.

Woodruff Formation Discussion

As a result of source-rock screening, the Devonian Woodruff Formation displayed the best OM quantity, quality, and thermal maturity among analyzed candidate units. A total of 24 outcrop samples of Woodruff Fm. were collected from Fish Creek Range. Sample location map is displayed in Appendix 8. TOC analysis revealed up to 6.5%, with values of 0.7 to 3 % common. Pyrolysis peak S_2 yield values up to 44 mg HC/g rock, also indicating excellent source potential. HI values reached 739 mg HC/g TOC, which indicates type I and type II kerogens for samples with reliable Rock-Eval Pyrolysis results. Visual kerogen analysis also suggested highly oil prone and oil prone kerogens. All organic-rich shales and mudstones from these Woodruff outcrop samples appeared to be thermally immature based on T_{max} values (up to 430 ^{o}C). In contrast, R_o values range from 0.76 % to 1.02 %, indicating peak oil window maturity to late oil window level of thermal maturity. However, biomarker analysis of 10CW79 and 10CW95 samples revealed that samples appeared to be biodegraded and thermally immature.

The Woodruff Fm. is exposed not only in the Fish Creek Range, but according to Ransom and Hansen (1990) is also found in Pinon and Hot Creek Ranges. Sandberg et al. (2003) and Morrow and Sandberg (2008) discussed tectonic development and sedimentation history of the Woodruff basin. They indicated that development of the Devonian Woodruff basin was related to proto-Antler forebulge evolution (Fig. 5). The

Woodruff formation was deposited west of Pilot (backbulge) basin and dated by conodonts as early Frasnian t*ransitans* Zone to the late Famennian Early *expansa* Zone in age (Sandberg et al., 2003). Due to similar lithology, the Woodruff can be confused with the lower member of the Pilot Shale to the east, and the upper part of the Slaven Chert to the west (Ransom and Hansen, 1990; Sandberg et al., 2003).

The Woodruff beds were involved in movement along the Roberts Mountains thrust and thermal maturity can vary significantly along the thrust front (Ransom and Hansen, 1990). According to Ransom and Hansen (1990), in Pinon Range the Woodruff Fm. was thrusted on top of Chainman Shale. In some localities Woodruff is mature and even overmature, while the Chainman Sh. is in the oil-window (Ransom and Hansen, 1990). This suggests that Woodruff Fm. could have been affected by local thermal events before and after thrusting.

Thus, this brief discussion of depositional environment of the Woodruff Fm., complex tectonic evolution, and thermal history of the area, lead us to the conclusion that thermally mature Woodruff could be present and responsible for oil accumulation in valleys other than Railroad Valley and Pine Valley.

CHAPTER 6

CONCLUSIONS

This research project performed an evaluation of possible source rock units in northern Nye County, that included the Paleozoic Pogonip Group, Vinini Formation, Devonian Slaven Chert, Guilmette Formation, Woodruff Formation, Pilot Shale, Joana Limestone, Eleana Formation, Ely Limestone and Cretaceous Newark Canyon Formation. This study resulted in a complete geochemical dataset, describing petroleum potential (quantity), kerogen type (quality) and level of thermal maturation of analyzed candidate rocks.

As a result of this evaluation, the Devonian Woodruff Formation displayed excellent organic matter quantity (TOC up to 6%), and type I and type II kerogens, which are favorable for oil generation, however samples appeared to be thermally immature. None of the other analyzed candidate units met the requirements for organic matter quantity, quality, and thermal maturity in order to be called source rocks. However I consider this assessment sample/location specific. Analyzed samples were collected from outcrops, easily affected by weathering. This could significantly change TOC values and affect thermal maturation and Rock-Eval pyrolysis parameters in general. TOC values and thermal maturity can also vary depending on facies changes and with depth.

Biomarker analysis of the Woodruff Formation provided contradictory interpretations of depositional environment. Samples appeared to be biodegraded and thermally immature, which affects certain biomarker parameters and decreases their reliability. Although one of the most powerful indicators of marine organic matter - C_{30} 24-*n*-propylcholestanes is present in all samples.

Additionally, rough oil – source rock correlation suggests, but doesn't prove, genetic relationship between the Woodruff Formation and Chainman-derived oils from Railroad and Pine Valleys. More detailed and reliable oil-source rock correlation requires equivalent or at least a similar level of thermal maturity of source-rock extracts and analyzed oils (Peters et al., 2007). However, thermally mature Woodruff could be present and responsible for oil accumulation in valleys other than Railroad Valley and Pine Valley. Thus, geochemical confirmation of good to excellent source rock characteristics of Woodruff Formation has important implications for future hydrocarbon exploration in northern Nye County and Nevada in general.

APPENDIX 1

FIGURES

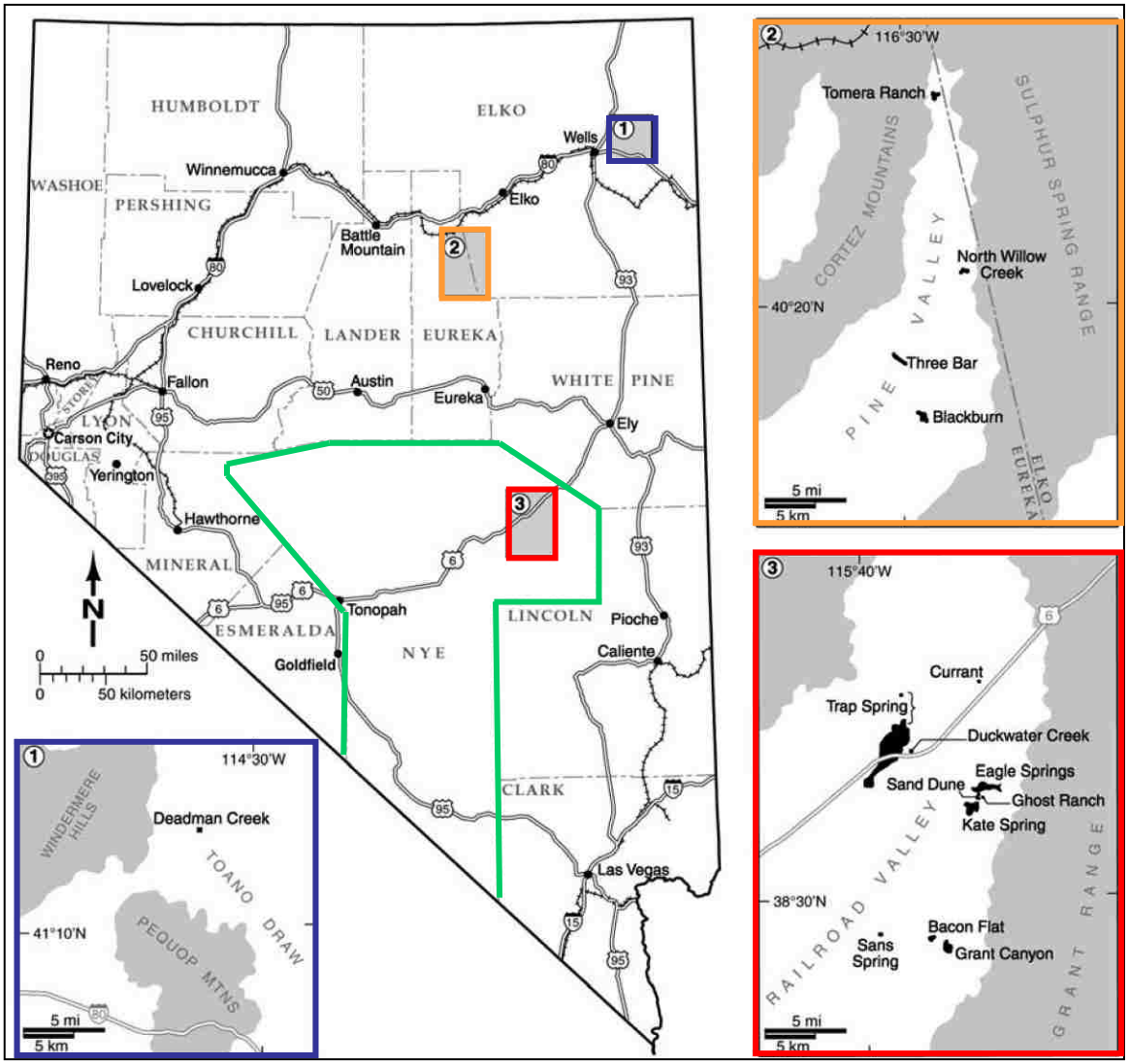

Figure 1. Location of producing oil fields in Nevada (LaPointe et al., 2007).

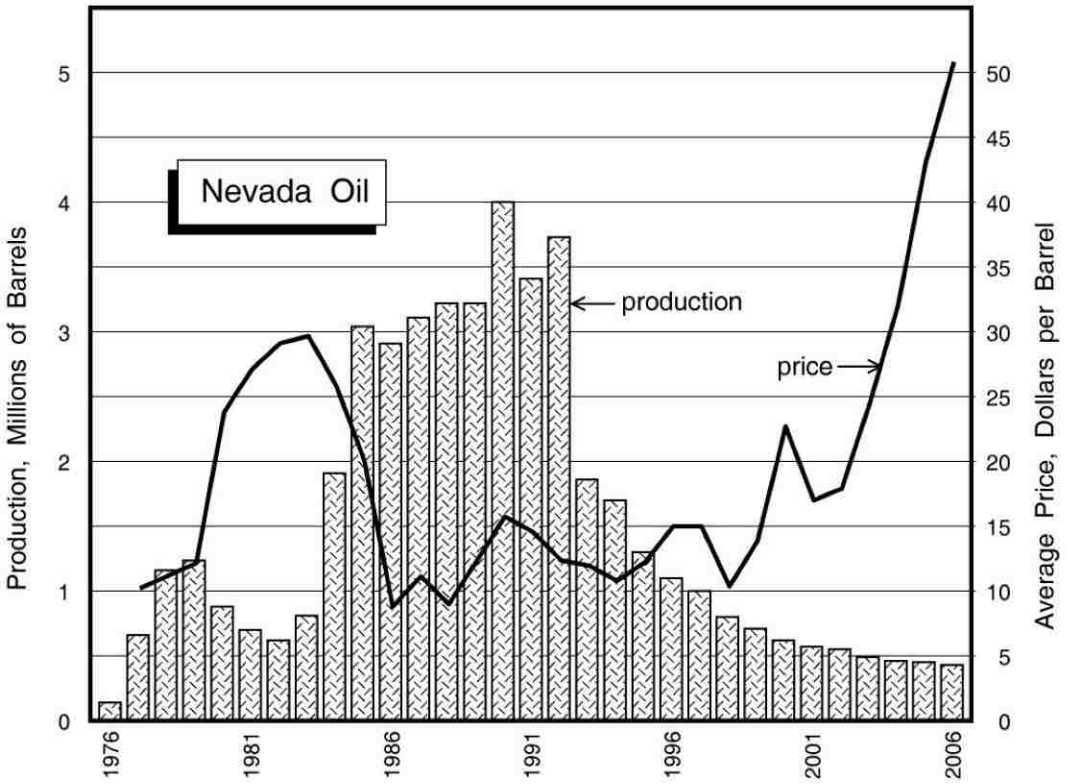

Figure 2. Production and price history for Nevada oil, 1976-2006 (Price and Meeuwig, 2007).

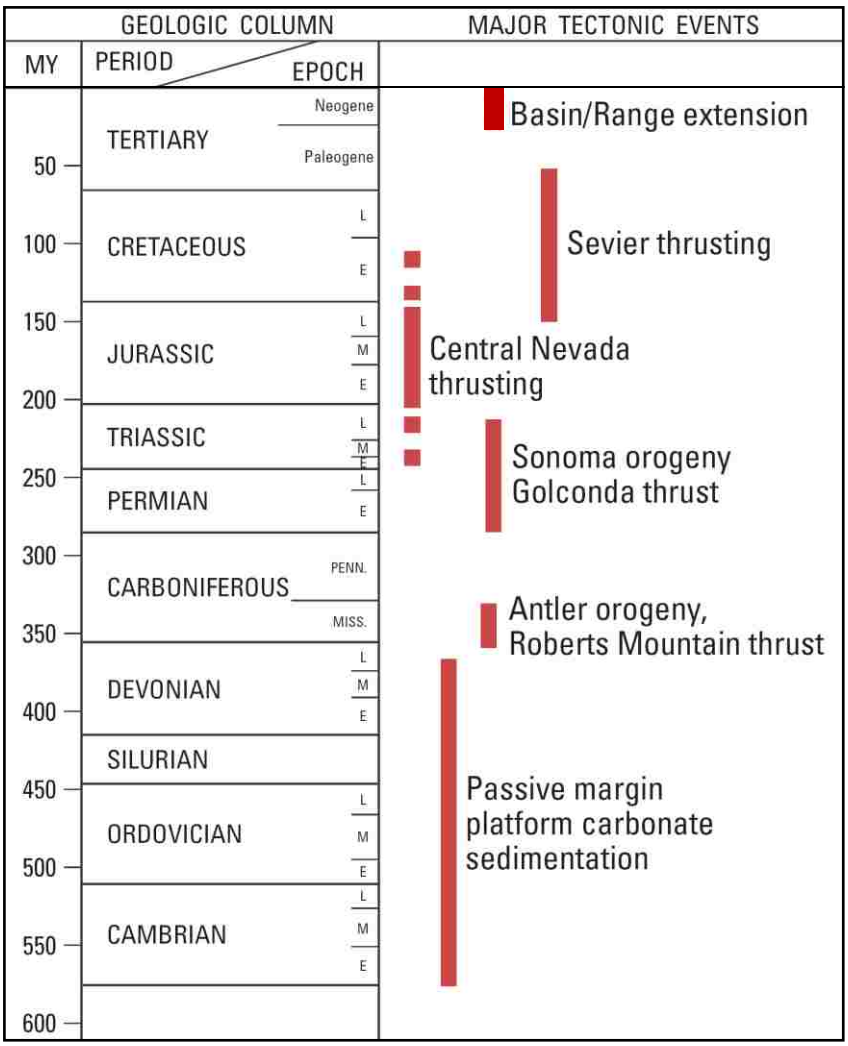

Figure 3. Sequence of major tectonic events of the eastern Great Basin. E, Early; M, Middle; L, Late; Miss., Mississippian; Penn., Pennsylvanian (Anna et al., 2007).

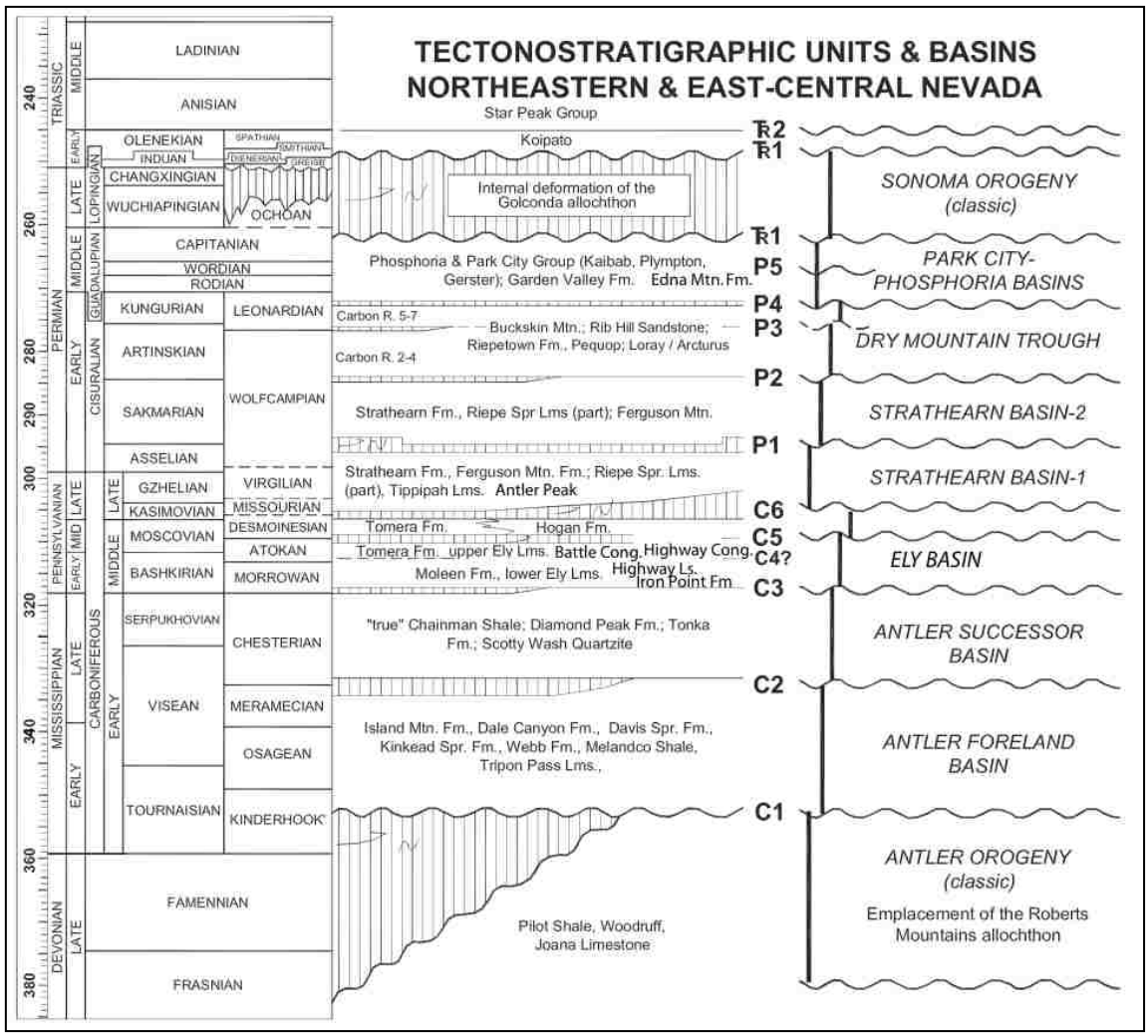

Figure 4. Tectonostratigraphic units and basins of northeastern and east-central Nevada (Cashman et al., 2008).

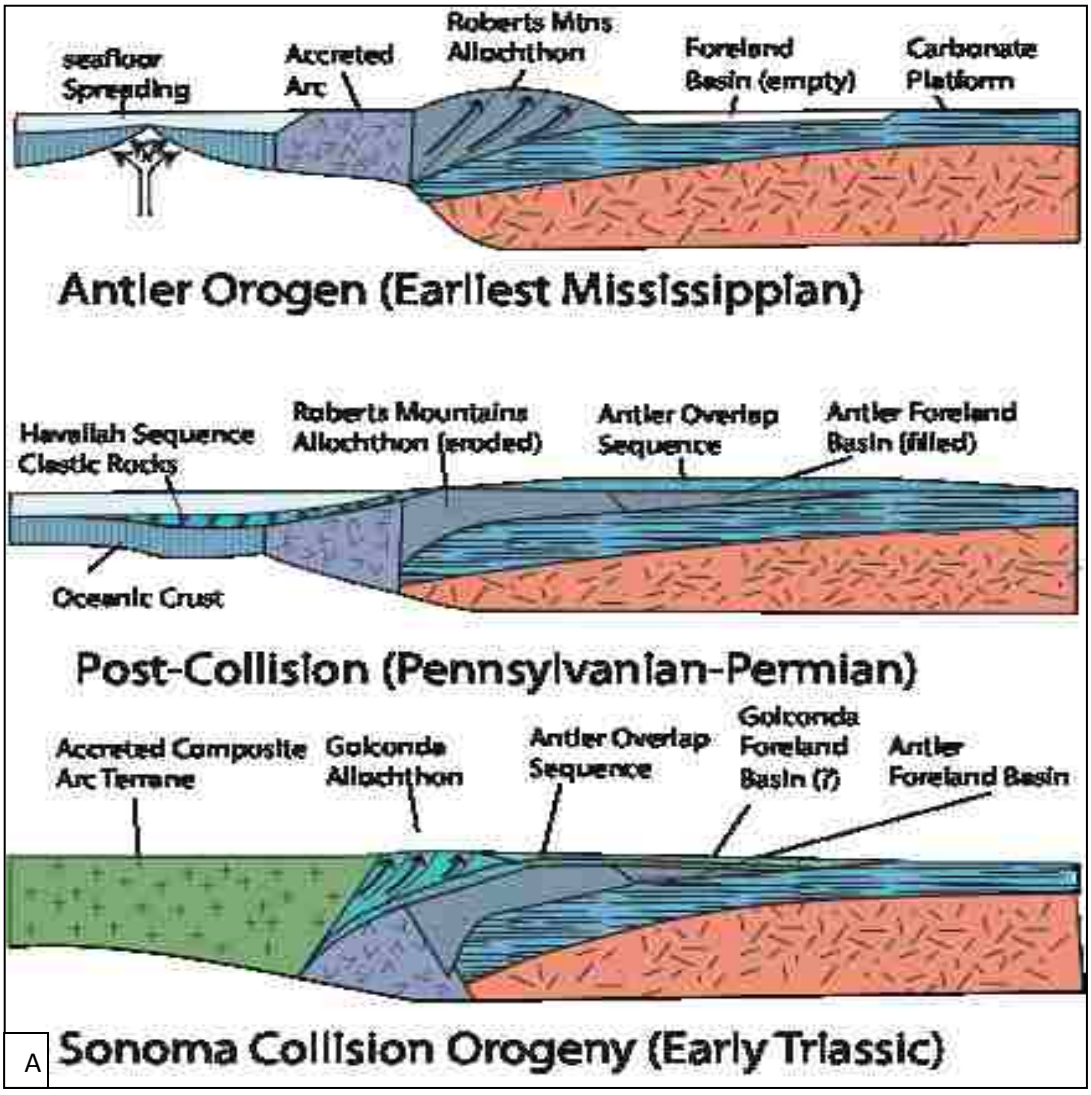

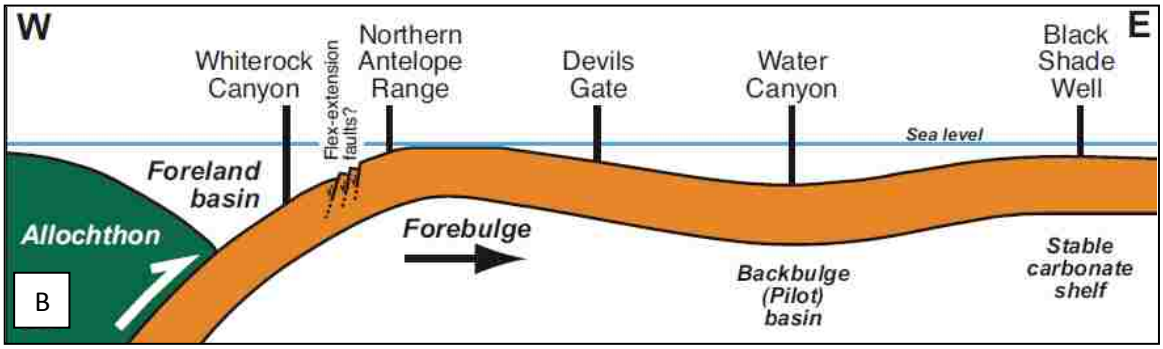

Figure 5. A - Model of Late Devonian and Mississippian time with hypothesized tectonic setting of the Antler orogeny. Modified by Siebenaler (2010) after Burchfiel et al. (1992). B - Model for the eastward migrating Antler foreland system (Morrow and Sandberg, 2008).

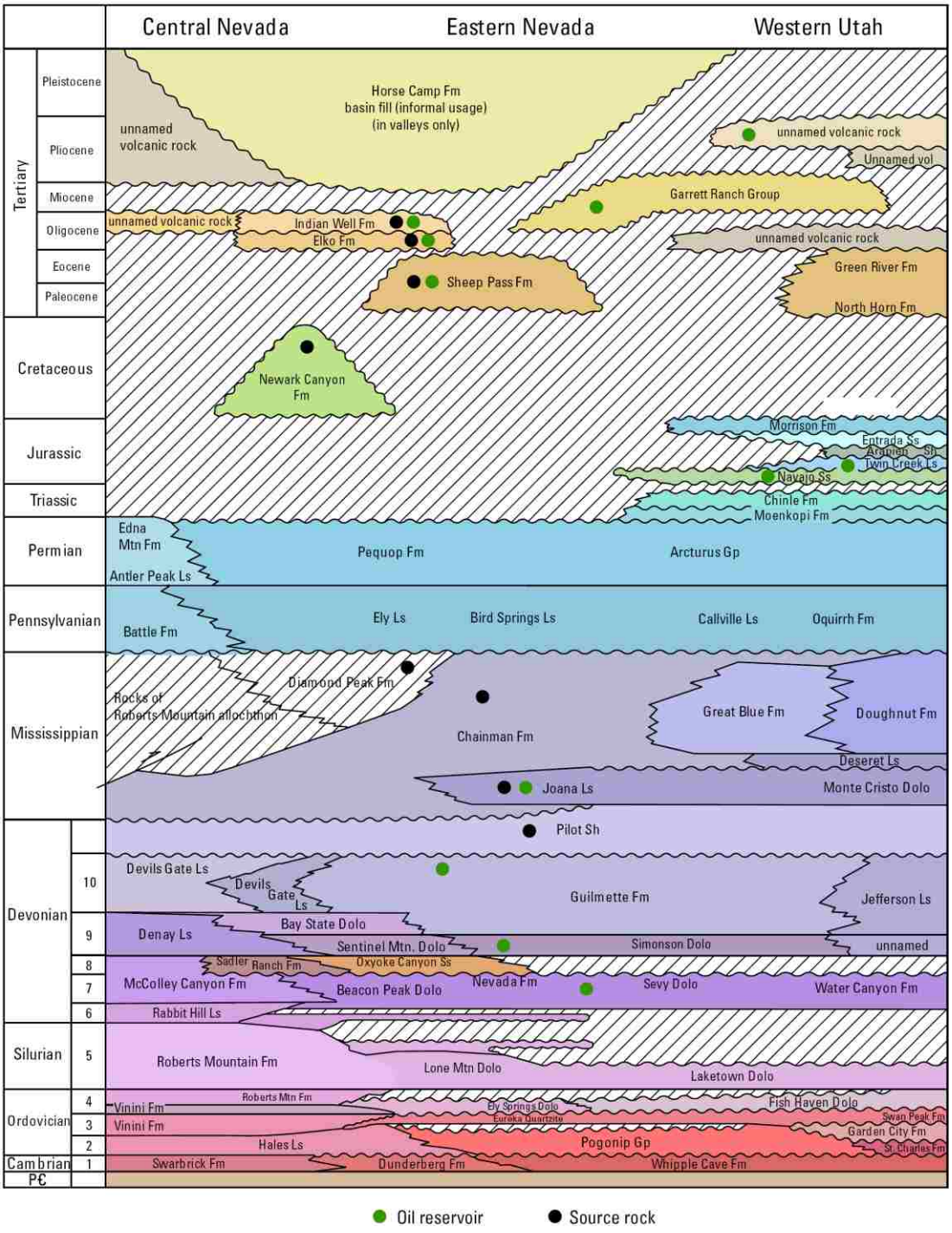

Figure 6. Generalized stratigraphic column of Phanerozoic strata in the eastern Great Basin showing oil reservoirs, source rocks, major sequence boundaries, hiatus intervals (hachured), and unconformities (Anna et al., 2007). Paleozoic section modified from Cook and Corboy (2004). Ls, limestone; Dolo, dolomite; Fm, formation; Vol, volcanic; Ss, sandstone. A newer and more detail stratigraphic column for the Late Devonian to Early Triassic is shown in Figure 4.

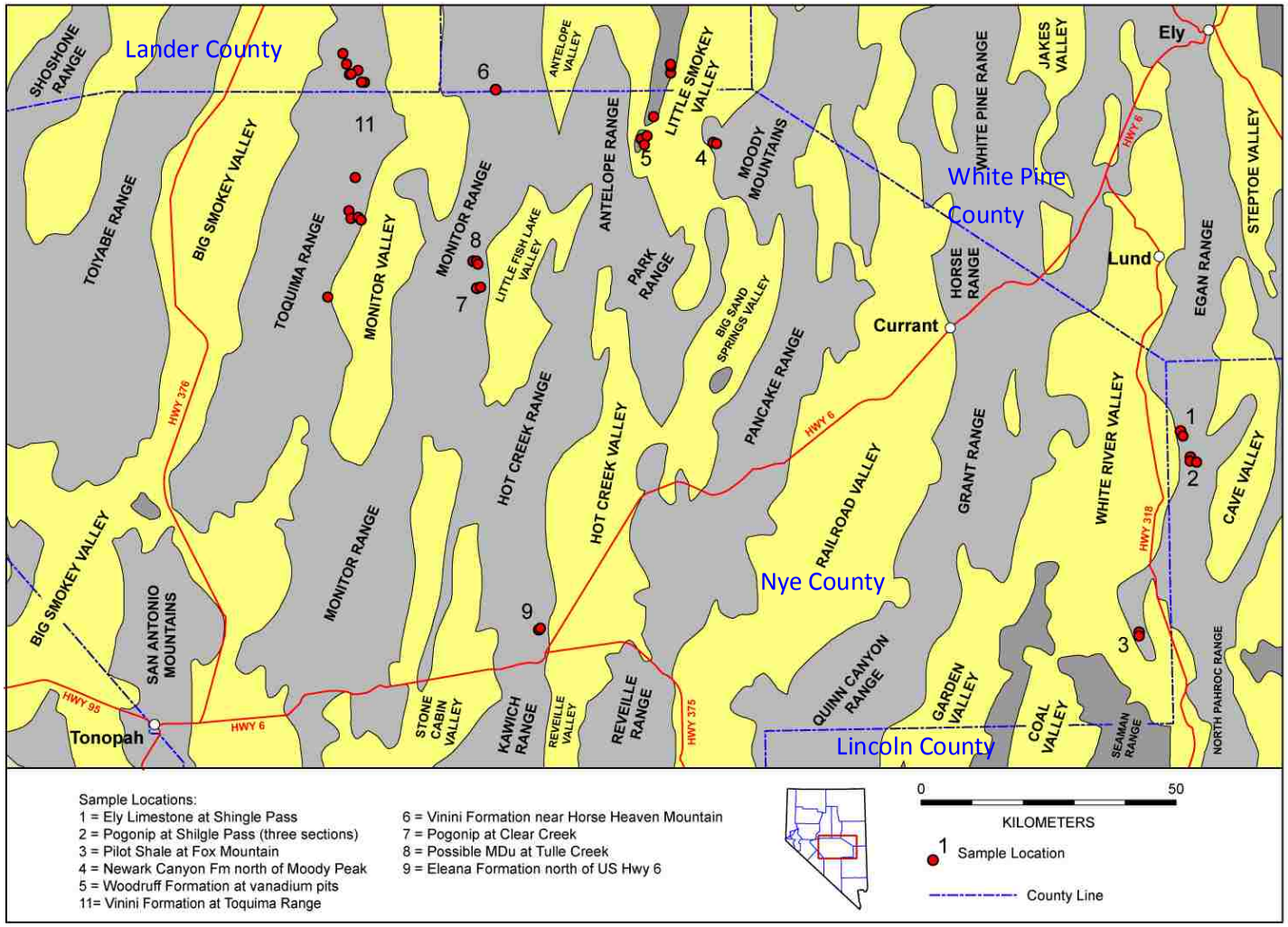

Figure 7. Sample location map showing mountain ranges and valleys in the vicinity of northern Nye County, Nevada. Base map is modified from Kleinhampl and Ziony (1984).

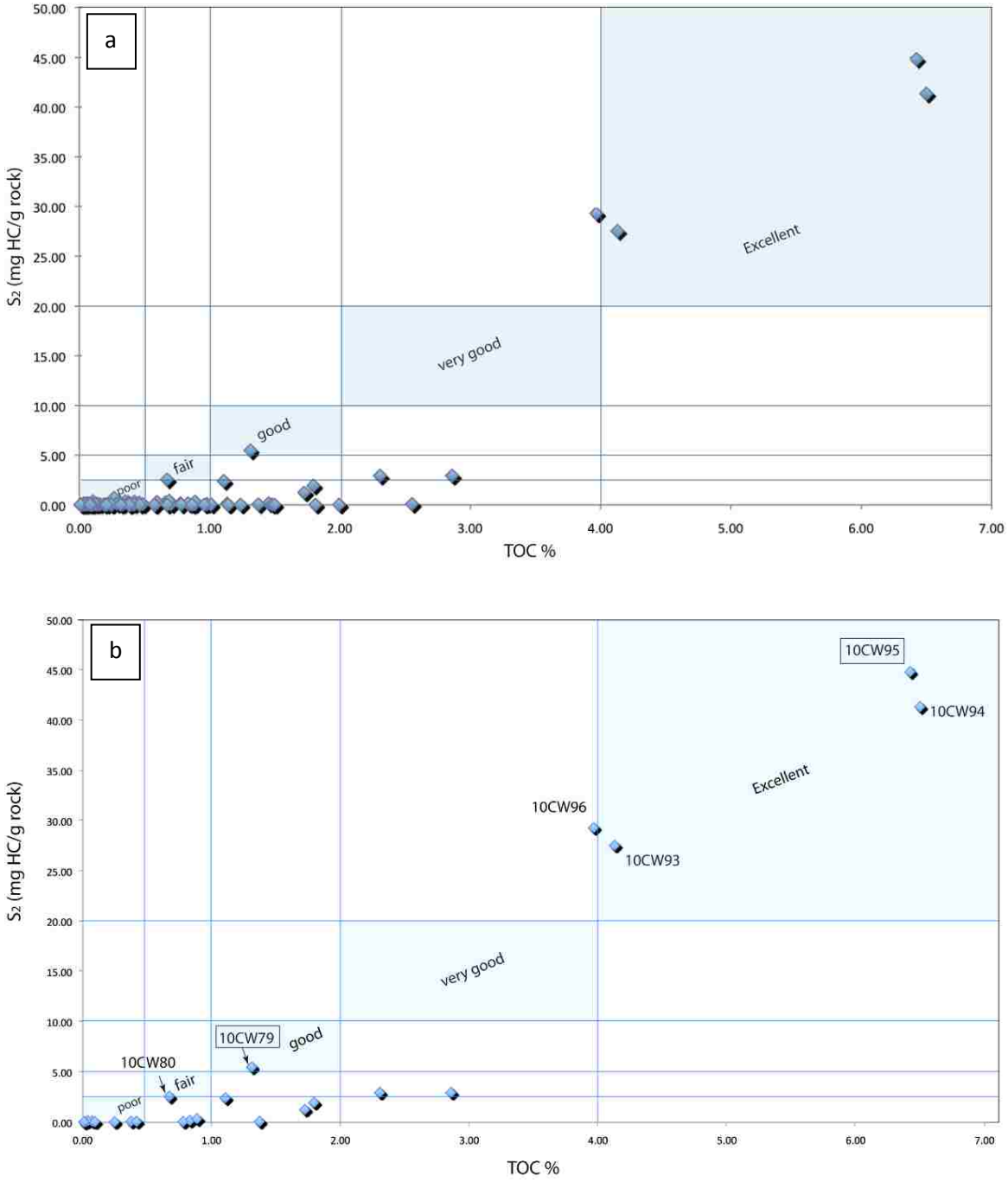

Figure 8. Total organic carbon (TOC) (wt. %) versus Rock-Eval S_2 peak, describing quantity of OM for the (a) complete sample set, and (b) Woodruff Formation

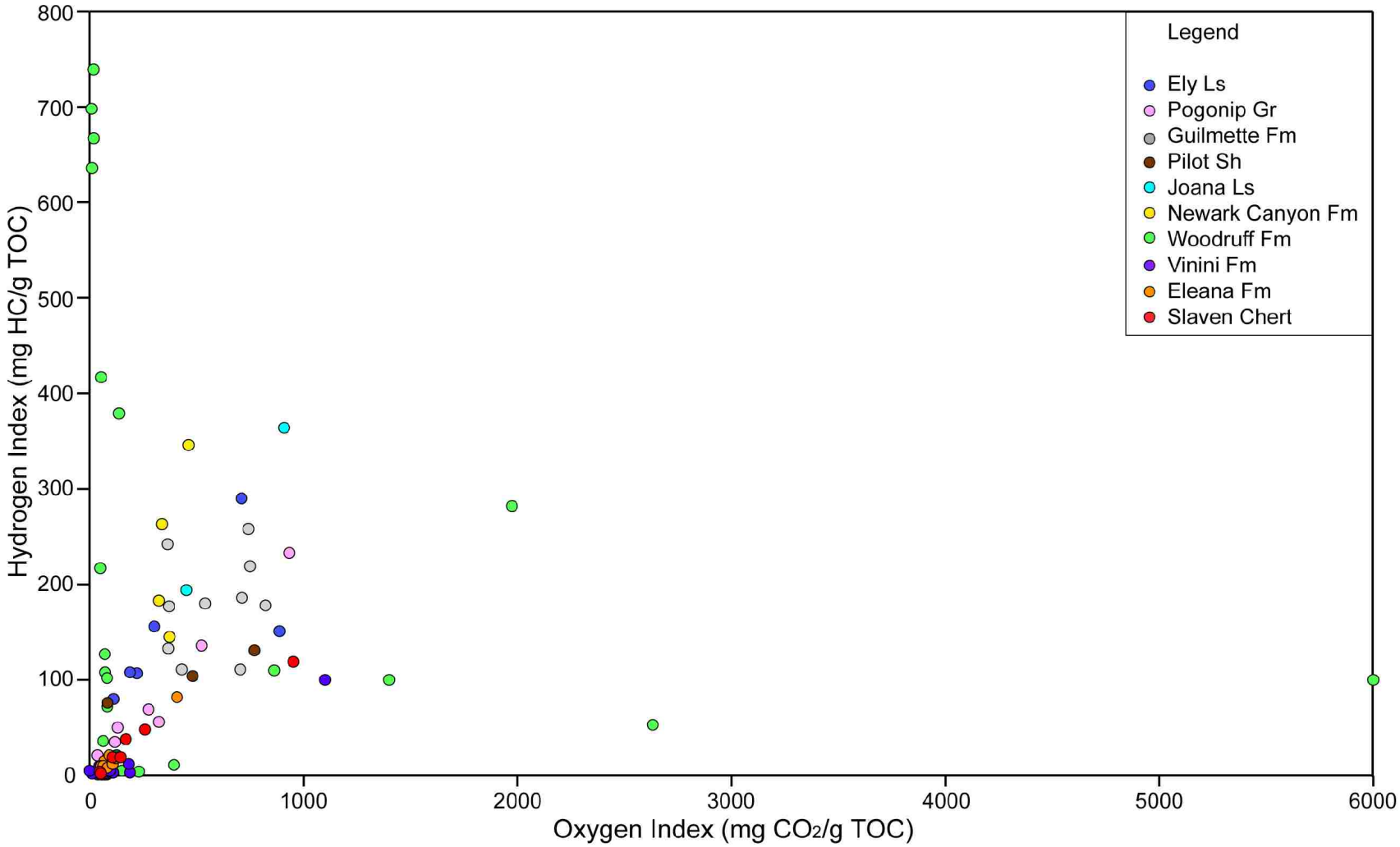

Figure 9. Oxygen Index versus Hydrogen Index plot for complete sample set.

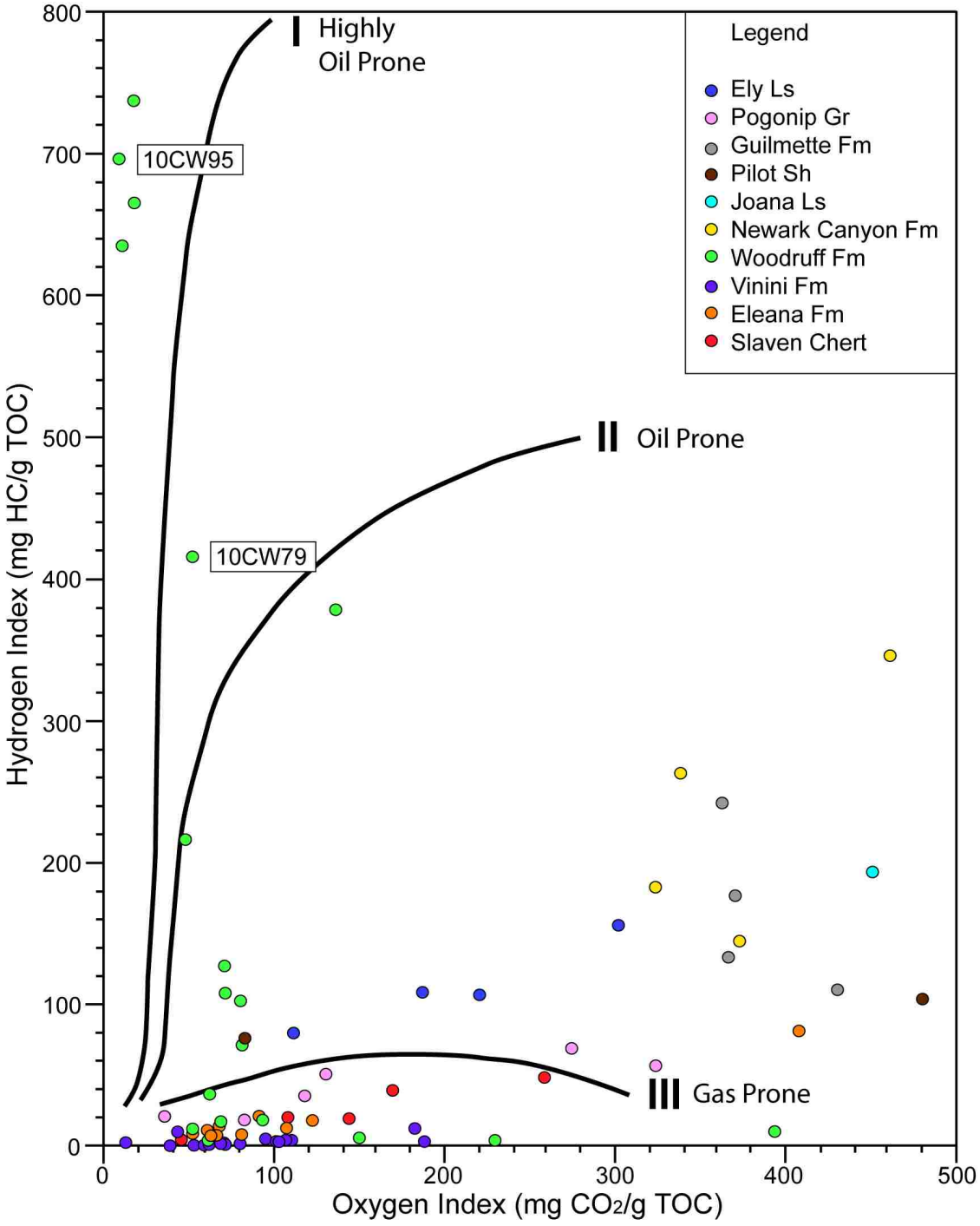

Figure 10. Modified van Krevelen diagram for analyzed samples.

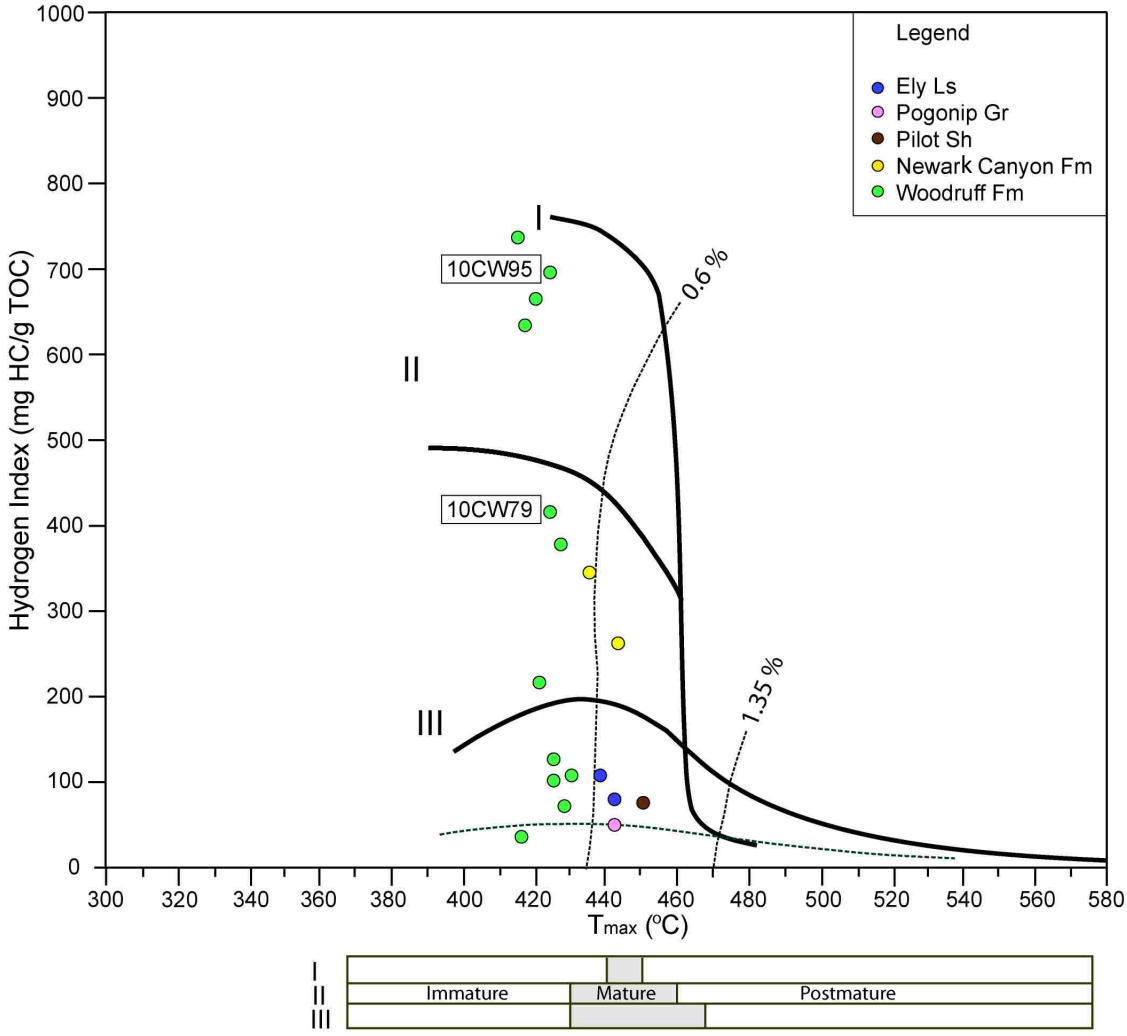

Figure 11. General Hydrogen Index versus T_{max} diagram modified from Espitalié et al. (1984).

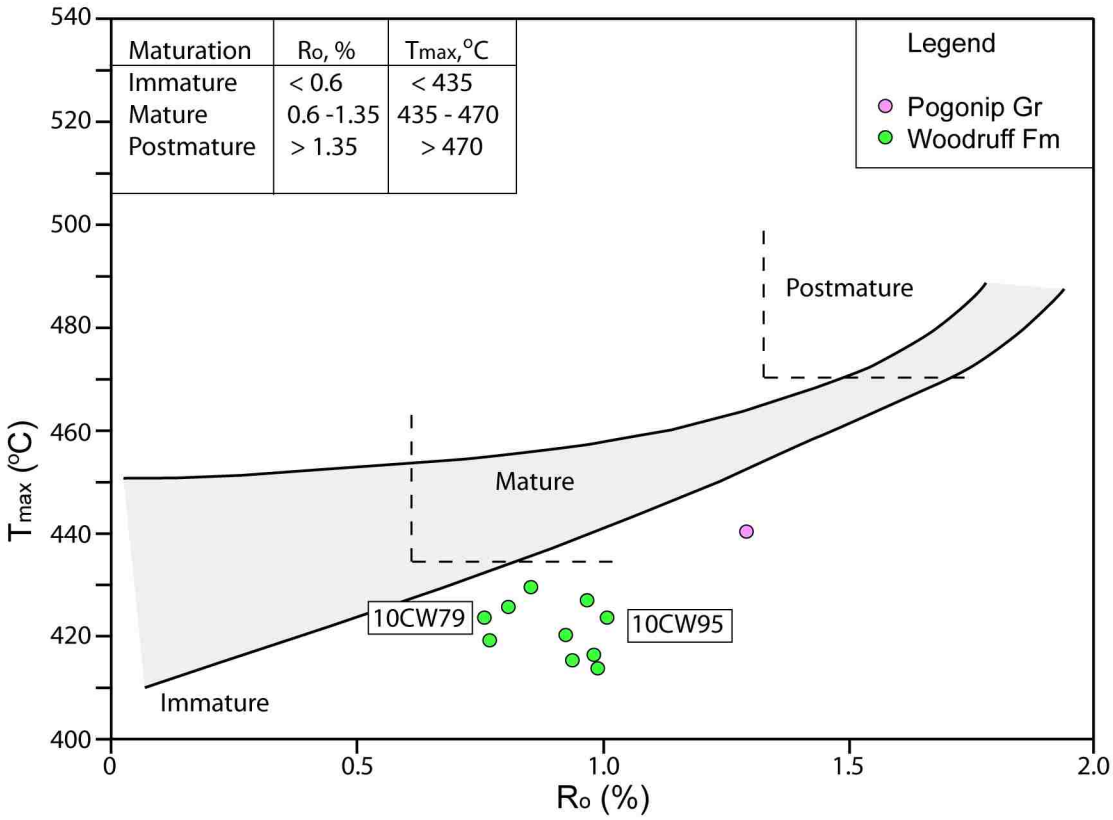

Figure 12. Vitrinite reflectance versus T_{max} plot, modified from Peters (1986).

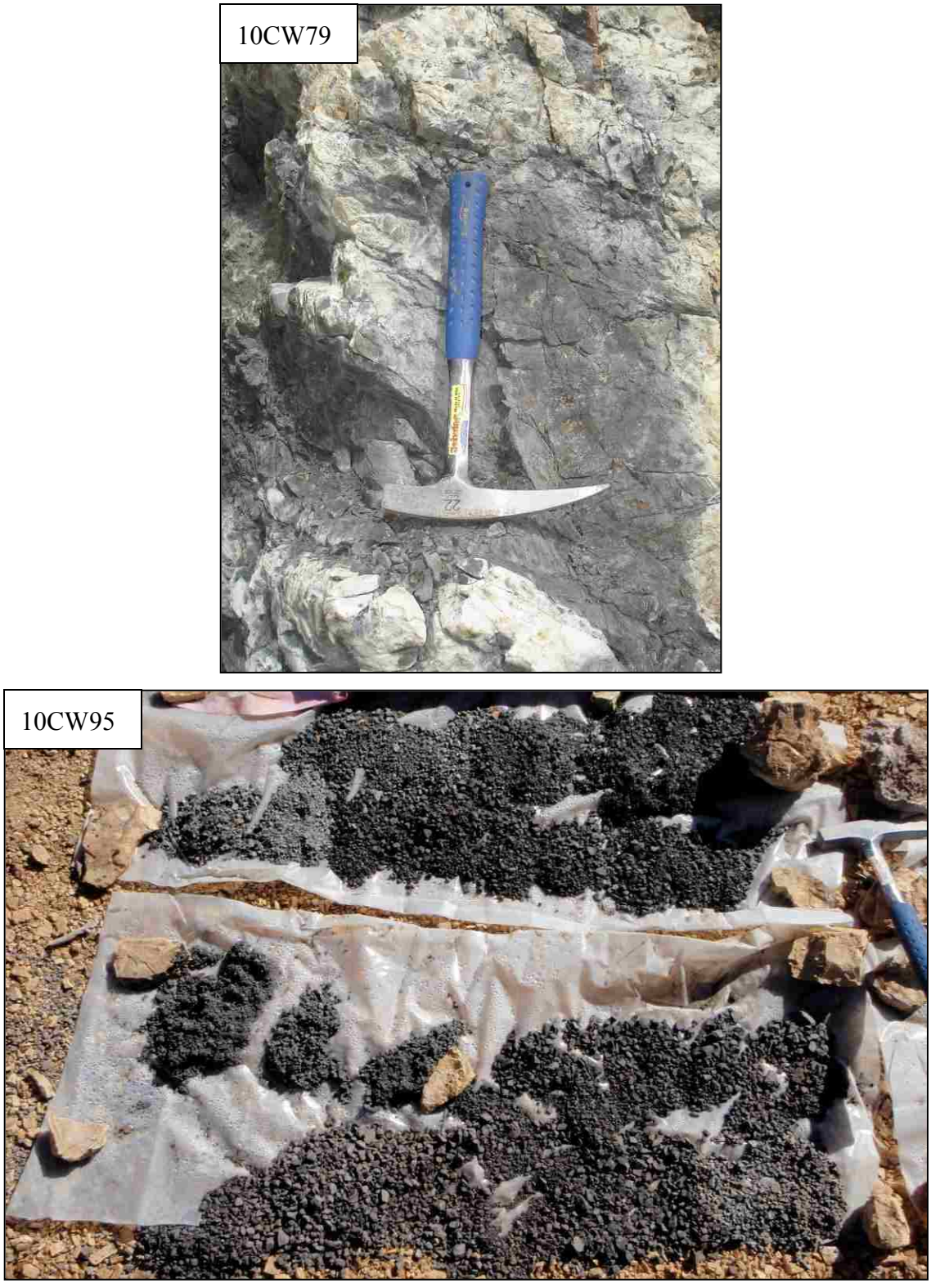

Figure 13. Photographs of 10CW79 and 10CW95 samples of the Woodruff Formation.

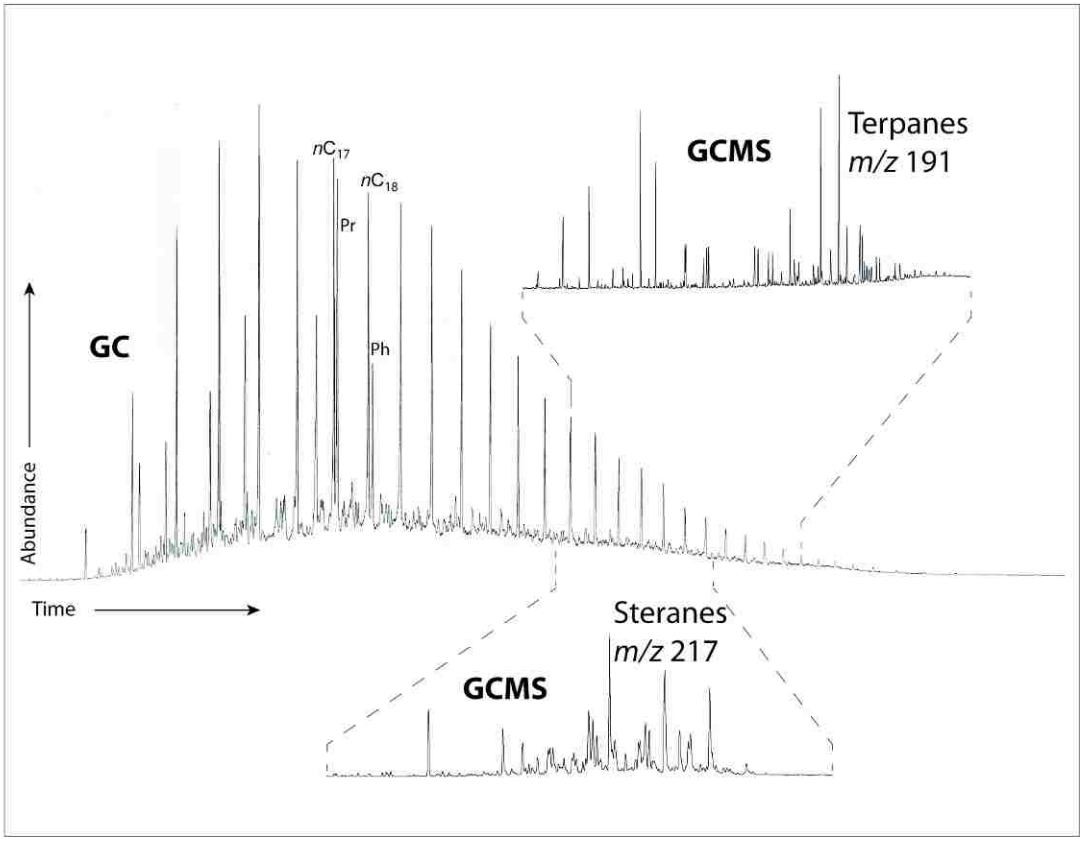

Figure 14. Gas chromatogram of 10CW95p sample illustrates the relationship (at different scale) between GC and GCMS data.

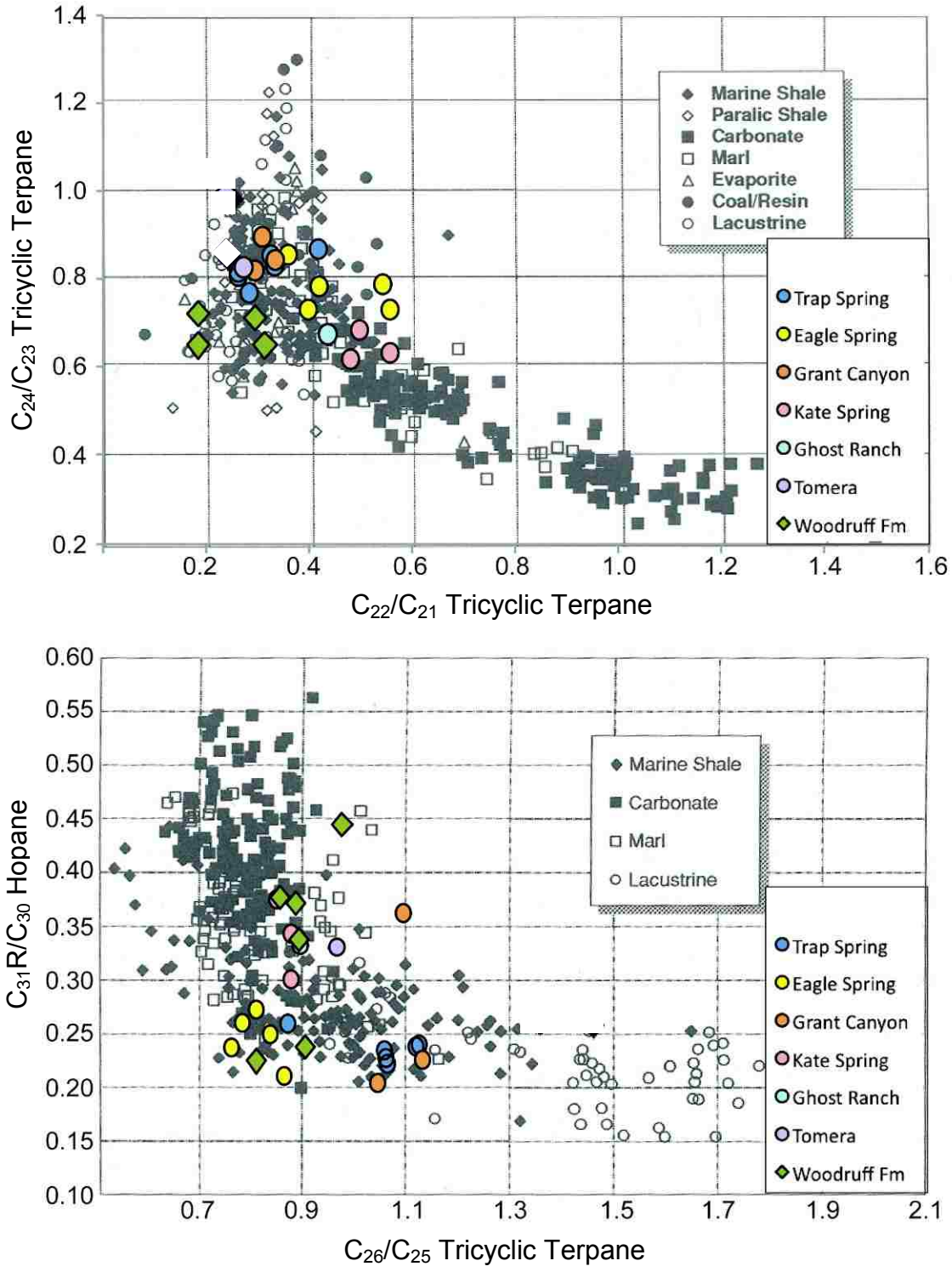

Figure 15. Relative amounts of tricyclic terpanes suggest interpretation of Woodruff Formation as marine shale source-rock and support oil - source rock correlation (modified from Peters et al., 2007).

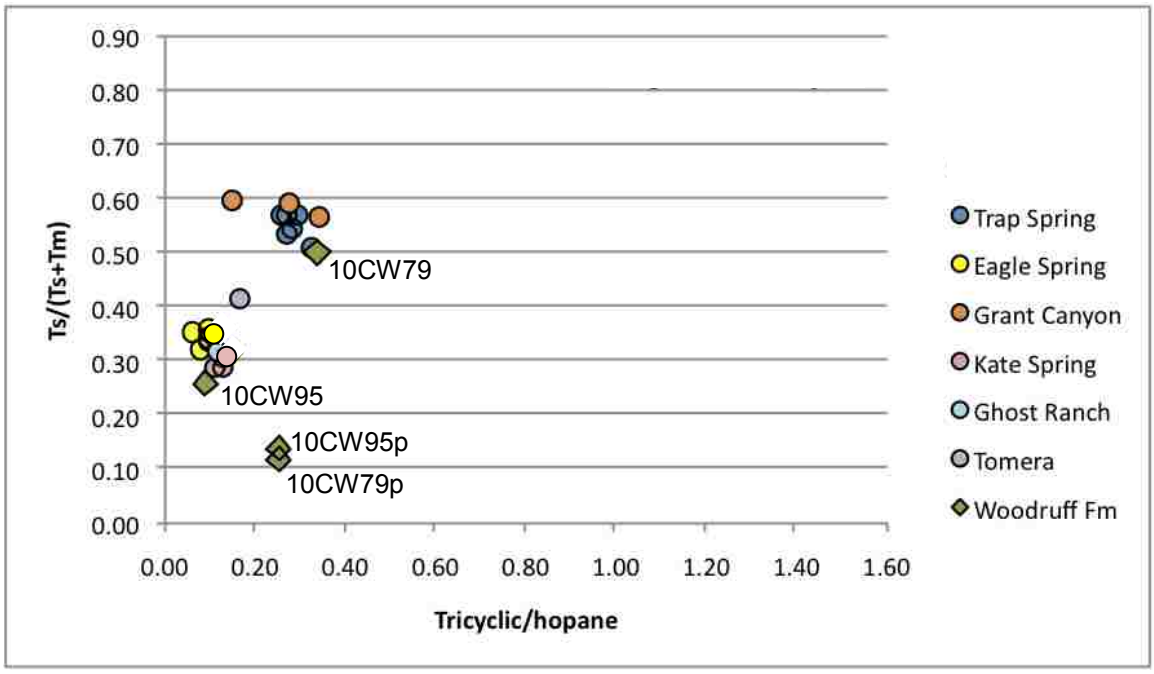

Figure 16. Tricyclic/17α-hopane vs Ts/(Ts+Tm) plot suggests interpretation of Woodruff Formation as algal-rich and clay-rich source-rock and supports oil-source rock correlation.

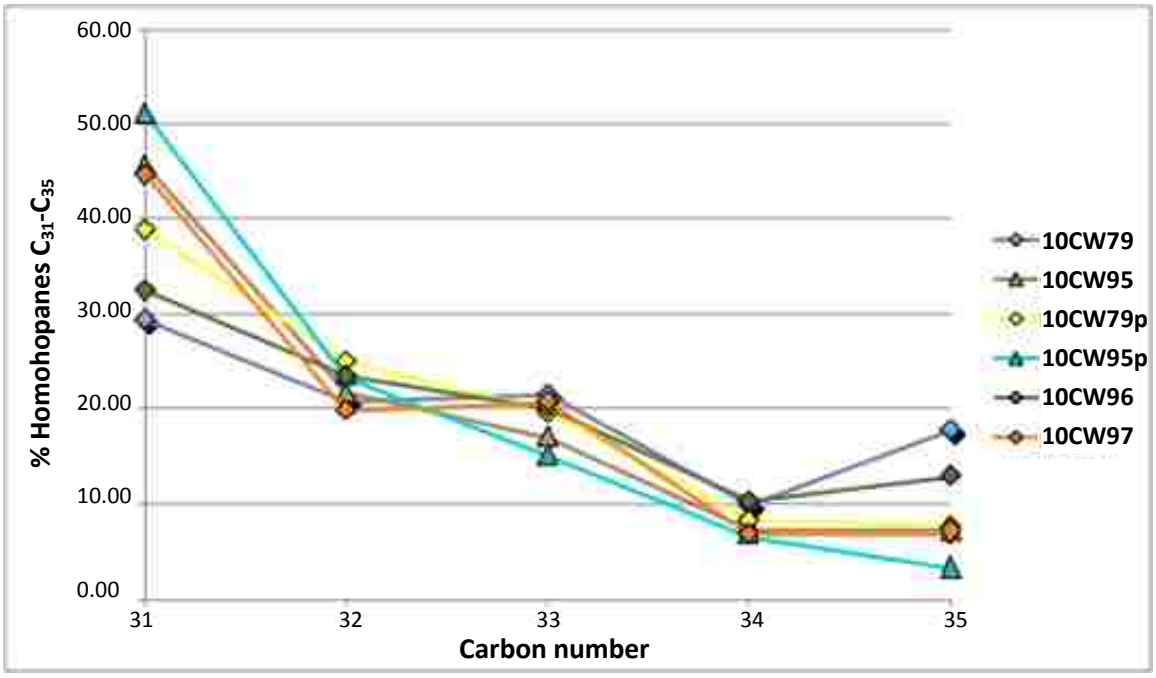

Figure 17. Homohopane distributions suggest highly reducing conditions during 10CW79 and 10CW96 deposition. Presence of C_{34}-C_{35} homohopanes in other samples indicate somewhat anoxic conditions.

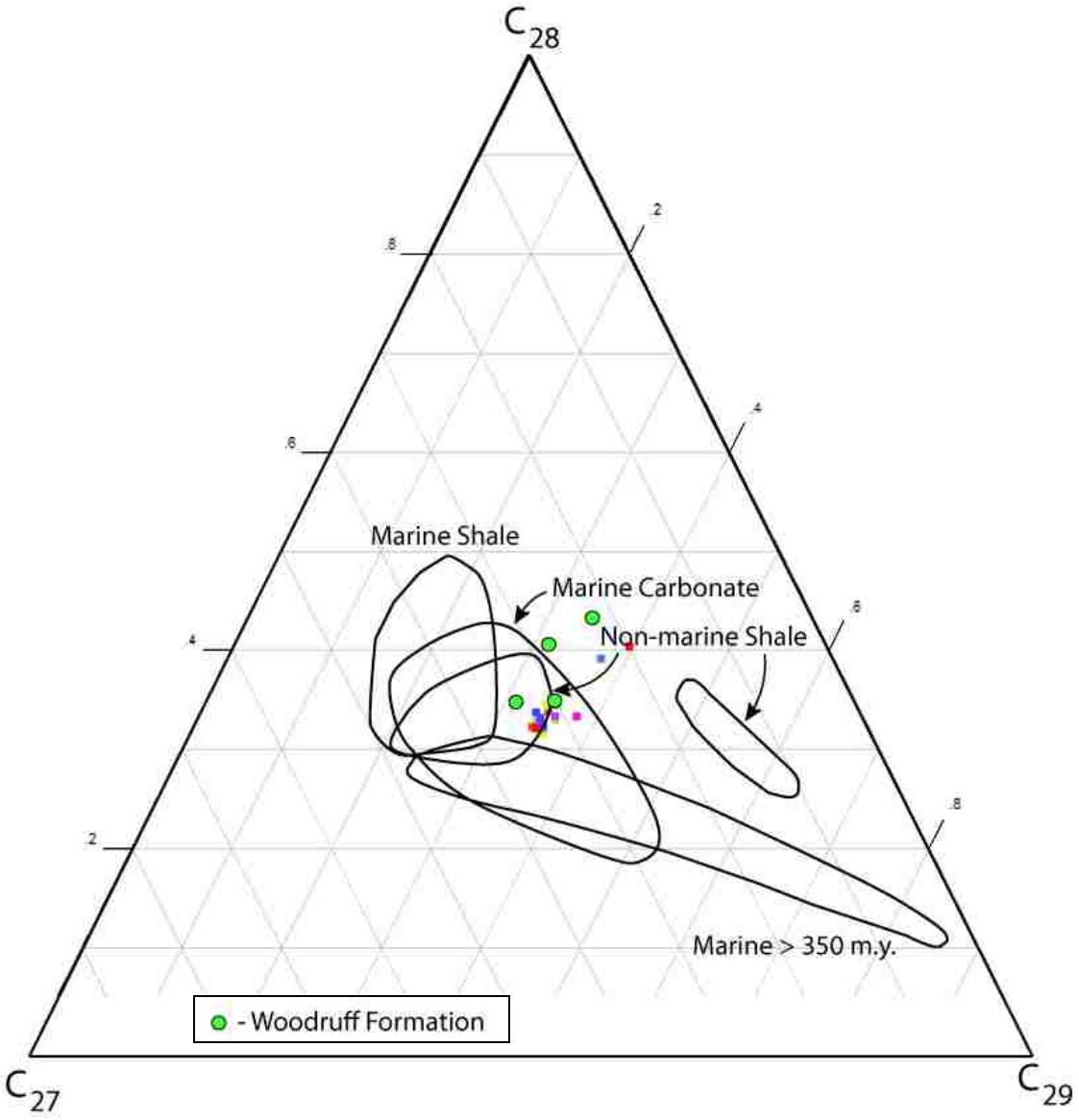

Figure 18. Ternary diagram showing the relative abundance of C_{27}, C_{28} and C_{29} regular steranes (Moldowan et al., 1985). Woodruff Formation samples are plotted as green dots, oils from Ahdyar (2011) are plotted as colored squares for oil-source rock correlation.

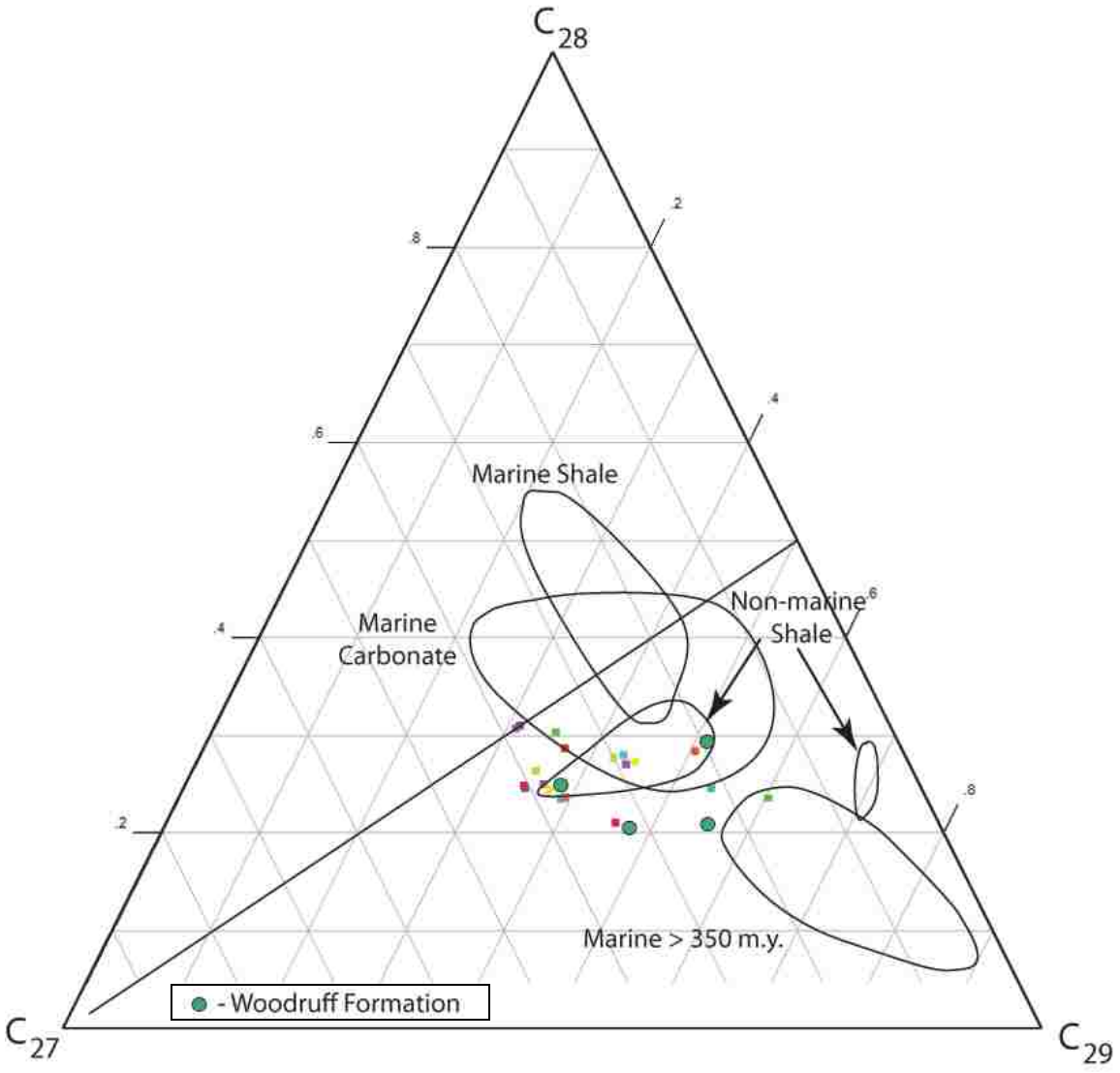

Figure 19. Monoaromatic steroids ternary diagram suggests that Woodruff Formation has non-marine or marine carbonate organic matter source. Woodruff Formation samples are plotted as green dots, oils from Ahdyar (2011) are plotted as colored squares for oil-source rock correlation.

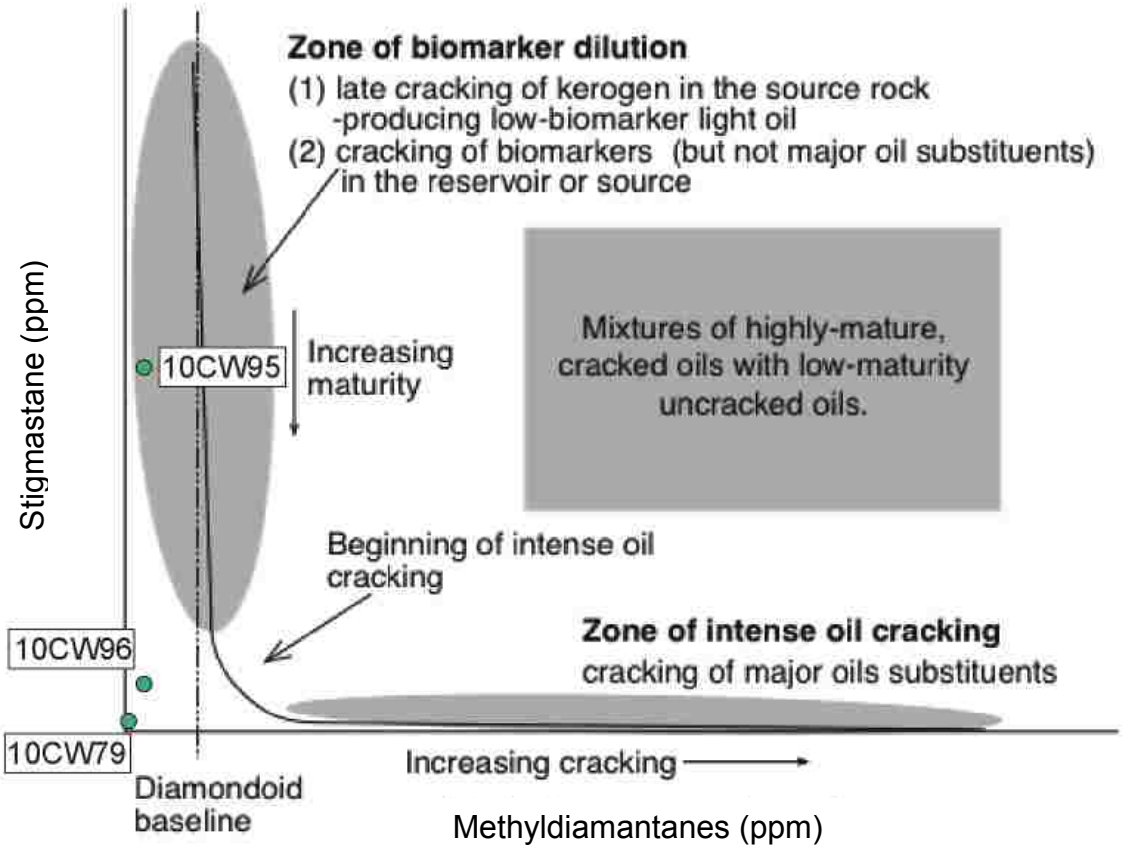

Figure 20. Schematic relationship between concentrations of 3- and 4-methyldiamantanes (diamondoids) and stigmastane for four Woodruff samples (Dahl et al., 1999).

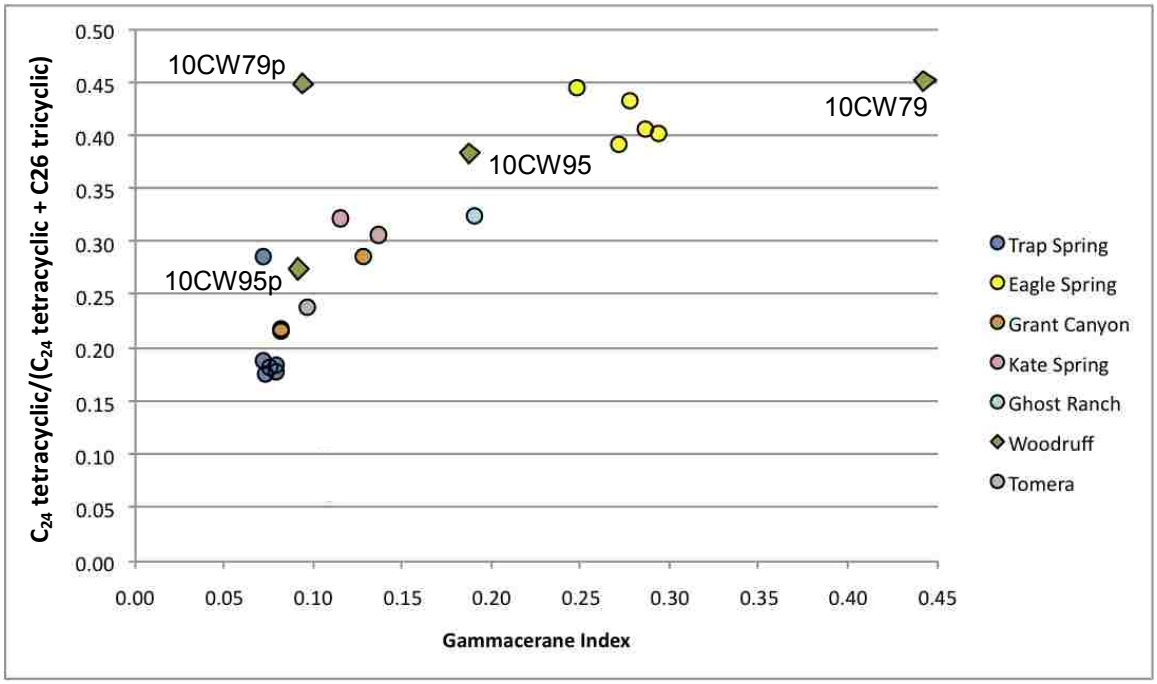

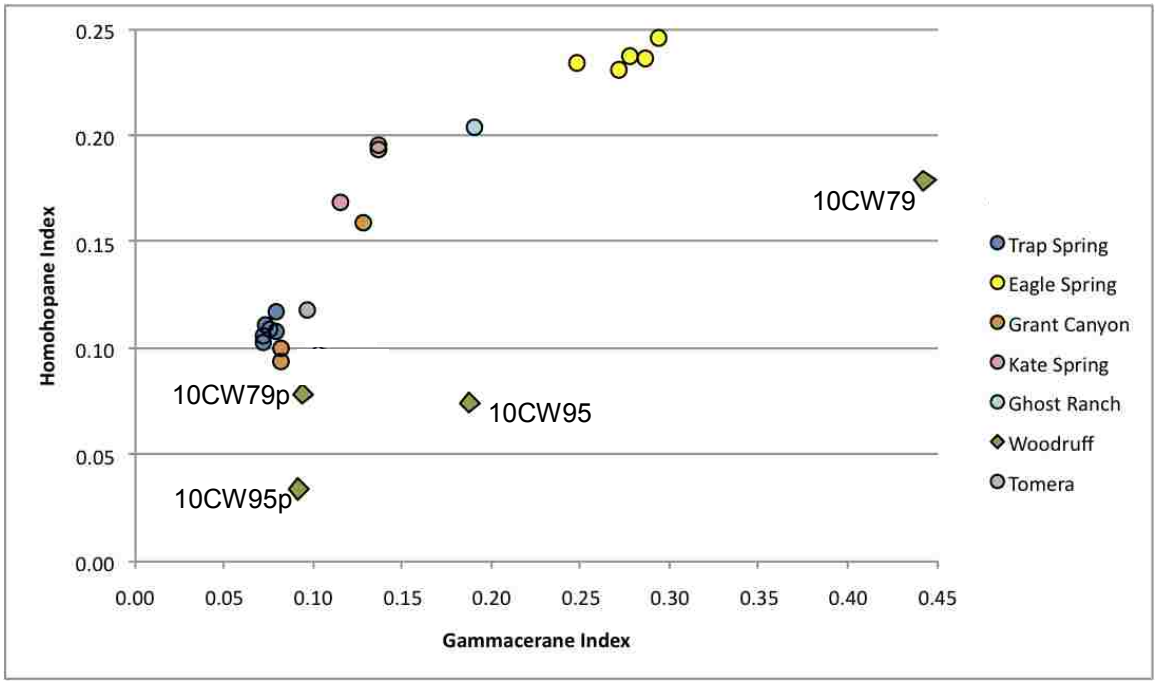

Figure 21. Cross-plots of gammacerane and homohopane indices, and C_{24} tetracyclic / (C_{24} tetracyclic + C_{26} tricyclic). Oil-source rock correlation is poor, only samples 10CW79p and 10CW95 p are similar to type I oils.

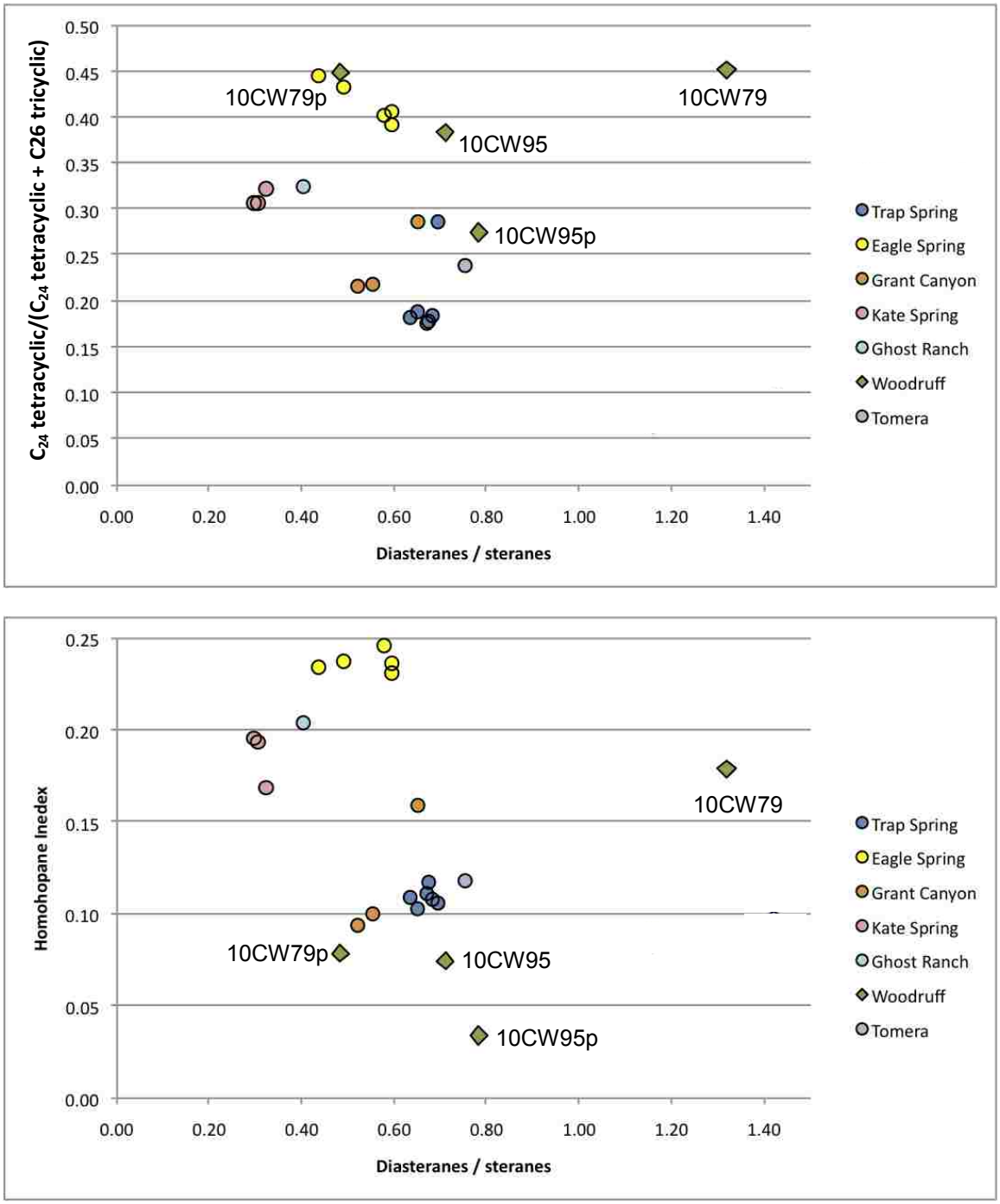

Figure 22. Cross-plots of diasteranes/steranes, homohopane index, and C_{24} tetracyclic / (C_{24} tetracyclic + C_{26} tricyclic). Samples 10CW79, 10CW79p and 10CW95 display some correlation with Railroad Valley oils. Sample 10CW79 has relatively high diasteranes/steranes ratio, presumably due to higher degree of biodegradation.

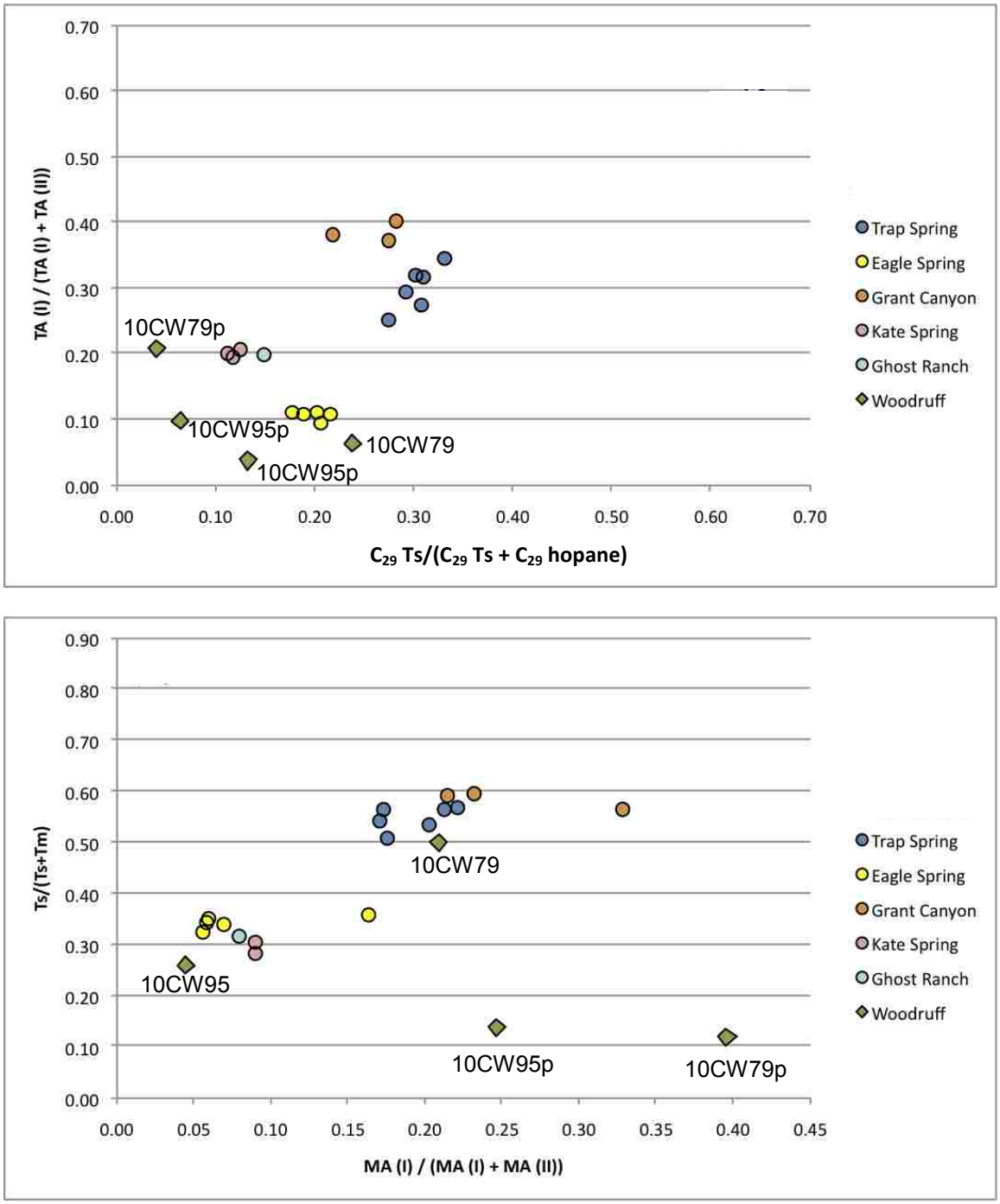

Figure 23. Cross-plots of maturity related parameters. The Woodruff Formation is less thermally mature than oils from Railroad Valley.

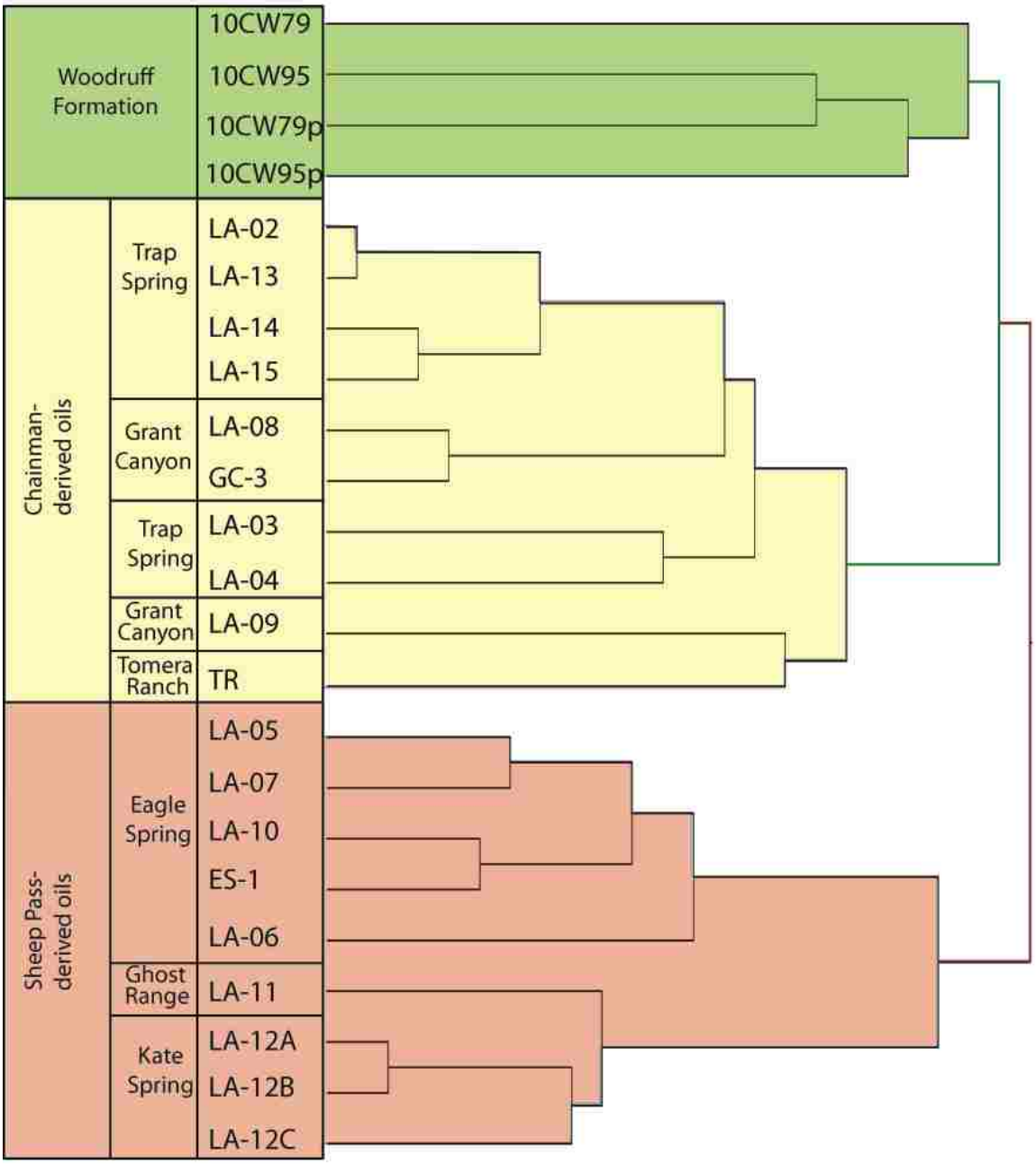

Figure 24. Dendrogram showing genetic relationship between 18 oil samples from Railroad Valley, one oil sample from Pine Valley, and two source rock extracts and two pyrolyzates from the Woodruff Formation. This dendrogram is based on statistical analysis using Ward's method. All input parameters for the cluster analysis are provided in Appendix 13.

APPENDIX 2

TABLES

Table 1. Producing oil fields in Nevada (from Nevada Oil Patch Newsletter, 2009).

Field Name	Location	County	Production, Start Date	Production, Barrels
Eagle Springs	Railroad Valley	Nye	1954	**5,387,785**
Trap Springs	Railroad Valley	Nye	1976	**14,290,584**
Currant	Railroad Valley	Nye	1979	**1,823**
Bacon Flat	Railroad Valley	Nye	1981	**1,021,542**
Blackburn	Pine Valley	Eureka	1982	**5,344,773**
Grant Canyon	Railroad Valley	Nye	1983	**21,117,309**
Kate Spring	Railroad Valley	Nye	1986	**2,370,194**
Tomera Ranch	Pine Valley	Eureka	1987	**36,472**
N Willow Creek	Pine Valley	Eureka	1988	**51,841**
Three Bar	Pine Valley	Eureka	1990	**23,837**
Duckwater	Railroad Valley	Nye	1990	**18,700**
San Spring	Railroad Valley	Nye	1993	**272,254**
Ghost Ranch	Railroad Valley	Nye	1996	**575,718**
Dead-Man Creek	Toano Draw	Elko	1996	**367**
Sand Dune	Railroad Valley	Nye	1998	**147,538**
Toana Draw	Toano Draw	Elko	2007	**1,964**
TOTAL				**50,662,701**

Table 2. Summarized source rock characteristics of the eastern Great Basin. Data tabulated by Anna et al. (2007) from Poole and Sandberg (1977), Maughan (1984), Nevada Bureau of Mines and Geology (2004), Palmer (1984), Poole and Claypool (1984), Barker and Peterson (1991), Inan and Davis (1994).

Formation	Age	TOC (%)		S_1		S_2		S_3		$S_1/(S_1+S_2)$		S_1+S_2		S_2/S_3	
		Mean	SD	Mean	SD	Mean	SD	Mean	SD	Mean	SD	Mean	SD	Mean	SD
Western Assemblage	Paleozoic	4.35	3.13												
Manning Canyon Fm	Permian	3.06	3.28							0.11		0.41	0.53		
Sheep Pass Fm	Paleogene	2.51	1.87	0.66	0.52	7.54	11.39	2.26	3.15	0.09	0.05	14.26	11.31	2.82	1.55
Phosphoria Fm	Permian	1.66													
Ochre Mtn. Ls	Mississippian	1.6								1		0.46			
Elko Fm	Oligocene	1.58	1.25	0.28	0.11	3.08	3.27	0.92	0.69	0.14	0.16			3.75	3.26
Chainman Fm	Mississippian	1.53	1.3	0.29	0.43	3.33	6.48	0.68	0.48	1.08	7.34	5.82	8.87	5.94	10.2
Joana Ls	Mississippian	1.21	1.3	0.44	0.59	2.96	3.14	0.51	0.14	0.08	0.04	0.4		6.39	6.51
Dell Phosphatic Mbr	Mississippian	1.15	1.22												
Pilot Sh	Mississippian	1.09	0.67	0.16	0.09	1.7	3.08	0.52	0.26	0.15	0.09	0.24		2.21	3.11
Mississippian	Mississippian	1.08	0.97	0.2	0.18	0.49	1.28	0.28	0.14	0.34	0.22	0.63		1.4	2.93
Webb Fm	Mississippian	1.02	1.01							0.04	0.06	2.63	4.34		
Indian Well Fm	Oligocene	0.91		0.19		4.69		1.53		0.03				3.06	
Diamond Pk Fm	Mississippian	0.83	0.51	0.19	0.31	1.01	1.99	1.32	1.21	0.06	0.05	0.14	0.03	0.65	0.89

Formation	Age	T_{max} (°C)		C_{15+} (ppm)		HC/TOC		HI		OI		Ro (%)		TAI	
		Mean	SD	Mean	SD	Mean	SD	Mean	SD	Mean	SD	Mean	SD	Mean	SD
Western Assemblage	Paleozoic	459	42			2.5		82.8	13.8	22.4	16.2	1.55	0.88		
Manning Canyon Fm	Permian	506						0.2		119					
Sheep Pass Fm	Paleogene	472	25	3294	2914	4.03		360		73.8		0.86	0.17	2.13	0.25
Phosphoria Fm	Permian														
Ochre Mtn. Ls	Mississippian					0.2		0		87.5		1.7			
Elko Fm	Oligocene	446	6	2189	1787									2	0
Chainman Fm	Mississippian	444	30	1691	3095	2	2	111	118	111	89	1.18	0.92	3.37	0.94
Joana Ls	Mississippian	440				0.97	0.8					2.8		3.35	1.2
Dell Phosphatic Mbr	Mississippian														
Pilot Sh	Mississippian	461	60	1392	93							1.37		2.6	0.22
Mississippian	Mississippian	464	25	686	868							1.6	0.88	2.79	0.34
Webb Fm	Mississippian	482	63			0.89		110	94	30	30	4.32			
Indian Well Fm	Oligocene	448													
Diamond Pk Fm	Mississippian	420	26	466	225							1.72			

Table 3. List of collected samples and geographic coordinates.

Sample number		Formation	Location	Latitude	Longitude
1	**10SH1**	Ely Limestone	Shingle Pass	38 33 37.7	114 58 34.3
2	**10SH2**				
3	**10SH3**				
4	**10SH4**				
5	**10SH5**				
6	**10SH6**				
7	**10SH7**	Pogonip Group		38 30 53.4	114 57 29.5
8	**10SH8**				
9	**10SH9**			38 30 48.6	114 56 56.3
10	**10SH10**			38 30 54.2	114 56 47.4
11	**10SH11**				
12	**10FM12**	Guilmette Formation	Fox Mtn	38 12 37.2	115 04 20.9
13	**10FM13**				
14	**10FM14**				
15	**10FM15**				
16	**10FM16**				
17	**10FM17**				
18	**10FM18**				
19	**10FM19**				
20	**10FM20**				
21	**10FM22**				
22	**10FM23**	Pilot Shale		38 12 42.5	115 04 52.5
23	**10FM24**				
24	**10FM25**				
25	**10FM26**	Joana Ls			
26	**10FM27**				
27	**10NC28**	Newark Canyon Fm	N of Moody Peak	39 04 16.3	115 59 49.3
28	**10NC29**				
29	**10NC30**				
30	**10NC31**				
31	**10CW36**	Woodruff Formation	Fish Creek Range	39 04 13.4	116 09 18.8
32	**10CW37**				
33	**10CW38**			39 04 13.4	116 09 18.8
34	**10CW39**				
35	**10CW40**			39 04 58.3	116 08 55.9
36	**10CW41**				
37	**10VI43**	Vinini Fm	Horse Heaven	39 09 46.1	116 28 26.1
38	**10PO45**	Pogonip Group	Clear Creek	38 49 08.8	116 30 47.5
39	**10MD46**		Tulle Creek	38 51 50.7	116 31 26.8
40	**10MD47**		Monitor Range	38 51 46.8	116 31 08.8

41	**10HC49**	Eleana Formation	North of Hwy 6	38 13 21.4	116 22 53.5
42	**10HC50**				
43	**10HC51**				
44	**10HC52**				
45	**10HC53**				
46	**10HC54**				
47	**10HC55**				
48	**10HC56**				
49	**10HC57**				
50	**10HC58**				
51	**10SL72**	Slaven Chert	Toquima Range	38 56 16.1	116 46 29.5
52	**10SL73**			38 56 16.2	116 46 29.9
53	**10SL74**			38 56 22.5	116 47 45.7
54	**10SL75**			38 57 10.0	116 48 03.9
55	**10SL76**				
56	**10SL77**			38 56 28.3	116 46 51.5
57	**10SL78**			38 56 16.1	116 46 30.4
58	**10CW79**	Woodruff Formation	Fish Creek Range	39 04 09.3	116 09 19.0
59	**10CW80**				
60	**10CW81**		Gibellini Hill	39 12 25.2	116 05 43.4
61	**10CW82**				
62	**10CW83**				
63	**10CW84**			39 12 21.1	116 05 41.3
64	**10CW85**				
65	**10CW86**				
66	**10CW87**			39 12 20.6	116 05 39.4
67	**10CW88**				
68	**10CW89**				
69	**10CW91**		LouieHill	39 11 45	116 05 55.7
70	**10CW92**			39 11 42.1	116 05 44.9
71	**10CW93**		Gibellini Hill	39 12 37.0	116 05 46.1
72	**10CW94**			39 12 28.4	116 05 40.6
73	**10CW95**				
74	**10CW96**			39 12 15.8	116 05 33.0
75	**10CW97**		LouieHill	39 11 35.9	116 05 47.5
76	**11MC1**	Vinini Formation	Toquima Range	38 59 59.5	116 46 45.4
77	**11MC2**				
78	**11MC3**				
79	**11MC4**				
80	**11MC5**				
81	**11MC6**				
82	**11MC7**				
83	**11MC8**				
84	**11MC9**				
85	**11MC10**				
86	**11MC11**				
87	**11MC12**				

89	**11MC13**	Vinini Formation	Toquima Range		
88	**11TC14**			39 09 59.8	116 45 39.2
90	**11TC15**			39 13 25.6	116 48 32.8
91	**11TC16**			39 12 20.2	116 48 15.5
92	**11TC17**			39 11 31.9	116 47 43.9
93	**11TC18**			39 11 16.8	116 47 41.1
94	**11TC19**			39 10 59.0	116 47 27.9
95	**11TC20**			39 10 24.4	116 46 20.1

Table 4. Total organic carbon, Rock-Eval pyrolysis, vitrinite reflectance, and thermal alteration index results for source rock samples.

Sample number	Formation	Location	TOC (%)	S_1	S_2	S_3	T_{max} (°C)	HI	OI	S_2/S_3	S_1/TOC *100	PI	R_o %	TAI	Spore Color
10SH1	Ely Limestone	Shingle Pass	0.10	0.02	0.15	0.29	438	156	302	1	21	0.12			
10SH2			0.12	0.02	0.13	0.27	435	107	221	0	16	0.13			
10SH3			0.03	0.01	0.09	0.22	445	290	710	0	32	0.10			
10SH4			0.05	0.01	0.08	0.47	449	151	887	0	19	0.11			
10SH5			0.35	0.02	0.38	0.66	438	108	188	1	6	0.05			
10SH6			0.38	0.03	0.30	0.42	442	80	112	1	8	0.09			
10SH7	Pogonip Group	Shingle Pass	0.03	0.01	0.07	0.28	342	233	933	0	33	0.13			
10SH8			0.04	0.01	0.06	0.23	448	136	523	0	23	0.14			
10SH9			0.14	0.01	0.08	0.46	483	56	324	0	7	0.11			
10SH10			0.77	0.04	0.16	0.28	523	21	36	1	5	0.20			
10SH11			0.10	0.01	0.07	0.28	457	69	275	0	10	0.13		3 to 3+	RB
10FM12	Guilmette Formation	Fox Mtn	0.03	0.02	0.08	0.12	431	242	364	1	61	0.20			
10FM13			0.06	0.01	0.08	0.22	450	133	367	0	17	0.11	1.14		
10FM14			0.05	0.01	0.09	0.27	465	180	540	0	20	0.10			
10FM15			0.05	0.01	0.06	0.38	449	111	704	0	19	0.14			
10FM16			0.06	0.02	0.11	0.42	446	186	712	0	34	0.15			
10FM17			0.06	0.02	0.11	0.23	432	177	371	0	32	0.15			
10FM18			0.07	0.01	0.08	0.31	433	111	431	0	14	0.11			
10FM19			0.06	0.02	0.16	0.46	447	258	742	0	32	0.11			
10FM20			0.05	0.02	0.08	0.37	437	178	822	0	44	0.20			
10FM22			0.03	0.01	0.07	0.24	464	219	750	0	31	0.13	1.36		
10FM23	Pilot Shale		0.08	0.03	0.08	0.37	467	104	481	0	39	0.27			
10FM24			0.42	0.04	0.32	0.35	450	76	83	1	10	0.11			
10FM25			0.06	0.01	0.08	0.47	494	131	770	0	16	0.11	1.24		
10FM26	Joana Ls		0.03	0.01	0.06	0.14	443	194	452	0	32	0.14			
10FM27			0.01	0.01	0.04	0.10	445	364	909	0	91	0.20			

10NC28	Newark Canyon Fm	N of Moody Peak	0.07	0.02	0.13	0.23	440	183	324	1	28	0.13			
10NC29			0.27	0.04	0.70	0.90	443	263	338	1	15	0.05			
10NC30			0.08	0.02	0.12	0.31	433	145	373	0	24	0.14			
10NC31			0.10	0.06	0.36	0.48	435	346	462	1	58	0.14			
10CW36	Woodruff Formation	Fish Creek Range	1.80	0.05	1.94	1.29	430	108	72	2	3	0.03	0.85		
10CW37			2.31	0.07	2.93	1.64	425	127	71	2	3	0.02			
10CW38			2.86	0.09	2.93	2.31	425	102	81	1	3	0.03			
10CW39			1.73	0.03	1.24	1.42	428	72	82	1	2	0.02	0.97		
10CW40			0.07	0.02	0.08	0.63	403	110	863	0	27	0.20			
10CW41			0.04	0.02	0.11	0.77	378	282	1974	0	51	0.15			
10VI43	Vinini Fm	Horse Heaven	1.45	0.02	0.15	0.66	493	10	45	0	1	0.12		4+ to 5	DB
10PO45	Pogonip Group	Clear Creek	0.40	0.01	0.07	0.33	453	18	83	0	3	0.13		5	DGB
10MD46		Tulle Creek	0.29	0.02	0.10	0.34	437	35	118	0	7	0.17	1.32		
10MD47		Monitor Range	0.46	0.04	0.23	0.60	442	50	131	0	9	0.15	1.30		
10HC49	Eleana Formation	North of Hwy 6	0.10	0.02	0.08	0.40	448	82	408	0	20	0.20			
10HC50			0.67	0.02	0.10	0.46	567	15	68	0	3	0.17	0.95		
10HC51			0.70	0.01	0.07	0.37	532	10	53	0	1	0.13			
10HC52			0.98	0.01	0.08	0.65	577	8	66	0	1	0.11			
10HC53			0.89	0.01	0.07	0.56	525	8	63	0	1	0.13			
10HC54			1.14	0.02	0.11	0.71	529	10	63	0	2	0.15			
10HC55			0.84	0.02	0.07	0.69	515	8	82	0	2	0.22			
10HC56			0.48	0.02	0.06	0.52	456	12	108	0	4	0.25			
10HC57			0.38	0.01	0.08	0.35	389	21	92	0	3	0.11			
10HC58			0.49	0.02	0.09	0.60	344	18	123	0	4	0.18	1.00		
10SL72	Slaven Chert	Toquima Range	0.32	0.02	0.06	0.34	368	19	108	0	6	0.25			
10SL73			1.01	0.01	0.04	0.46	546	4	46	0	1	0.20	1.35		
10SL74			1.48	0.01	0.03	0.75	349	2	51	0	1	0.25			
10SL75			0.21	0.01	0.04	0.30	437	19	144	0	5	0.20			
10SL76			0.13	0.01	0.05	0.22	467	38	169	0	8	0.17			

10SL77	Slaven Chert	Toquima Range	0.12	0.01	0.06	0.32	456	48	258	0	8	0.14			
10SL78			0.04	0.01	0.05	0.40	380	119	952	0	24	0.17	1.79		
10CW79	Woodruff Formation	Fish Creek Range	1.31	0.08	5.47	0.69	424	417	53	7.9	6	0.01	0.76		
10CW80			0.67	0.10	2.55	0.92	427	379	137	2.8	15	0.04	0.81		
10CW81		Gibellini Hill	0.02	0.01	0.01	0.50	-1	53	2632	0.0	54	0.50	0.84		
10CW82			0.01	0.01	0.01	0.60	-1	100	6000	0.0	100	0.50	0.00		
10CW83			0.01	0.01	0.01	0.14	-1	100	1400	0.1	98	0.49	0.89		
10CW84			0.38	0.02	0.06	0.26	308	16	69	0.2	5	0.25	0.96		
10CW85			0.83	0.03	0.15	0.78	424	18	94	0.2	4	0.17	0.88		
10CW86			0.42	0.02	0.05	0.22	363	12	53	0.2	5	0.29	0.97		
10CW87			0.89	0.05	0.32	0.56	416	36	63	0.6	6	0.14	0.94		
10CW88			1.37	0.04	0.05	0.85	345	4	62	0.1	3	0.45	0.83		
10CW89			0.78	0.04	0.04	1.17	-1	5	150	0.0	5	0.49	0.86		
10CW91		Louie Hill	0.09	0.01	0.01	0.37	-1	11	394	0.0	11	0.50	0.68		
10CW92			0.25	0.01	0.01	0.57	-1	4	230	0.0	4	0.50	0.78		
10CW93		Gibellini Hill	4.13	1.45	27.53	0.77	420	667	19	35.8	35	0.05	0.77		
10CW94			6.50	1.66	41.34	0.74	417	636	11	55.9	26	0.04	0.98		
10CW95			6.42	2.31	44.82	0.61	424	698	9	73.5	36	0.05	1.02		
10CW96			1.11	0.48	2.40	0.54	421	217	49	4.4	43	0.17	0.99		
10CW97		Louie Hill	3.97	1.13	29.30	0.72	415	739	18	40.7	28	0.04	0.92		
11MC1	Vinini Formation	Toquima Range	0.38	0.00	0.01	0.72	-1	3	188	0.0					
11MC2			0.96	0.01	0.01	0.57	-1	1	59	0.0	1	0.51			
11MC3			1.50	0.00	0.01	0.59	-1	1	39	0.0					
11MC4			1.14	0.01	0.01	0.78	-1	1	68	0.0	1	0.50			
11MC5			1.99	0.00	0.01	1.07	-1	1	54	0.0					
11MC6			1.81	0.01	0.01	1.29	-1	1	71	0.0	1	0.51			
11MC7			1.24	0.01	0.01	0.73	321	1	59	0.0	1	0.51			
11MC8			0.67	0.00	0.01	0.54	-1	1	80	0.0					
11MC9			0.58	0.00	0.01	0.41	-1	2	70	0.0					
11MC10			0.39	0.00	0.01	0.40	-1	3	104	0.0					
11MC11			0.57	0.00	0.01	0.07	-1	2	12	0.1					

11MC12	Vinini Formation	Toquima Range	0.87	0.00	0.01	0.61	-1	1	71	0.0					
11MC13			0.01	0.00	0.01	0.11	-1	100	1100	0.1					
11TC14			0.46	0.00	0.01	0.29	-1	2	63	0.0					
11TC15			0.24	0.00	0.01	0.26	-1	4	107	0.0					
11TC16			0.19	0.00	0.01	0.00	-1	5							
11TC17			0.38	0.03	0.01	0.39	-1	3	102	0.0	7	0.74			
11TC18			0.32	0.00	0.01	0.35	-1	3	110	0.0					
11TC19			0.08	0.01	0.01	0.15	-1	12	183	0.1	13	0.51			
11TC20			0.21	0.02	0.01	0.20	-1	5	96	0.0	9	0.66			

"-1" – not measured or invalid value for T_{max}

S_1 - volatile hydrocarbon (HC) content, mg HC/ g rock

S_2 - remaining HC generative potential, mg HC/ g rock

S_3 - carbon dioxide content, mg CO_2 / g rock

TOC - total organic carbon, wt. %

Ro - vitrinite reflectance, %

DB - dark brown

HI - Hydrogen index = S_2 * 100 / TOC, mg HC/ g TOC

OI - Oxygen Index = S_3 * 100 / TOC, mg CO_2/ g TOC

PI - Production Index = S_1 / (S_1+S_2)

TAI - thermal alteration index

RB - red-brown

DGB - dark grey-brown

Table 5. Geochemical parameters describing petroleum potential (quantity), kerogen type (quality), character of expelled products and level of thermal maturation of a source rock (from Peters and Cassa, 1994).

Petroleum Potential	TOC (wt. %)	S_1 (mg HC/g rock)	S_2 (mg HC/g rock)
Poor	0 - 0.5	0 - 0.5	0 - 2.5
Fair	0.5 - 1	0.5 - 1	2.5 - 5
Good	1 - 2	1 - 2	5 - 10
Very Good	2 - 4	2 - 4	10 - 20
Excellent	> 4	> 4	> 20
Kerogen Type	HI (mg HC/g TOC)	S_2/S_3	Product
I	> 600	> 15	Oil
II	300 - 600	10 - 15	Oil
II/III	200 - 300	5 - 10	Mixed oil and gas
III	50 - 200	1 - 5	Gas
IV	> 50	< 1	None

Maturity	R_o (%)	T_{max} (^oC)	TAI	PI
Immature	0.2 - 0.6	< 435	1.5 - 2.6	< 0.10
Mature				
Early	0.6 - 0.65	435 - 445	2.6 - 2.7	0.10 - 0.15
Peak	0.65 - 0.9	445 - 450	2.7 - 2.9	0.25 - 0.40
Late	0.9 - 1.35	450 - 470	2.9 - 3.3	> 0.40
Postmature	> 1.35	> 470	> 3.3	-

Table 6. TOC, Rock Eval pyrolysis and vitrinite reflectance for source rock samples with S_2 peak more than 0.2 mg HC/g rock.

Sample Number		Formation	TOC	S_1	S_2	S_3	T_{max}	HI	OI	S_2/S_3	PI	R_o
1	10SH5	Ely Ls	0.35	0.02	0.38	0.66	438	108	188	6	0.05	
2	10SH6		0.38	0.03	0.30	0.42	442	80	112	8	0.09	
3	10FM24	Pilot Sh	0.42	0.04	0.32	0.35	450	76	83	10	0.11	
4	10NC29	Newark Canyon Fm	0.27	0.04	0.70	0.90	443	263	338	15	0.05	
5	10NC31		0.10	0.06	0.36	0.48	435	346	462	58	0.14	
6	10CW36	Woodruff Fm	1.80	0.05	1.94	1.29	430	108	72	3	0.03	0.85
7	10CW37		2.31	0.07	2.93	1.64	425	127	71	3	0.02	
8	10CW38		2.86	0.09	2.93	2.31	425	102	81	3	0.03	
9	10CW39		1.73	0.03	1.24	1.42	428	72	82	2	0.02	0.97
10	10CW79		1.31	0.08	5.47	0.69	424	417	53	6	0.01	0.76
11	10CW80		0.67	0.10	2.55	0.92	427	379	137	15	0.04	0.81
12	10CW87		0.89	0.05	0.32	0.56	416	36	63	6	0.14	0.94
13	10CW93		4.13	1.45	27.53	0.77	420	667	19	35	0.05	0.77
14	10CW94		6.50	1.66	41.34	0.74	417	636	11	26	0.04	0.98
15	10CW95		6.42	2.31	44.82	0.61	424	698	9	36	0.05	1.02
16	10CW96		1.11	0.48	2.40	0.54	421	217	49	43	0.17	0.99
17	10CW97		3.97	1.13	29.30	0.72	415	739	18	28	0.04	0.92
18	10MD47	Pogonip Gr	0.46	0.04	0.23	0.60	442	50	131	9	0.15	1.30

Table 7. Geochemical parameters describing OM quantity, quality and thermal maturity of 10CW79 and 10CW95 samples of the Woodruff Formation.

Woodruff Formation 10CW79

Petroleum Potential	TOC (wt. %)	S_1 (mg HC/g rock)	S_2 (mg HC/g rock)
Poor	0 - 0.5	0 - 0.5 (0.08)	0 - 2.5
Fair	0.5 - 1	0.5 - 1	2.5 - 5
Good	1 - 2 (1.31)	1 - 2	5 - 10 (5.47)
Very Good	2 - 4	2 - 4	10 - 20
Excellent	> 4	> 4	> 20
Kerogen Type	HI (mg HC/g TOC)	S_2/S_3	Product
I	> 600	> 15	Oil
II	300 - 600 (417)	10 - 15	Oil
II/III	200 - 300	5 - 10 (7.9)	Mixed oil and gas
III	50 - 200	1 - 5	Gas
IV	> 50	< 1	None
Maturity	R_o (%)	T_{max} (^oC)	PI
Immature	0.2 - 0.6	< 435 (424)	< 0.10 (0.01)
Mature			
Early	0.6 - 0.65	435 - 445	0.10 - 0.15
Peak	0.65 - 0.9 (0.76)	445 - 450	0.25 - 0.40
Late	0.9 - 1.35	450 - 470	> 0.40
Postmature	> 1.35	> 470	-

Woodruff Formation 10CW95

Petroleum Potential	TOC (wt. %)	S_1 (mg HC/g rock)	S_2 (mg HC/g rock)
Poor	0 - 0.5	0 - 0.5	0 - 2.5
Fair	0.5 - 1	0.5 - 1	2.5 - 5
Good	1 - 2	1 - 2	5 - 10
Very Good	2 - 4	2 - 4 (2.31)	10 - 20
Excellent	> 4 (6.42)	> 4	> 20 (44.82)
Kerogen Type	HI (mg HC/g TOC)	S_2/S_3	Product
I	> 600 (698)	> 15 (73.5)	Oil
II	300 - 600	10 - 15	Oil
II/III	200 - 300	5 - 10	Mixed oil and gas
III	50 - 200	1 - 5	Gas
IV	> 50	< 1	None
Maturity	R_o (%)	T_{max} (^oC)	PI
Immature	0.2 - 0.6	< 435 (424)	< 0.10 (0.05)
Mature			
Early	0.6 - 0.65	435 - 445	0.10 - 0.15
Peak	0.65 - 0.9	445 - 450	0.25 - 0.40
Late	0.9 - 1.35 (1.02)	450 - 470	> 0.40
Postmature	> 1.35	> 470	-

Table 8. Measured peak heights (in centimeters) and calculated ratios on GC.

Identification	10CW79	10CW95	10CW79p	10CW95p
n-C_{11}			0	0
n-C_{12}			0	3.9
n-C_{13}			4.3	7.1
n-C_{14}			7.8	8.7
n-C_{15}			9.5	9.4
n-C_{16}			9.35	8.1
Pr	1	2.4	3.1	7.5
Ph	1.2	3.3	1.9	3.5
n-C_{17}			9.2	8
n-C_{18}			8.85	7.2
n-C_{19}			8.5	7
n-C_{20}			8.4	6.5
n-C_{21}			7.4	5.6
n-C_{22}			6.4	4.5
n-C_{23}			5.75	3.9
n-C_{24}			4.9	2.9
n-C_{25}			4	2.6
n-C_{26}			3.8	2.3
n-C_{27}			3.3	1.8
n-C_{28}			3.05	1.6
n-C_{29}			2.55	1.4
n-C_{30}			2	0.95
n-C_{31}			1.7	0.85
n-C_{32}			1.45	0.65
n-C_{33}			1	0.55
n-C_{34}			0.9	0.45
Carotanes	No	No	No	No
Botryococcane	No	No	No	No
Biodegraded	Yes	Yes	No	No
Calculated Ratio	**10CW79**	**10CW95**	**10CW79p**	**10CW95p**
Pr/Ph	0.83	0.73	1.63	2.14
Pr/(Pr+Ph)	0.45	0.42	0.62	0.68
Ph/*n*-C_{18}			0.21	0.49
Pr/*n*-C_{17}			0.34	0.94
OEP 1			1.02	1.07
OEP 2			0.96	0.95
OEP 3			1.00	1.10
TAR			0.28	0.17
CPI			0.97	1.03
CPI(1)			0.98	1.02

Table 9. Measured peak heights and calculated ratios on GC-MSD *m/z* 191.

Peak #	Identification	10CW79	10CW95	10CW79p	10CW95p	10CW96	10CW97
2	C_{19} Tricyclic (Cheilanthane)	0,6	0,2	1,5	0,9	0	0
3	C_{20} Tricyclic (Cheilanthane)	3,8	1,2	4,95	4,2	0	0
38	C_{21} Tricyclic (Cheilanthane)	6,75	1,9	7,2	5,9	0	0
39	C_{22} Tricyclic (Cheilanthane)	2	0,6	1,4	1,1	0	0
40	C_{23} Tricyclic (Cheilanthane)	11,7	3,85	13,25	10,1	2,6	2,3
41	C_{24} Tricyclic (Cheilanthane)	8,3	2,5	8,6	7,3	1,7	1,25
42	C_{25} Tricyclic (Cheilanthane) (22S + 22R)	5,75	2,1	5,6	5	0,9	1
4	C_{24} Tetracyclic	6,55	1,15	3,65	1,7	0,95	0,9
43	C_{26} Tricyclic (Cheilanthane) (22S + 22R)	8,15	1,85	4,5	4,5	1,6	1,7
5	C_{25} Tricyclic (Cheilanthane)	1,4	0,15	0,45	0,3	0	0
44	C_{27} Tricyclic (Cheilanthane) (22R + 22S)	1,8	0,4	0,9	0,8	0	0
10	C_{26} Tetracyclic	0,9	0,15	0,5	0,55	0	0
6	C_{28} Tricyclic (Cheilanthane)	2,8	0,9	2,3	2,3	0,7	0,7
7	C_{28} Tricyclic (Cheilanthane)	1	0,8	2,15	2,2	0,6	0,4
8	C_{29} Tricyclic (Cheilanthane)	3	0,9	2,25	1,95	0,6	1,4
9	C_{29} Tricyclic (Cheilanthane)	2,2	0,9	2,25	1,9	0,9	0,9
13	22,29,30-Trisnorneohopane (Ts)	3,6	1,2	0,9	0,7	1,1	0,6
14	22,29,30-Trisnorhopane (Tm)	3,6	3,45	6,65	4,4	2	1,3
11	C_{30} Tricyclic (Cheilanthane)	2,9	0,8	1,4	1,5	0,5	0,95
12	C_{30} Tricyclic (Cheilanthane)	4	1,5	1,3	1,9	1,4	1,1
17	C_{31} Tricyclic (Cheilanthane)	2,5	1,15	0,95	1,1	9,9	1
18	17α,21β(H)-30-Norhopane	6,4	9,8	11,9	10,5	4	5,2
16	18α(H)-30-Norneohopane (C_{29}Ts)	2	1,5	0,5	0,7	1	1,05
36	C_{29} 17β,21α(H)-30-Norhopane	2	1,95	1,5	1,95	1,8	1,4
20	17α,21β(H)-Hopane	6,4	11,85	11	11,9	9,5	6,25
21	17β,21α(H)-Hopane (Moretane)	1,5	1,65	1,4	3,2	2,1	0,9
22	17α,21β(H)-29-Homohopane 22S	3,2	4,3	3,3	3,3	1,95	3,1
23	17α,21β(H)-29-Homohopane 22R	2,4	4,4	2,45	2,8	3,2	2,85
31	Gammacerane	5,1	2,75	1,15	1,2	5,8	1,75
25	17α,21β(H)-29-Bishomohopane 22S	2,4	2,2	2,1	1,5	1	2,4
26	17α,21β(H)-29-Bishomohopane 22R	1,6	1,95	1,6	1,3	1,3	1,9
29	17α,21β(H)-29-Trishomohopane 22S	2,6	1,8	1,7	1	1	2,1
30	17α,21β(H)-29-Trishomohopane 22R	1,5	1,45	1,2	0,8	1,4	1,6
32	17α,21β(H)-29-Tetrakishomohopane 22S	1,2	0,8	0,75	0,45	0,3	1,1
33	17α,21β(H)-29-Tetrakishomohopane 22R	0,7	0,7	0,5	0,35	0,5	0,8
34	17α,21β(H)-29-Pentakishomohopane 22S	2,3	0,8	0,7	0,2	0,35	1,5
35	17α,21β(H)-29-Pentakishomohopane 22R	1,1	0,6	0,45	0,2	0,5	0,9

Calculated Ratios	10CW79	10CW95	10CW79p	10CW95p	10CW96	10CW97
C_{22} tricyclic/ C_{21} tricyclic	0,30	0,32	0,18	0,19		
C_{24} tricyclic/ C_{23} tricyclic	0,71	0,65	0,65	0,72	0,54	0,65
C_{26} tricyclic/ C_{25} tricyclic	0,85	0,88	0,80	0,90	0,97	0,89
C_{29} tricyclic/ C_{30} tricyclic	0,96	1,06	1,67	1,33	1,27	0,79
C_{23} tricyclic / (C_{23} + C_{29}) tricyclic	0,69	0,68	0,75	0,72	0,47	0,63
C_{23} tricyclic /(C_{23} tricyclic +C_{30} hopane)	0,65	0,25	0,55	0,46	0,26	0,21
C_{24} tetracyclic / (C_{24} tetra + C_{26}tricyclic)	0,45	0,38	0,45	0,27	0,35	0,37
C_{26} tricyclic / C_{24} tetracyclic	1,21	1,61	1,23	2,65	1,89	1,68
C_{24} tetra / (C_{24} tetracyclic + C_{30} hopane)	0,51	0,09	0,25	0,13	0,12	0,09
C_{25} / C_{24} tricyclic	1,30	0,90	0,70	0,73	1,40	1,06
C_{25} / C_{26} tricyclic	1,35	1,22	1,34	1,18	1,03	1,13
(C_{28}+C_{29}) tricyclic/(C_{28}+C_{29})+ hopane	0,58	0,22	0,45	0,41	0,37	0,23
C_{29} hopane / (C_{29} hopane + C_{30} hopane)	0,50	0,45	0,52	0,46	0,45	0,30
C_{29}/ C_{30} Hopane	1,00	0,83	1,08	0,84	0,81	0,42
C_{29} Ts / (C_{29}Ts + C_{29} Hopane)	0,24	0,13	0,04	0,07	0,17	0,20
Ts/(Ts+Tm)	0,50	0,26	0,12	0,14	0,32	0,35
Gammacerane / C_{31} 22S	1,59	0,64	0,35	0,36	0,56	2,97
C_{31} 22R / C_{30} hopane	0,38	0,37	0,22	0,24	0,45	0,34
C_{31} 22S / (C_{31} 22S + 22R) hopane	0,57	0,49	0,57	0,54	0,52	0,38
C_{32} 22S / (C_{32} 22S+22R) hopane	0,60	0,53	0,57	0,54	0,56	0,43
C_{33} 22S / (C_{33} 22S + 22R) hopane	0,63	0,55	0,59	0,56	0,57	0,42
C_{34} 22S / (C_{34} 22S + 22R) hopane	0,63	0,53	0,60	0,56	0,58	0,38
C_{35} 22S / C_{34} 22S hopane	1,92	1,00	0,93	0,44	1,36	1,17
C_{35} 22S / C_{34} 22S + C_{35} 22S	0,66	0,50	0,48	0,31	0,58	0,54
% C_{31} Homohopane	29,47	45,79	38,98	51,26	32,60	44,78
% C_{32} Homohopane	21,05	21,84	25,08	23,53	23,56	20,00
% C_{33} Homohopane	21,58	17,11	19,66	15,13	20,27	20,87
% C_{34} Homohopane	10,00	7,89	8,47	6,72	10,41	6,96
% C_{35} Homohopane	17,89	7,37	7,80	3,36	13,15	7,39
Tricyclics/17α-hopanes	0,34	0,09	0,26	0,26	0,15	0,12
Moretane / Hopane	0,23	0,14	0,13	0,27	0,14	0,22
Homohopane index	0,18	0,07	0,08	0,03	0,13	0,07
Gammacerane Index	0,44	0,19	0,09	0,09	0,21	0,38
Diahopane / (Diahopane + C_{30} Hopane)	0,24	0,14	0,12	0,14	0,18	0,16
Diahopane / (Diahopane + C_{29} Hopane)	0,24	0,17	0,11	0,16	0,21	0,31
Diahopane / (Diahopane + C_{29}Ts)	0,50	0,57	0,75	0,74	0,57	0,64

Table 10. Measured peak heights and calculated ratios on GC-MRM.

Peak #	Identification	Carbon #	10CW79	10CW95	10CW79p	10CW95p
6	5α,14α,17α(H)-Cholestane 20S	27	1,6	1,5	2	1,05
7	5α,14β,17β(H)-Cholestane 20R		1,15	0,7	1,9	0,3
8	5α,14β,17β(H)-Cholestane 20S		1,2	0,7	2,05	0,4
9	5α,14α,17α(H)-Cholestane 20R		1,05	2,15	1,6	2,2
21	13β,17α(H)-Diacholestane 20S		1,8	1,8	0,7	1
22	13β,17α(H)-Diacholestane 20R		2,3	0,95	0,8	0,9
23	13α,17β(H)-Diacholestane 20S		1	0,35	0,3	0,3
24	13α,17β(H)-Diacholestane 20R		1,5	0,5	1,85	0,9
10	5α,14α,17α(H)-Ergostane 20S	28	1,7	0,95	1,8	1,6
11	5α,14β,17β(H)-Ergostane 20R		1,05	1,6	1,7	2,1
12	5α,14β,17β(H)-Ergostane 20S		2	0,65	2	1,6
13	5α,14α,17α(H)-Ergostane 20R		0,9	4	2	2,2
25	13β,17α(H)-Diaergostane 20S (24S + 24R)		1,85	1,1	0,55	1,3
26	13β,17α(H)-Diaergostane 20R (24S + 24R)		1	0,85	0,95	1,7
14	5α,14α,17α(H)-Stigmastane 20S	29	2,4	1,3	2,1	1,45
15	5α,14β,17β(H)-Stigmastane 20R		1,2	0,85	1,8	0,6
16	5α,14β,17β(H)-Stigmastane 20S		1,1	1,3	1,65	1,5
17	5α,14α,17α(H)-Stigmastane 20R		0,85	2,1	1,2	2,4
27	13β,17α(H)-Diastigmastane 20S		2,6	0,9	0,7	1
28	13β,17α(H)-Diastigmastane 20R		2,4	0,8	1,1	1
18	5α,14α,17α(H)-24-*n*-Propylcholestane 20S	30	1,55	0,4	2	0,7
19	5α,14β,17β(H)-24-*n*Propylcholestane20R+20S		2	0,8	3,5	1,1
20	5α,14α,17α(H)-24-*n*-Propylcholestane 20R		1,7	2,2	2,1	2,25
29	13β,17α(H)-Dia-24-*n*-propylcholestane 20S		1,9	0,5	0,9	0,8
30	13β,17α(H)-Dia-24-*n*-propylcholestane 20R		1	0,2	1	1

Calculated Ratios				
C_{27} 20S (C_{27} ααα 20S + C_{27} αββ 20S)	2,80	2,20	4,05	1,45
C_{27} 20R (C_{27} ααα 20R + C_{27} αββ 20R)	2,20	2,85	3,50	2,50
C_{27} (20S + 20R)	5,00	5,05	7,55	3,95
C_{28} 20S (C_{28} ααα 20S + C_{28} αββ 20S)	3,70	1,60	3,80	3,20
C_{28} 20R (C_{28} ααα 20R + C_{28} αββ 20R)	1,95	5,60	3,70	4,30
C_{28} (20S + 20R)	5,65	7,20	7,50	7,50
C_{29} 20S (C_{29} ααα 20S + C_{29} αββ 20S)	3,50	2,60	3,75	2,95
C_{29} 20R (C_{29} ααα 20R + C_{29} αββ 20R)	2,05	2,95	3,00	3,00
C_{29} (20S + 20R)	5,55	5,55	6,75	5,95
C_{27} + C_{28} + C_{29} Steranes	16,20	17,80	21,80	17,40
C_{27} + C_{28} + C_{29} Diasteranes	14,45	7,25	6,95	8,10
Diasterane/sterane	1,32	0,71	0,48	0,78
C_{27} diasterane/(Dia+Reg) sterane	0,57	0,42	0,33	0,44
Sterane % C_{27} (Total C_{27}/Total C_{27}+C_{28}+C_{29})*100	30,86	28,37	34,63	22,70
Sterane % C_{28} (Total C_{28}/Total C_{27}+C_{28}+C_{29})*100	34,88	40,45	34,40	43,10
Sterane % C_{29} (Total C_{29}/Total C_{27}+C_{28}+C_{29})*100	34,26	31,18	30,96	34,20
Diasterane % C_{27} (Total C_{27}/Total C_{27}+C_{28}+C_{29})*100	45,67	49,66	52,52	38,27
Diasterane % C_{28} (Total C_{28}/Total C_{27}+C_{28}+C_{29})*100	19,72	26,90	21,58	37,04
Diasterane % C_{29} (Total C_{29}/Total C_{27}+C_{28}+C_{29})*100	34,60	23,45	25,90	24,69
C_{29} 20S / (20S+20R)	0,63	0,47	0,56	0,50
C_{29} αββ/(αββ+ααα)	0,41	0,39	0,51	0,35
C_{28}/C_{29}	1,02	1,30	1,11	1,26
C_{30} / (C_{27} - C_{30}) Steranes	0,24	0,16	0,26	0,19

Table 11. Measured peak heights and calculated ratios on GC-MSD *m/z* 253.

Peak #	Identification	Carbon #	10CW79	10CW95	10CW79p	10CW95p
1	Pregnane	21	3,5	1,15	3,1	3,3
2	20-Methylpregnane	22	6,7	1,3	5,15	4,9
3	20-Ethylpregnane	23	11,4	1,2	4,25	3
1	Pregnane	21	3,5	1,15	3,1	3,3
4	5β-Cholestane 20S	27	2,7	3,35	1,4	2
5	Diacholestane		1,25	1,15	0,7	0,95
6	5β-Cholestane 20R; diacholestane 20R		1,75	3,25	1	2
7	5α-Cholestane 20S		0,9	2,2	0,9	2
9	5α-Cholestane 20R		1,1	2,8	0,7	1,2
8	5β-Ergostane 20S; diaergostane 20S	28	3,4	2,95	0,95	1,35
14	5α-Ergostane 20R		3,5	2	0,6	1,15
10	5α-Ergostane 20S		1,35	2,3	0,8	1,3
11	5β-Ergostane 20R; diaergostane 20R		2,9	3,5	0,75	1,2
12	5β-Stigmastane 20S; diastigmastane 20S	29	11,2	12,4	2,2	4,7
13	5α-Stigmastane 20S		2,25	5	1	2,8
15	5β-Stigmastane 20R; diastigmastane 20R		3,7	7,15	0,95	2,4
16	5α-Stigmastane 20R		2,45	4,2	0,6	1,95
Calculated Ratios						
% 27s			20,03	24,40	37,45	32,60
% 28s			29,00	20,57	24,70	20,00
% 29s			50,98	55,02	37,85	47,40
MA (I) (Sum of C21 to C22)			10,20	2,45	8,25	8,20
MA (II) (Sum of C27 to C29)			38,45	52,25	12,55	25,00
MA (I) / ((MA (I) + MA (II))			0,21	0,04	0,40	0,25

Table 12. Measured peak heights and calculated ratios on GC-MSD *m/z* 231.

Peak #	Identification	Carbon #	10CW79	10CW95	10CW79p	10CW95p
1	Pregnane	20	0,7	0,8	3,2	1,3
2	20-Methylpregnane	21	1,2	1,1	1,55	0,9
3	20-Ethylpregnane	22	3,2	1	1,5	1,2
4	Cholestane 20S	26	2,6	3,7	1,6	3,95
5	Cholestane 20R; ergostane 20S	26, 27	3,9	8,25	1	1,8
6	Stigmastane 20S	28	4,9	11,8	4,75	4,1
7	Ergostane 20R	27	5,8	3,2	3,5	5
8	Stigmastane 20R	28	6,95	12,1	2,5	1,8
9	24-*n*-Propylcholestane 20S	29	2,3	0,4	1	1,7
10	24-*n*-Propylcholestane 20R	29	2,1	0	2,5	2,8
11	20-*n*-Decylpregnane 20S	30	0	0	2	2,45
12	20-*n*-Decylpregnane 20R	30	0	0	2,6	3,35
Calculated Ratios						
C28 (20S+20R) Triaromatic			11,85	23,9	7,25	5,9
C26 / C28S Triaromatic steroid			0,53	0,31	0,34	0,96
C27 / C28S Triaromatic steroid			1,18	0,27	0,74	1,22
TA (I) (Sum of C20 to C21)			1,90	1,90	4,75	2,20
TA (II) (Sum of C26 to C28)			29,05	50,85	18,10	20,75
TA (I) / ((TA (I) + TA (II))			0,06	0,04	0,21	0,10

APPENDIX 3

TOC AND ROCK-EVAL PROCEDURES BY WEATHERFORD LABORATORIES

The following is verbatim from Weatherford Laboratories procedures description:

Sample Preparation

Samples for TOC and Rock-Eval analysis were ground, and material passing through a 60 mesh (250 micron) sieve was used for analysis. Samples were not high-graded prior to grinding.

Total Organic Carbon

Approximately 0.10 g of ground rock is accurately weighed and then treated with concentrated Hydrochloric Acid to remove carbonates. Sample weight may be varied depending on sample richness. The samples are left in acid for a minimum of two hours. The acid is removed from the sample with a filtration apparatus fitted with a glass microfiber filter. The filter is placed in a LECO crucible and dried at 110° C for a minimum of one hour. After drying the sample is analyzed with a LECO 600 Carbon Analyzer.

Rock-Eval Pyrolysis

Total organic carbon (TOC) and Rock-Eval pyrolysis were performed to assess source rock quality and thermal maturity (e.g., Peters, 1986; Peters and Casa, 1994). In Rock-Eval pyrolysis, ground samples are heated in an inert environment to measure the yield three groups of compounds (S_1, S_2, and S_3), measured as three peaks on a pyrogram. Sample heating at 300°C for 3 min. produces the S_1 peak by vaporizing the free (unbound) hydrocarbons. High S1 values indicate either large amounts of kerogen-derived bitumen (as in an active source rock) or the presence of migrated hydrocarbons.

The oven then increases in temperature by 25°C/minute to 600°C, and the S_2 and S_3 peaks are measured from the pyrolytic degradation of the kerogen in the sample. The S_2 peak is proportional to the amount of hydrogen-rich kerogen in the rock, and the S_3 peak measures the carbon dioxide released (to 390°C) providing an assessment of the oxygen content of the rock. The temperature at which the S_2 peak reaches a maximum, "T_{max}", is a measure of the source rock maturity. Accuracy of Tmax is 1-3°C, depending on the instrument, program rate and sample size. T_{max} also varies by organic matter type. T_{max} values for samples with S_2 peaks less than 0.2 mg HC/g rock are often inaccurate and should be rejected unless a definitive kerogen peak is noted from the pyrogram. A summary of operating conditions and analytical results from Rock-Eval pyrolysis follows.

Operating Conditions

S_1: 300°C for 3 minutes

S_2: 300°C to 600°C at 25°C/min; held at 600°C for 1 minute

S_3: trapped between 300 to 390°

S_4: oxidation at 580° for 12 minutes

Results

S_1: free oil content (mg hydrocarbons per gram of rock)

S_2: remaining hydrocarbon potential (mg hydrocarbons per gram of rock)

S_3: organic carbon dioxide (mg CO_2 per gram of rock)

TOC: total organic carbon content (wt. %)

T_{max}: temperature at maximum evolution of S_2 hydrocarbons

Ratios: hydrogen index (HI), oxygen index (OI), production index (PI), S_2/S_3, and S_1/TOC

APPENDIX 4

ORGANIC PETROLOGY ANALYTICAL PROCEDURES BY EGS-PLORATION COMPANY

The following is verbatim from EGS-ploration company procedures description:

Vitrinite reflectance measurements

Whole rock sample preparation for analysis in incident white light was performed on crushed (0.55 mm) whole rocks following the guidelines set out in the International Organization for Standardization publications ISO 7404-2, ISO 7404-3 and ISO 7404-5. Crushed particles were cold set into an epoxy resin block and sequentially ground then polished using decreasing abrasives and polishing powders using an automated Buehler Ecomet 3®, Automet 2® head, polishing system and isopropanol as lubricant. The reflectance of vitrinite particles was determined in a dark-room using a Zeiss Standard Universal research microscope-photometer system (UMSP-30) equipped with a 12V, 100W tungsten-halogen lamp, a 40-power Epiplan oil immersion objective, filtered 546 nm non-polarized incident light and Zeiss immersion oil with a refractive index of 1.517 at 23°C. Reflectance measurements (% R_o) were recorded on randomly-oriented particles. A Zeiss triple glass standard with reflectances of 0.506 %, 1.025 % and 1.817 % was used in addition to McCrone® Yttrium-aluminum-Garnet (0.917 %), Spinel (0.413 %) and Cubic Zirconium (3.256 %) mineral standards for photometer calibration and reflectance determination.

Visual kerogen analysis

Kerogen (insoluble, non-extractable organic matter) found in sedimentary rocks can be characterized under the microscope. This technique directly assesses the composition of the organic matter (facies), the relative contributions from different components, and the quality and degree of preservation of organic particles. This information is, in turn, used to infer paleodepositional environments. In addition, spore and amorphous matter color changes are also valuable and sensitive proxies for thermal maturity.

Sedimentary organic matter was excised from the mineral matrix according to the following protocol: Approximately 1 g crushed dry rock was exposed to sequential acid digestions using 1) 1 M Hydrochloric acid (HCL) to remove carbonate, and 2) Hydrofluoric acid (HF) (10% v/v; 5.6 M) to dissolve silicate minerals (Gelinas et al., 2001). Unreacted residue and precipitates were then separated using a high density solution of zinc bromide (2.00 SG) that allows the less dense kerogen to float, where it can be collected via pipette. This purified matter is then strewn onto a clear glass microscope slide using polyvinyl alcohol and Eukitt® mounting mediums.

Visual kerogen analysis was performed using a Zeiss Standard 14 microscope fitted for blue light excitation (450-490, FT 510, LP 520) and transmitted light (blue daylight filter). Thermal alteration Index (TAI), Spore Fluorescence Color (SFC) and percent distributions were made using a Zeiss Ph 2 40x/0.75 Neofluar lens.

APPENDIX 5

MEASURED SECTIONS

Measured Section of Ely Limestone at Shingle Pass, Nevada
(legend is applicable for all measured sections)

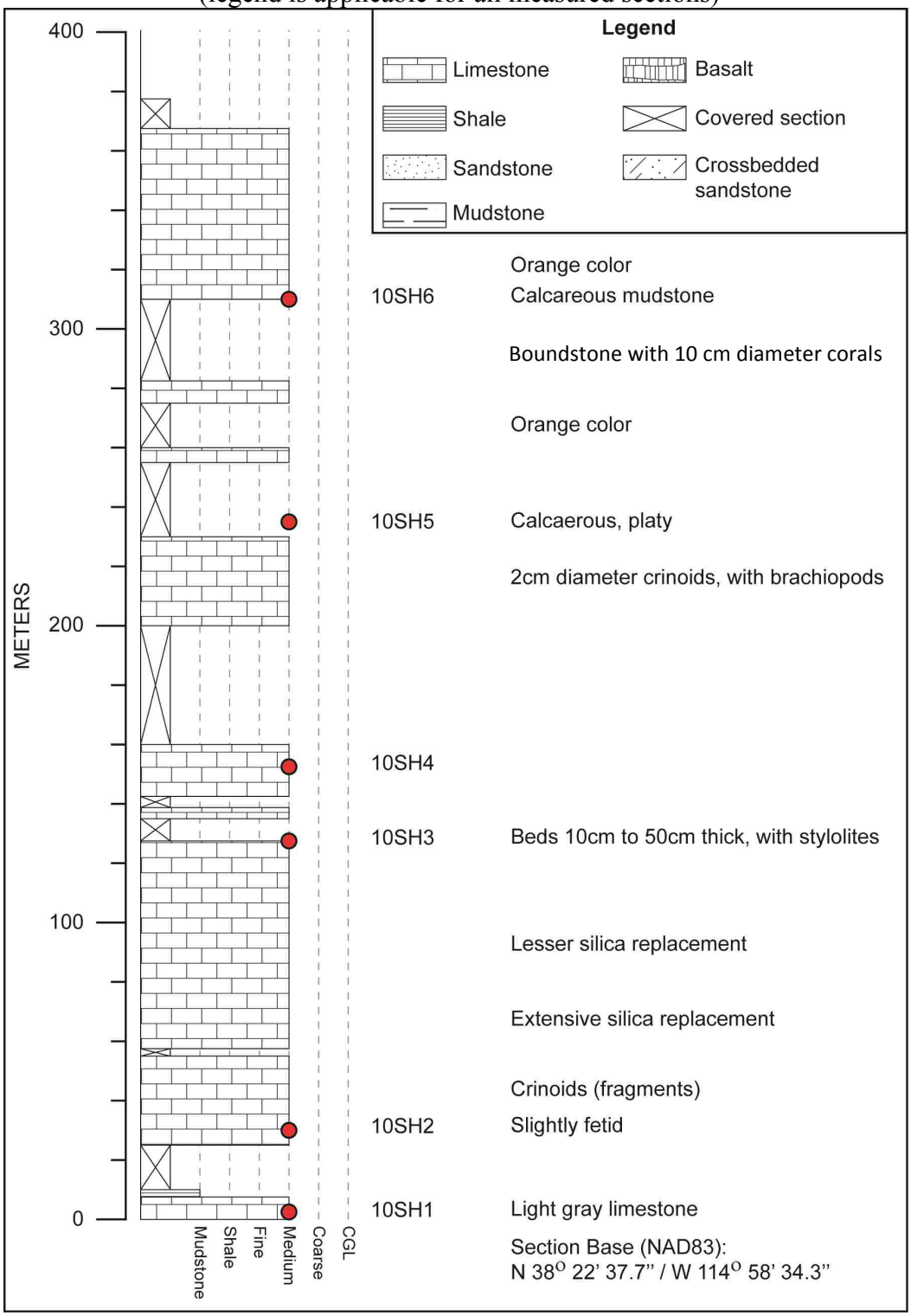

Measured Sections (1 and 2 of 3) of Pogonip Group at Shingle Pass

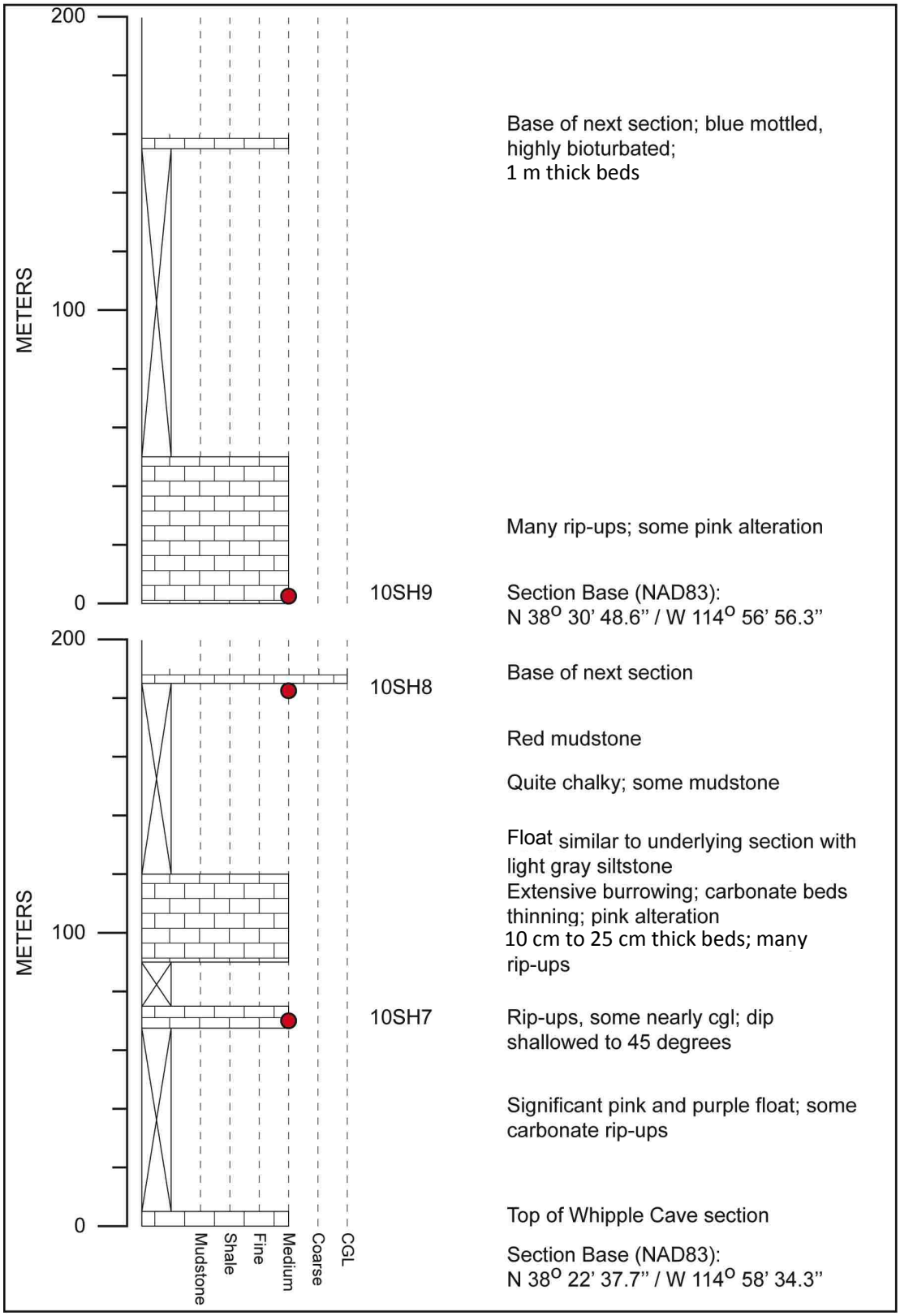

Measured Section (3 of 3) of Pogonip Group at Shingle Pass

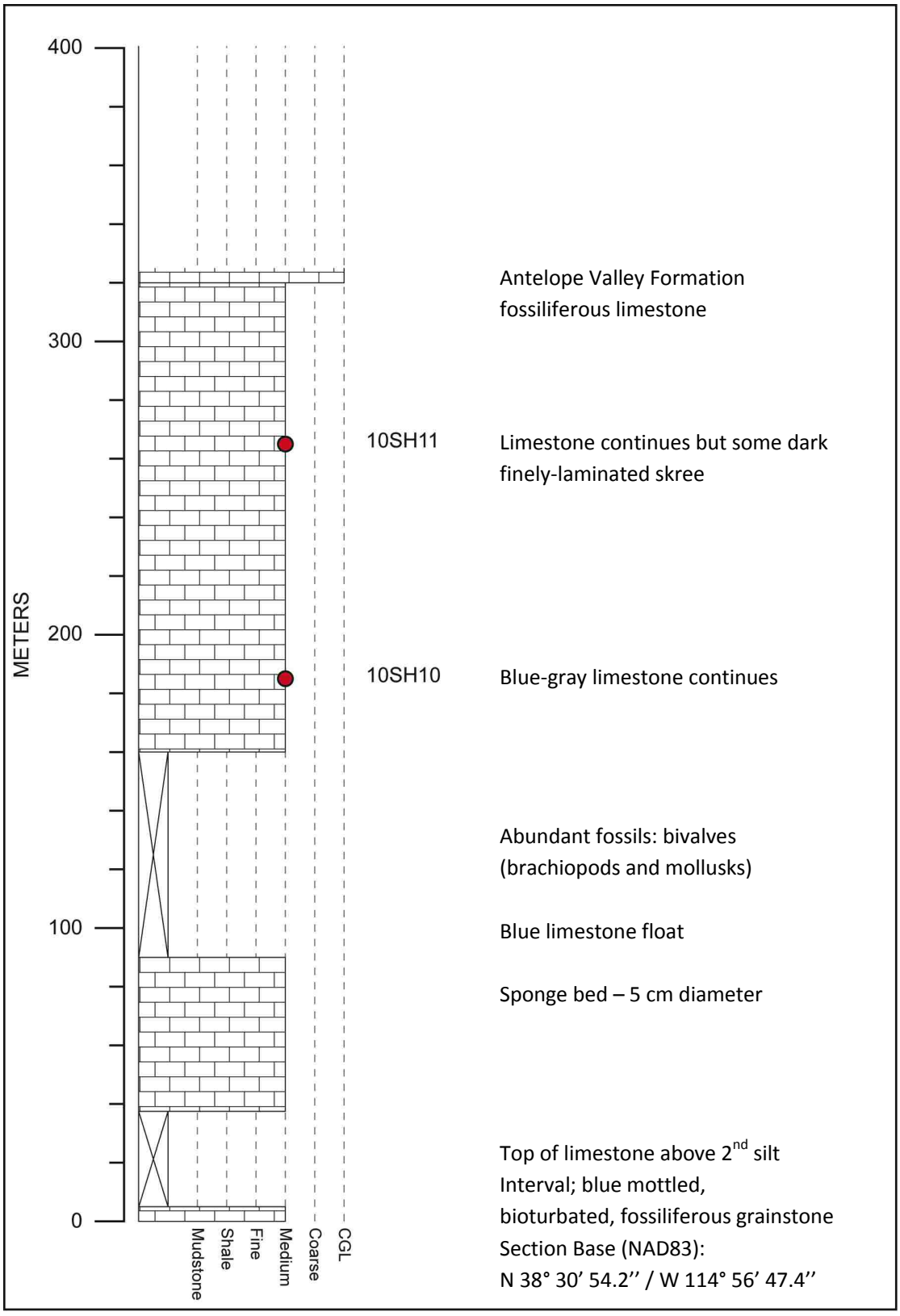

Measured Section of Guilmette Formation north of Fox Mountain, Nevada

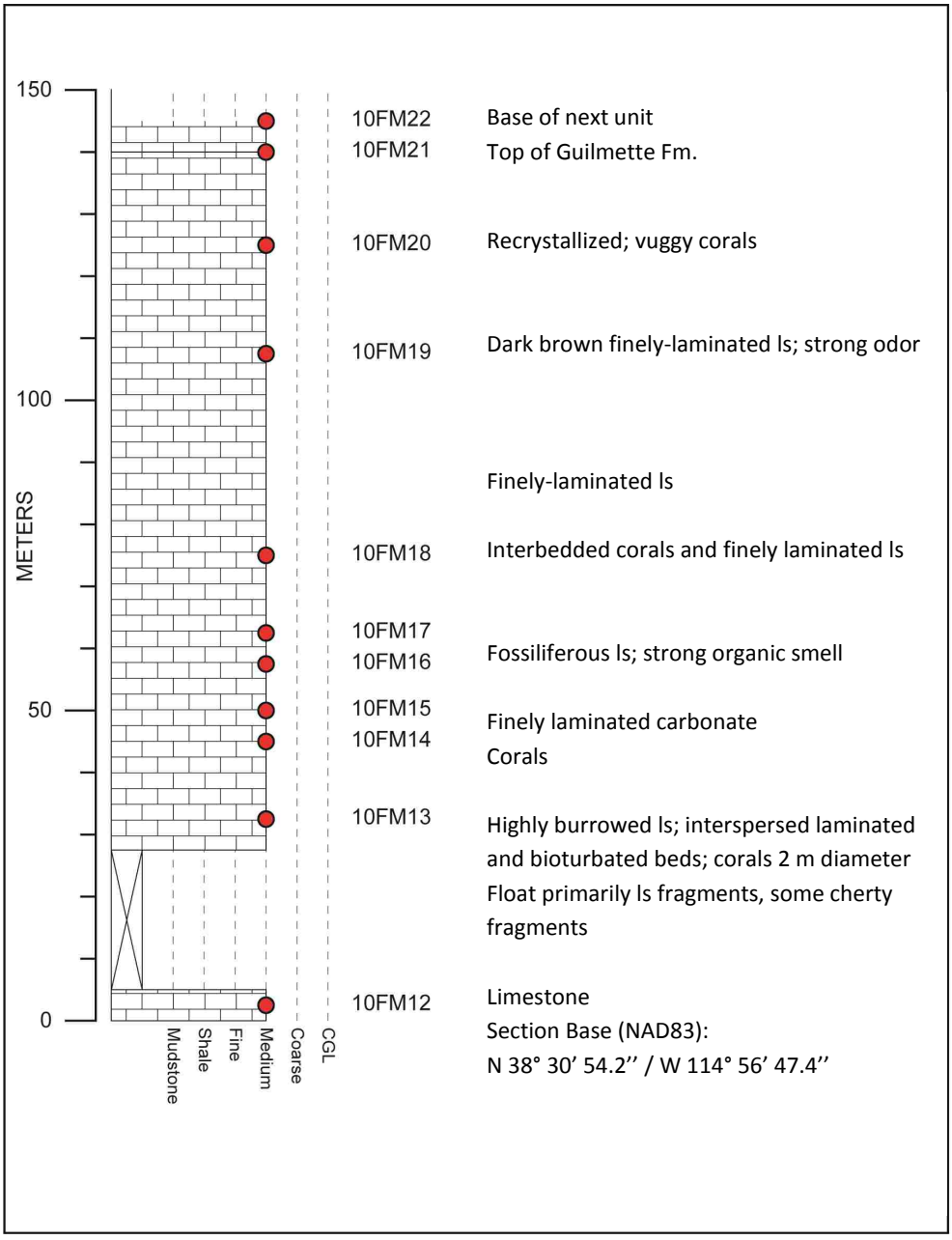

Measured Section of Pilot Shale, north of Fox Mountain, Nevada

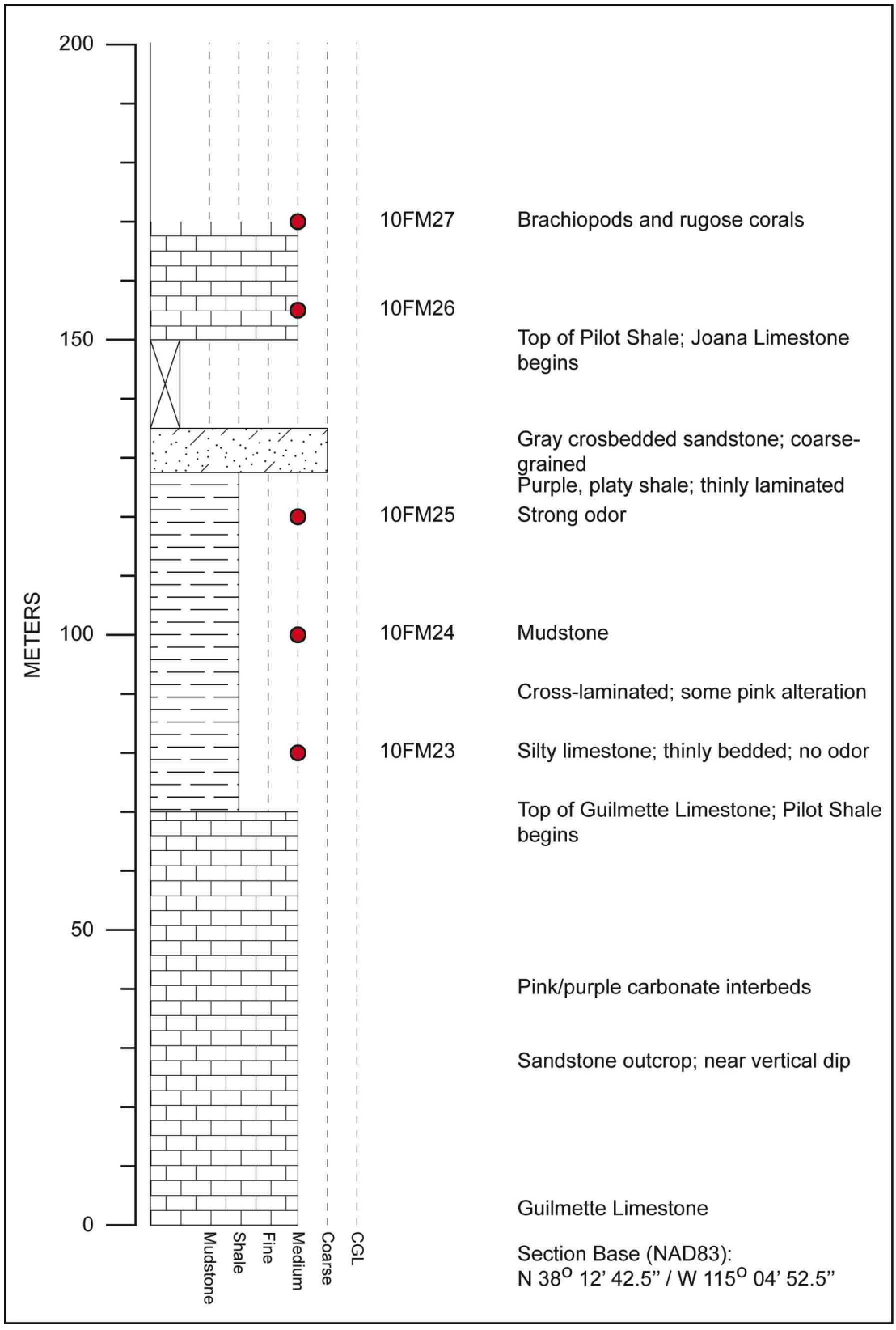

Measured Section of unidentified limestone unit (Cretaceous?) north of Moody Peak

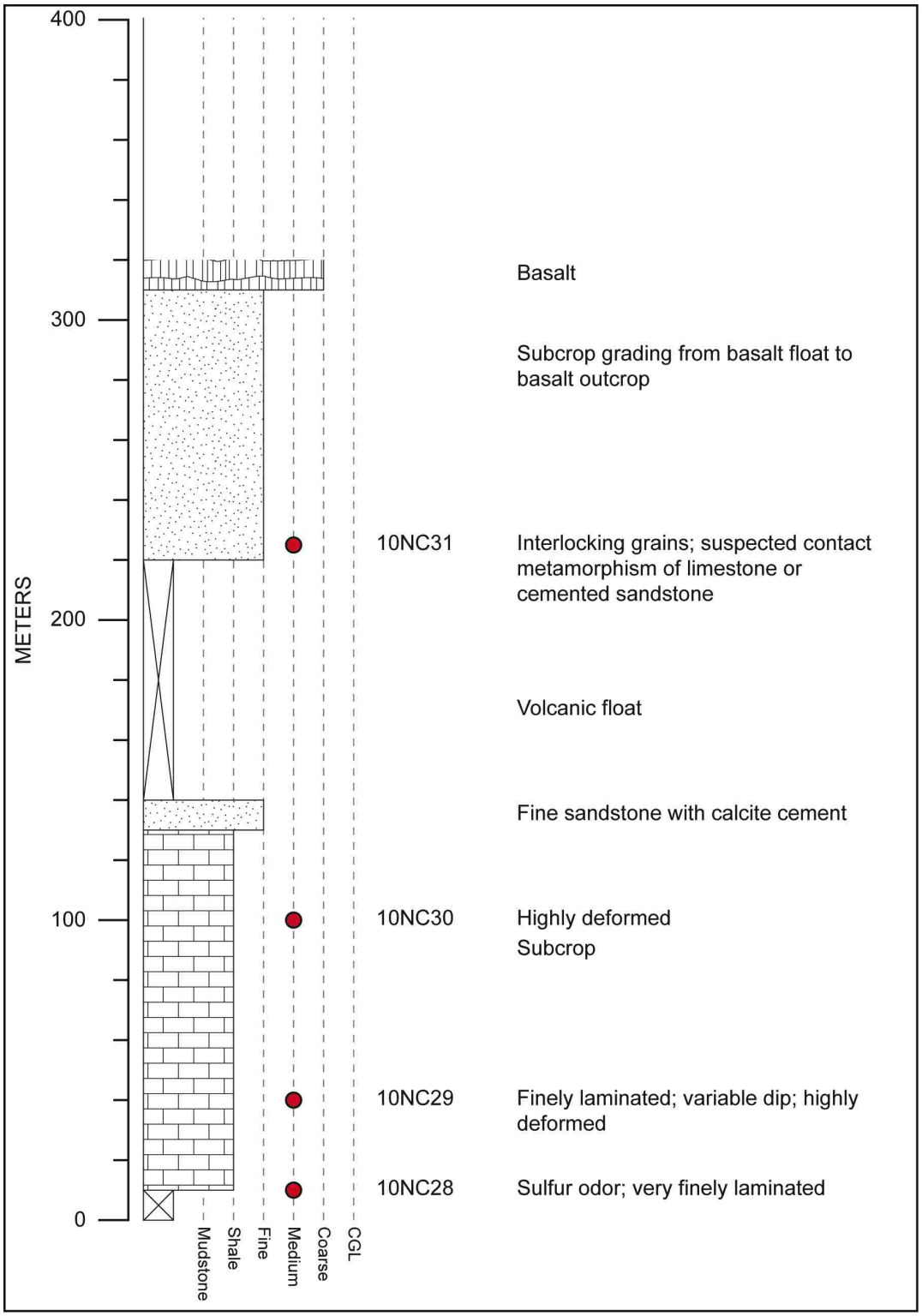

Measured Section of Eleana Formation north of US Highway 6, Nye County

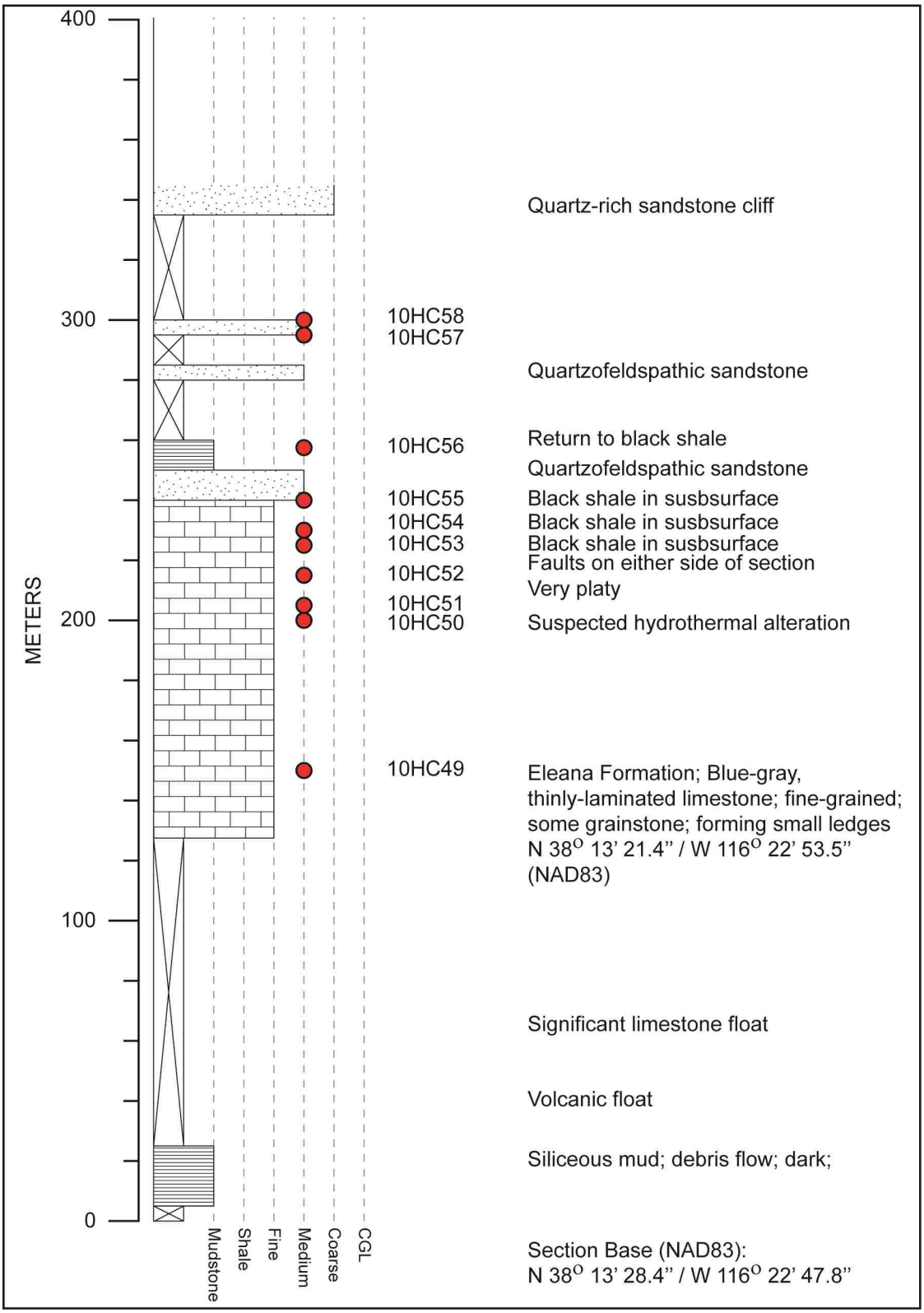

APPENDIX 6

ORGANIC PETROLOGY RESULTS BY EGS-PLORATION COMPANY

The following is verbatim from EGS-ploration company procedures description:

Thirty (31) outcrop samples, from undisclosed locations, were submitted for whole rock vitrinite reflectance (% Ro) determination and an additional five (5) samples were submitted or visual kerogen and thermal alteration index analysis. Organic petrology results are summarized below, while additional sample descriptions can be found on each analysis report. Photomicrographs in Plates 1 through 9 show typical views of the organic matter assemblages in incident white light (546 nm). A second series of photomicrographs labeled Plates 1 through 6 shows typical views of the organic matter assemblages in incident blue light (450-490, FT 510, LP 520).

Whole rock analysis 10CW-series

The 10CW outcrop series is comprised of nineteen (19) samples.

Mudstone, shale and marl have extremely low to moderately rich organic matter contents in general. However, five samples in this series are virtually barren in organic matter and in two samples it was impossible to make any maturity determination based on vitrinite reflectance. The majority of organic matter assemblages are characterized by contribution from terrestrially-derived organic matter. Vitrinite is typically present as recycled particles but there is often a minor contribution from primary vitrinite fragments. Differentiation of the two types was often difficult. Primary vitrinite is commonly present as very small lenses and very thin stringers that are difficult to measure accurately. However, there are occasional good quality stringers in some samples. In general, liptinite content is very low and appears to be algal, where present.

These results plot in a fairly tight range of vitrinite reflectance values. The minimum recorded vitrinite reflectance value is 0.76 % Ro for sample 10CW79, increasing to a maximum of 1.02 % Ro in sample 10CW95. However, the majority of values range between 0.80 % Ro and 0.90 %. To summarize findings, this series of outcrop samples indicate peak oil window maturity to late oil window level of thermal maturity.

Histogram populations were determined from notes taken for each measurement, and the level of confidence in the thermal maturity determinations is fair.

Whole rock analysis 10FM-series

The 10FM outcrop series is comprised of four (4) samples.

In general, these samples are characterized by marl and mudstone lithologies that typically have low organic matter contents and poor quality vitrinite. Indeed, marl lithologies are virtually barren in organic matter. Organic matter fluorescence has extinguished in all samples.

This sample series is characterized by vitrinite reflectance values that range 1.14 % Ro to 1.24% Ro (10FM25) reaching a maximum of 1.36 % Ro (10FM22), with one sample yielding no result (10FM23). These data indicate thermal maturity is in the zone of wet gas/condensate.

Histogram populations were determined from notes taken for each measurement, and the level of confidence in the thermal maturity determinations is poor to fair.

Whole rock analysis 10HC-series

The 10HC outcrop series is comprised of two (2) samples.

Shale and silty shale have moderately abundant organic matter contents. This is typically comprised of terrestrially-derive organic matter particles that are characterized by thin stringers of fair quality primary vitrinite as well as some poor quality lenses. There is a fair contribution from recycled vitrinite, and minor inertinite. Pyrite is abundant, and fluorescence appears to be mineral-derived and/or devoid of liptinite.

These two samples return vitrinite reflectance values of 0.95 % Ro (10HC50) and 1.00 % Ro (10HC58). These data indicate thermal maturity is late oil window mature.

Histogram populations were determined from notes taken for each measurement, and the level of confidence in the thermal maturity determinations is poor to fair.

Whole rock analysis 10MD-series

The 10MD outcrop series is comprised of two (2) samples.

Sample 10MD47 has slightly richer organic matter content. Shale in this sample has low to moderate organic matter content. This is comprised of fairly high maturity vitrinite which occurs as stringers, some of which are very thin and some poor quality. This is followed by minor recycled vitrinite and inertinite. Fluorescence appears to be mineral-derived. Sample 10MD46 is poor. There is a very low organic matter content that is comprised of a few small and sometimes poor quality lenses of vitrinite and minor inertinite. No organic matter fluorescence persists, but there is just a suggestion of a dull mineral fluorescence.

Vitrinite reflectance values are shown in Table 1. These two samples return vitrinite reflectance values of 1.32 % Ro (10MD46) and 1.30 % Ro (10MD47). These data indicate thermal maturity is early wet gas/condensate zone mature.

Histogram populations were determined from notes taken for each measurement, and the level of confidence in the thermal maturity determinations is poor to fair.

Whole rock analysis 10SL-series

The 10SL outcrop series is comprised of two (2) samples.

These two samples have very low organic matter contents and sample 10SL73 contains scattered particles of poor quality organic matter tend to be difficult to differentiate. Sample 10SL78 contains abundant hematite and a trace-level abundance of organic matter particles. However, three phytoclasts were deemed good enough quality to indicate thermal maturity in this sample. Pyrite is also abundant. Organic matter fluorescence has extinguished.

While vitrinite reflectance results in sample 10SL73 must be treated with caution, the data for sample 10SL78 is considered to be more reliable. The latter sample returns a vitrinite reflectance value of 1.79 % Ro and sample 10SL73, 1.35 % Ro. These data indicate thermal maturity is early wet gas/condensate zone to dry gas zone mature.

Histogram populations were determined from notes taken for each measurement, and the level of confidence in the thermal maturity determinations is poor to fair.

Whole rock analysis 10CW96

One outcrop sample comprises silty shale that has moderately abundant organic matter content. This is comprised of terrestrially-derived organic matter particles, of which vitrinite is the most abundant. This typically occurs as thin stringers and small lenses, followed by recycled vitrinite and inertinite. Pyrite is abundant and there is a moderate bitumen stain. Spores fluoresce mid to dark orange and algal matter fluoresces yellow-orange.

A vitrinite value of 0.92 % Ro indicates shale is late peak oil window mature.

The Histogram populations were determined from notes taken for each measurement, and the level of confidence in the thermal maturity determinations is fair.

Whole rock analysis 10CW97

One outcrop sample comprises shale that has a low to moderately rich organic matter content comprised of a mixture of terrestrially-derived and marine-derived organic matter. A low-reflecting population is deemed to be solid bitumen and this is accompanied by a more mature population of primary vitrinite stringers and lenses. Recycled vitrinite is present in moderate amounts and this is followed by a minor contribution from inertinite. Pyrite is abundant. Algal cysts fluoresce yellow, spores are not easy to identify.

A vitrinite value of 0.99 % Ro indicates shale is late peak oil window mature.

The Histogram populations were determined from notes taken for each measurement, and the level of confidence in the thermal maturity determinations is fair.

Visual kerogen analysis

Kerogen (insoluble, non-extractable organic matter) assemblages for three samples are characterized by high maturity organic matter that is transitioning into non-reactive material after exposure to higher levels of thermal stress. These kerogens are characterized by a dominance of poor quality non-fluorescing granular amorphous matter. Coaly matter is present in moderate amounts in most samples except 10SH11. Woody material is minor to moderate in abundance and present with smaller amounts of solid bitumen. Kerogen in sample 10SH11 indicates a possible marine-derived origin and is at a slightly lower level of thermal maturity relative to other samples in this series.

This kerogen is comprised mostly of non-fluorescing amorphous matter with very little contribution from coaly or woody particles. Sample 10SH7 was most likely a carbonate with trace organic carbon content. Following acid-digestion, no significant organic matter was recovered to allow for any characterization.

Kerogen in 10SH11 is classed as Type I/II, but has a poor potential for hydrocarbon generation. Kerogen in samples 10VI43, I0PO45 and 10HC48 has matured to a level where their components are being, and have been, transformedinto non-reactive organic matter. Kerogen in 10VI43 will currently plot as Type II/III on a van Krevelen diagram, while kerogen in samples I0PO45 and 10HC48 will currently plot as Type III/IV on a van Krevelen diagram. These kerogens have poor to no potential for the generation of gaseous hydrocarbons.

TAI is mainly based on red-brown, dark brown and dark grey-black amorphous kerogen color, which is less reliable than spore TAI. TAI (3 to 3+) is lowest in sample 10SH11 increasing to 4+ to 5 in sample 10VI43, and reaching 5 in samples I0PO45 and 10HC48. These data indicate kerogen in these samples varies from late oil window maturity through wet gas/condensate mature and into the zone of dry gas zone formation.

PHOTOMICROGRAPHS OF OM ASSEMBLAGES

IN INCIDENT WHITE LIGHT (546 nm)

10CW36 Woodruff Fm

10CW36 Woodruff Fm

10CW39 Woodruff Fm

10CW39 Woodruff Fm

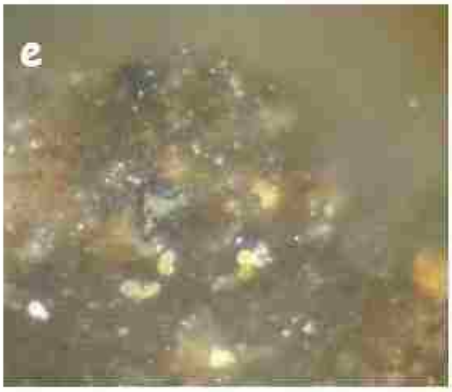

10CW79 Woodruff Fm

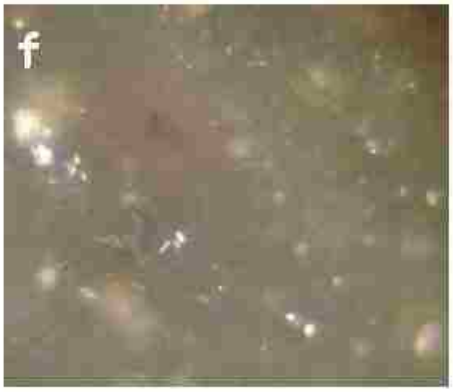

10CW36 Woodruff Fm

Plate 1

10CW79 Woodruff Fm

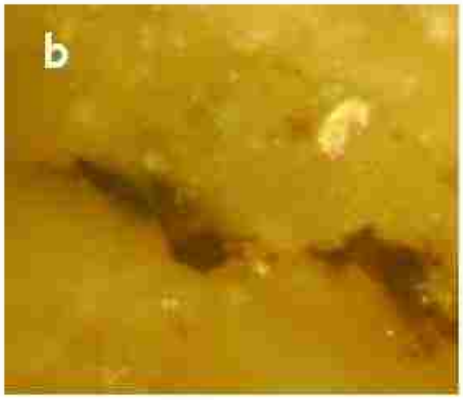

10CW80 Woodruff Fm

10CW80 Woodruff Fm

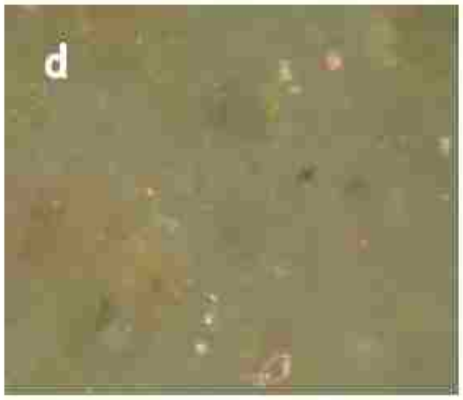

10CW81 Woodruff Fm

10CW81 Woodruff Fm

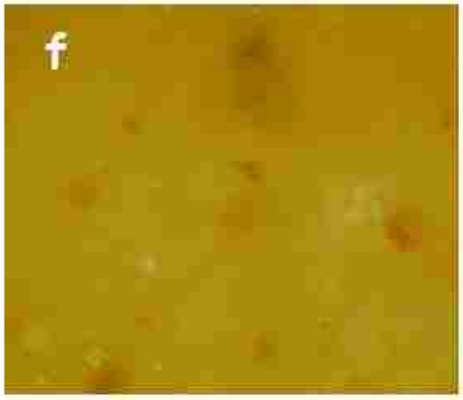

10CW82 Woodruff Fm

Plate 2

10CW82 Woodruff Fm

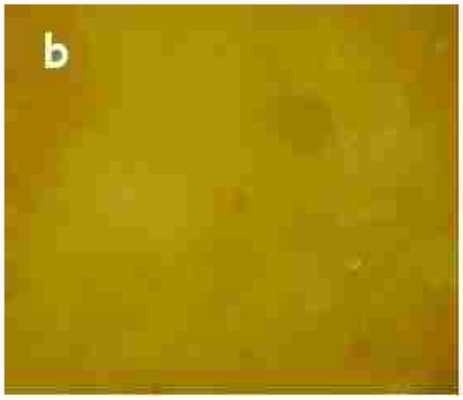

10CW83 Woodruff Fm

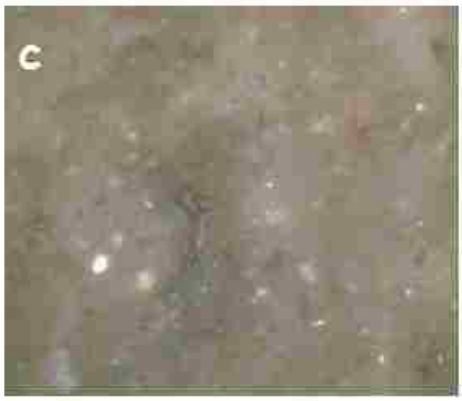

10CW84 Woodruff Fm

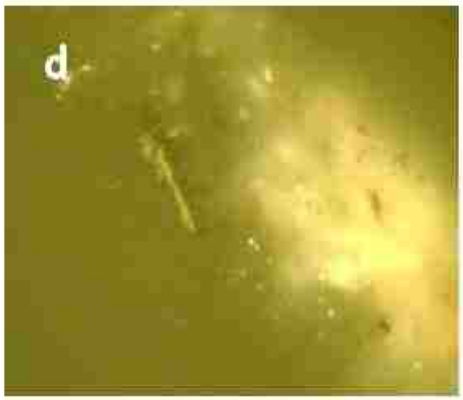

10CW84 Woodruff Fm

10CW85 Woodruff Fm

10CW85 Woodruff Fm

Plate 3

10CW86 Woodruff Fm

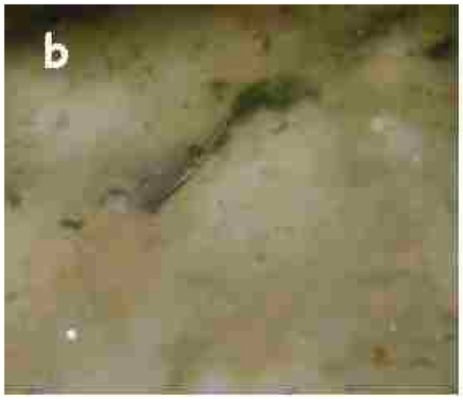

10CW86 Woodruff Fm

10CW87 Woodruff Fm

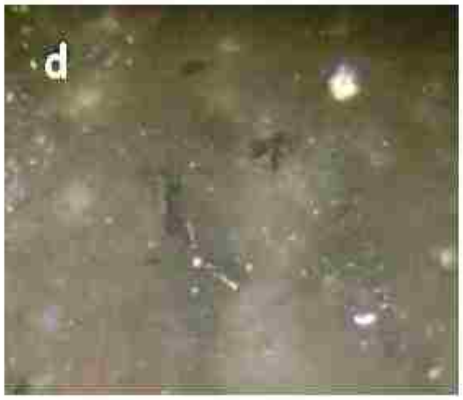

10CW87 Woodruff Fm

10CW88 Woodruff Fm

10CW88 Woodruff Fm

Plate 4

10CW89 Woodruff Fm

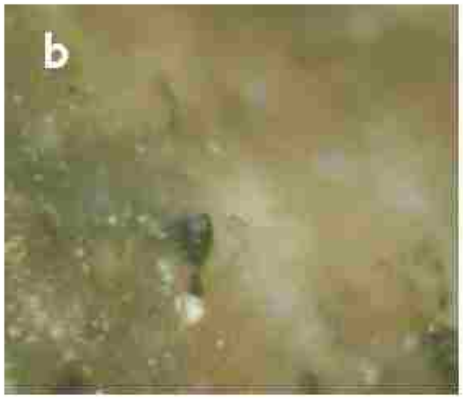

10CW89 Woodruff Fm

10CW91 Woodruff Fm

10CW92 Woodruff Fm

10CW92 Woodruff Fm

10CW92 Woodruff Fm

Plate 5

10CW93 Woodruff Fm

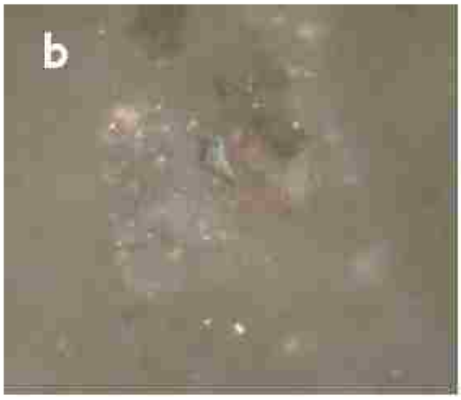

10CW93 Woodruff Fm

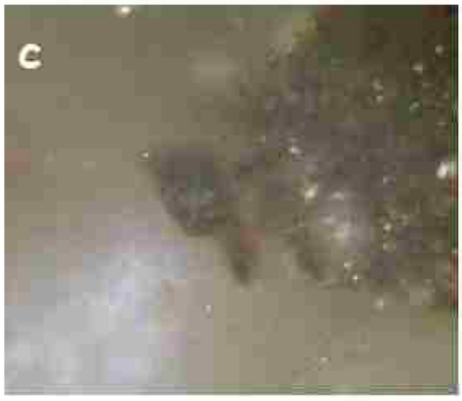

10CW93 Woodruff Fm

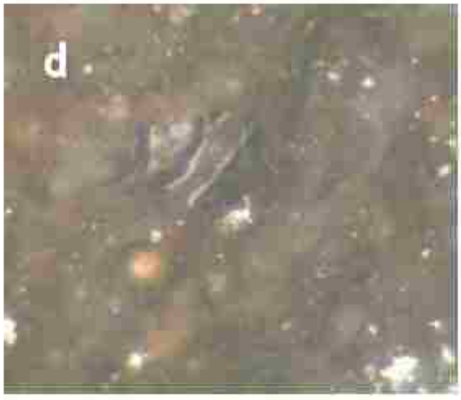

10CW94 Woodruff Fm

10CW94 Woodruff Fm

10CW94 Woodruff Fm

Plate 6

10CW95 Woodruff Fm

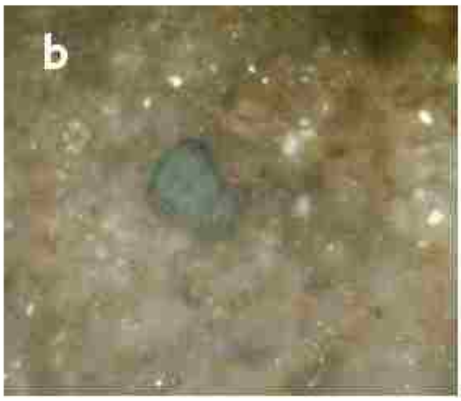

10CW95 Woodruff Fm

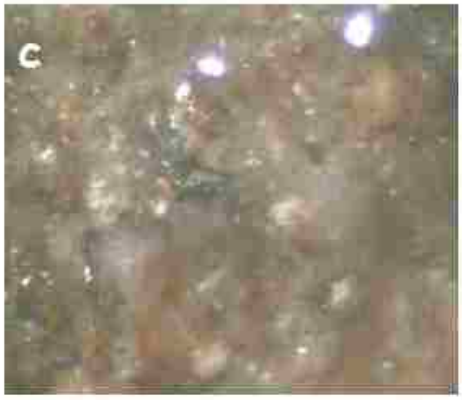

10CW95 Woodruff Fm

10FM13 Guilmette Fm

10FM13 Guilmette Fm

10FM25 Pilot Sh

Plate 7

10HC50 Eleana Fm

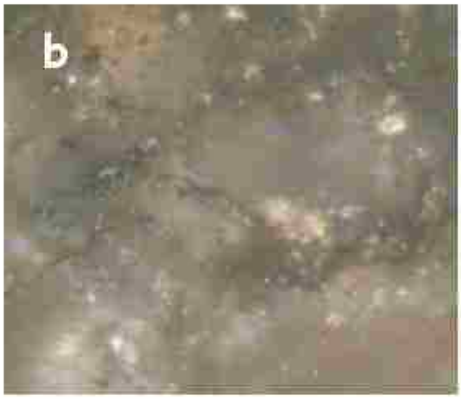

10HC50 Eleana Fm

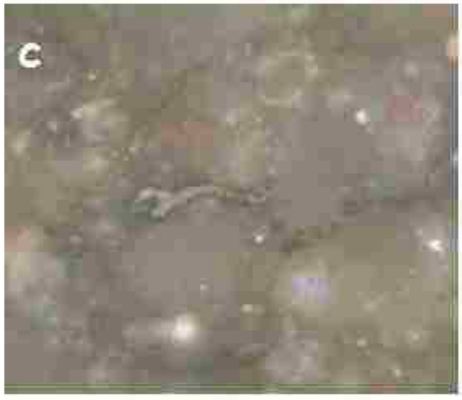

10HC50 Eleana Fm

10HC58 Eleana Fm

10HC58 Eleana Fm

10MD46 Pogonip Gr

Plate 8

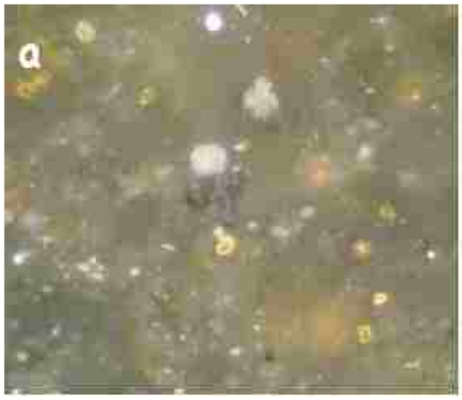

10MD46 Pogonip Gr

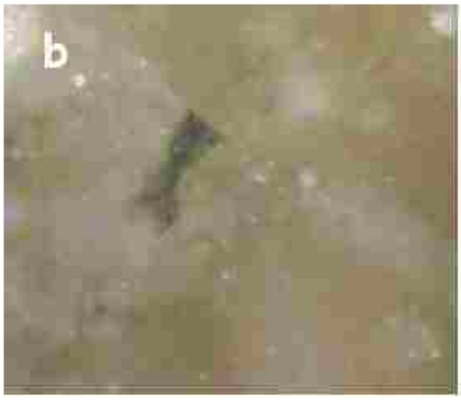

10MD47 Pogonip Gr

10MD47 Pogonip Gr

10SL73 Slaven Chert

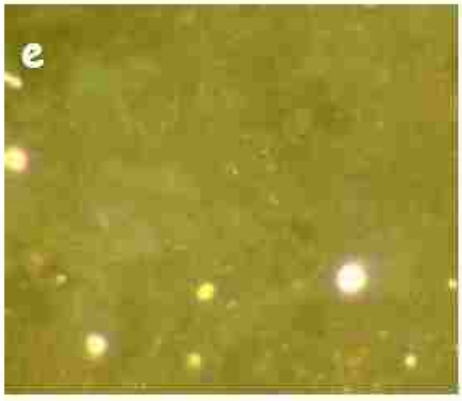

10SL73 Slaven Chert

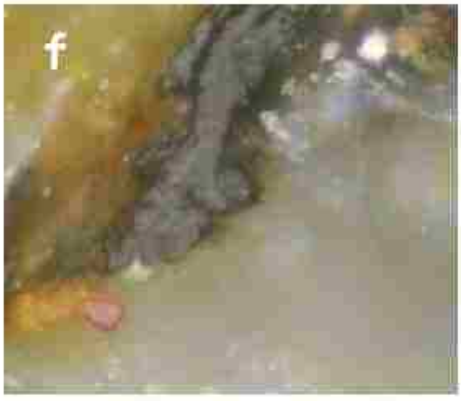

10SL78 Slaven Chert

Plate 9

PHOTOMICROGRAPHS OF OM ASSEMBLAGES IN INCIDENT BLUE LIGHT

(450-490, FT 510, LP 520)

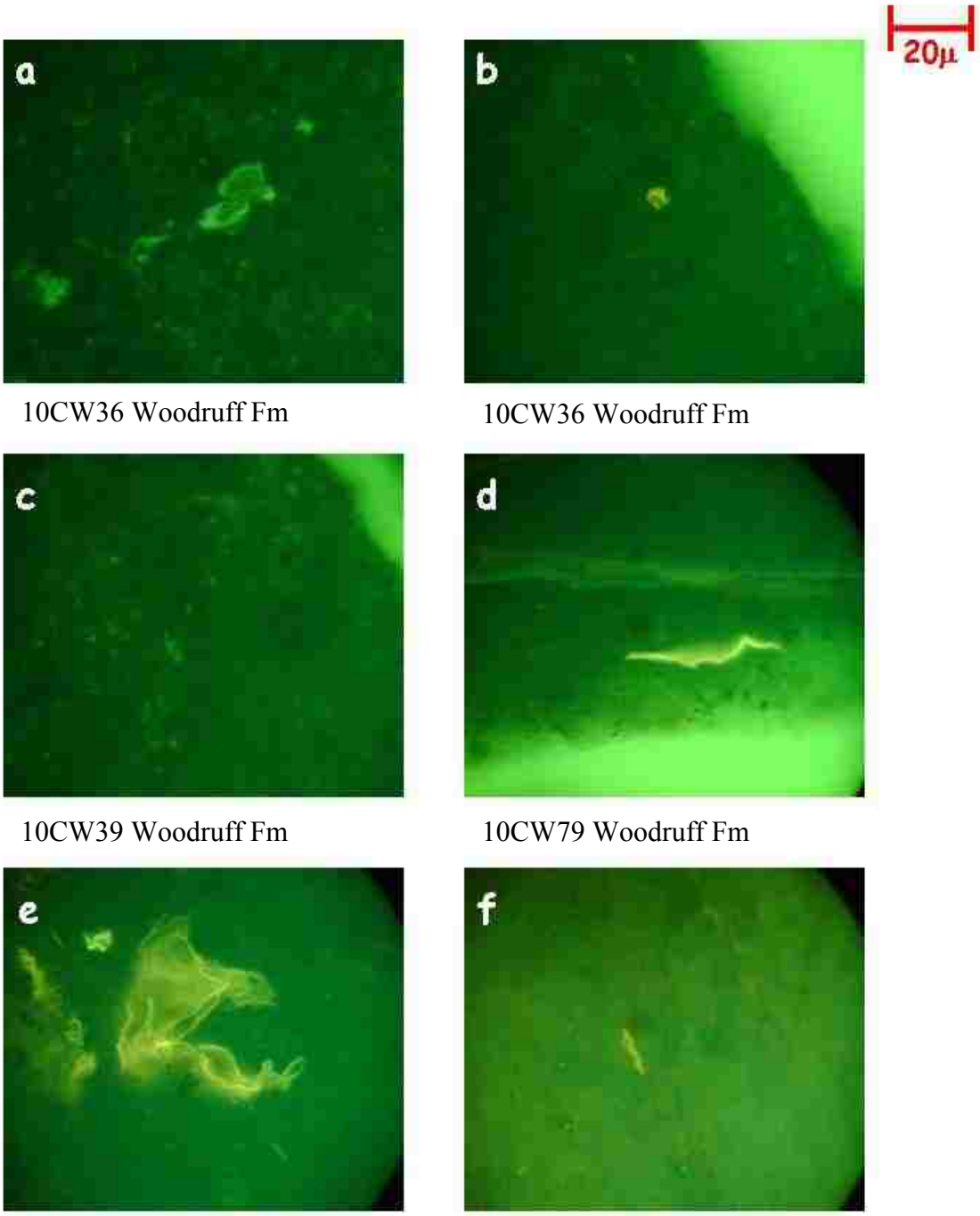

10CW36 Woodruff Fm

10CW36 Woodruff Fm

10CW39 Woodruff Fm

10CW79 Woodruff Fm

10CW79 Woodruff Fm

10CW80 Woodruff Fm

Plate 1

10CW80 Woodruff Fm

10CW81 Woodruff Fm

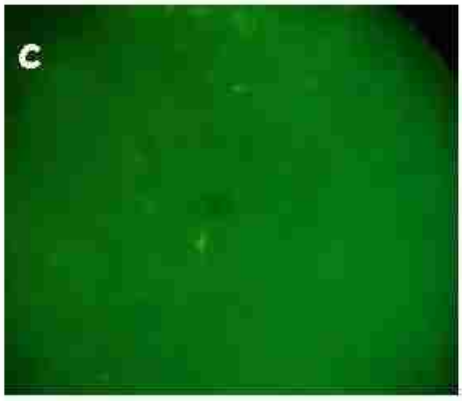

10CW82 Woodruff Fm

10CW83 Woodruff Fm

10CW84 Woodruff Fm

10CW89 Woodruff Fm

Plate 2

10CW89 Woodruff Fm

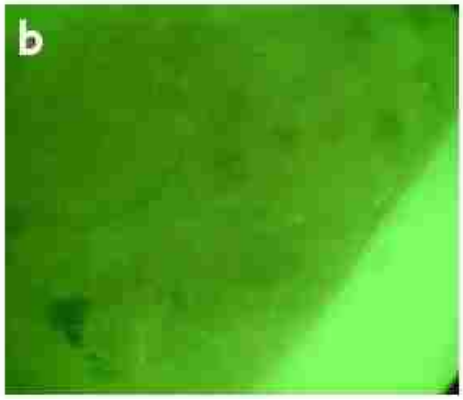

10CW91 Woodruff Fm

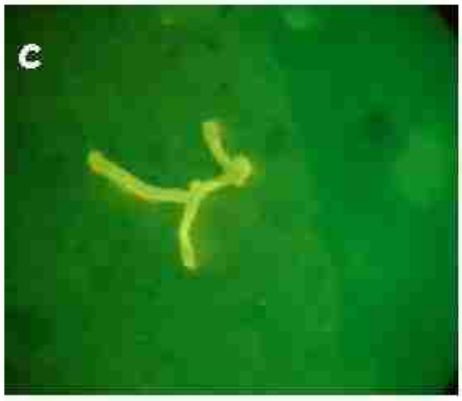

10CW93 Woodruff Fm

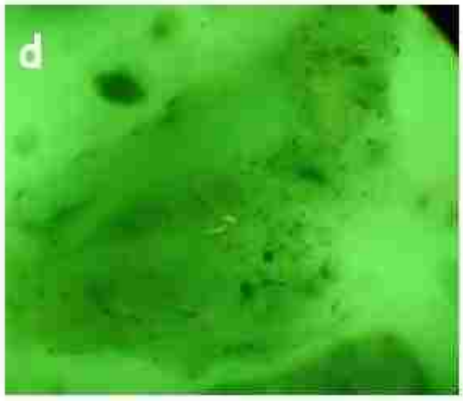

10CW93 Woodruff Fm

10CW93 Woodruff Fm

10CW93 Woodruff Fm

Plate 3

10CW93 Woodruff Fm

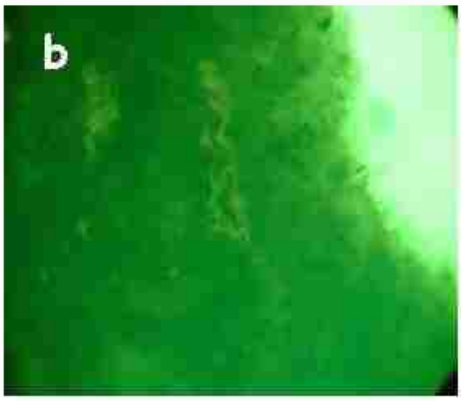

10CW94 Woodruff Fm

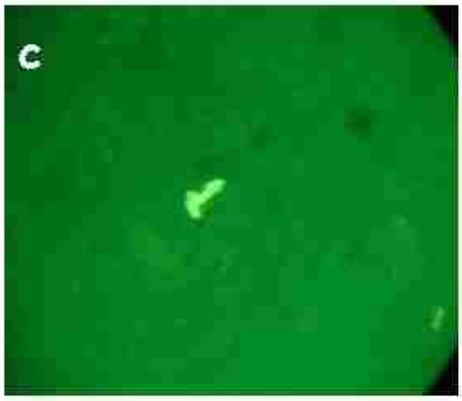

10CW94 Woodruff Fm

10CW94 Woodruff Fm

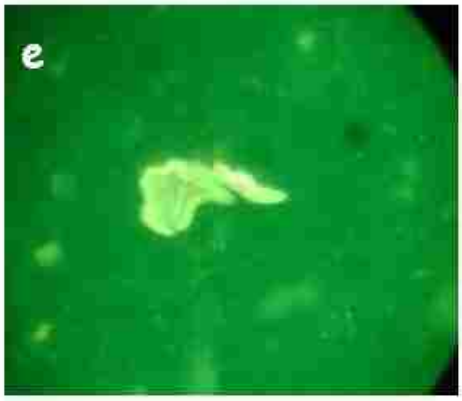

10CW94 Woodruff Fm

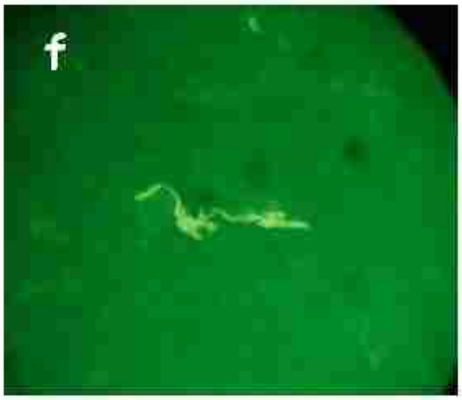

10CW94 Woodruff Fm

Plate 4

10CW94 Woodruff Fm

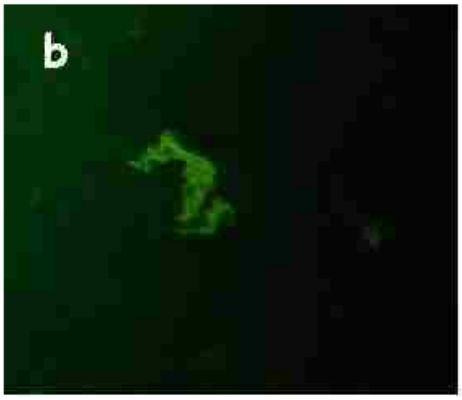

10CW95 Woodruff Fm

10CW95 Woodruff Fm

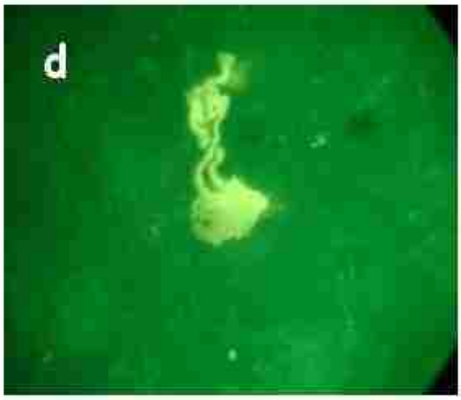

10CW95 Woodruff Fm

10CW95 Woodruff Fm

10HC58 Eleana Fm

Plate 5

10SL78 Slaven Chert

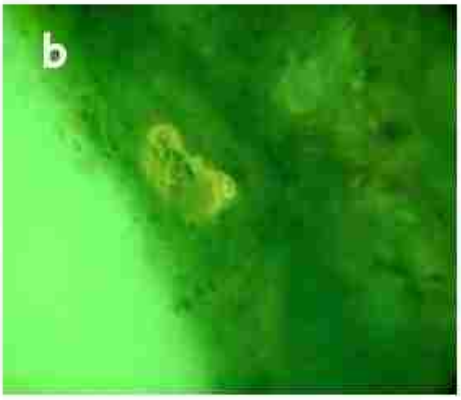

10CW95 Woodruff Fm

10CW95 Woodruff Fm

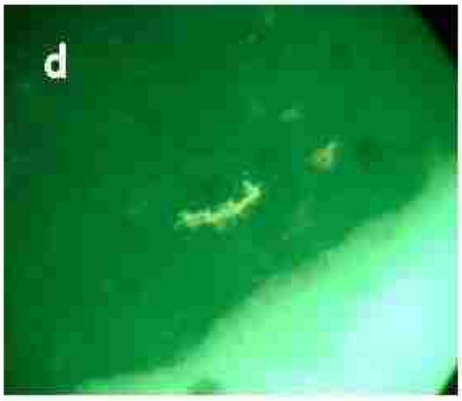

10CW97 Woodruff Fm

10CW97 Woodruff Fm

20µ

Plate 6

APPENDIX 7

PHOTOMICROGRAPHS OF THIN-SECTIONS

Images on the left are in plain polarized light, images on the right are in the crossed polarized light.

10VI43 Vinini Fm

Radiolarian mudstone, finely laminated; fracture filled with quartzous cement observed; some dolomitization present; disseminated OM more concentrated in some layers than others.

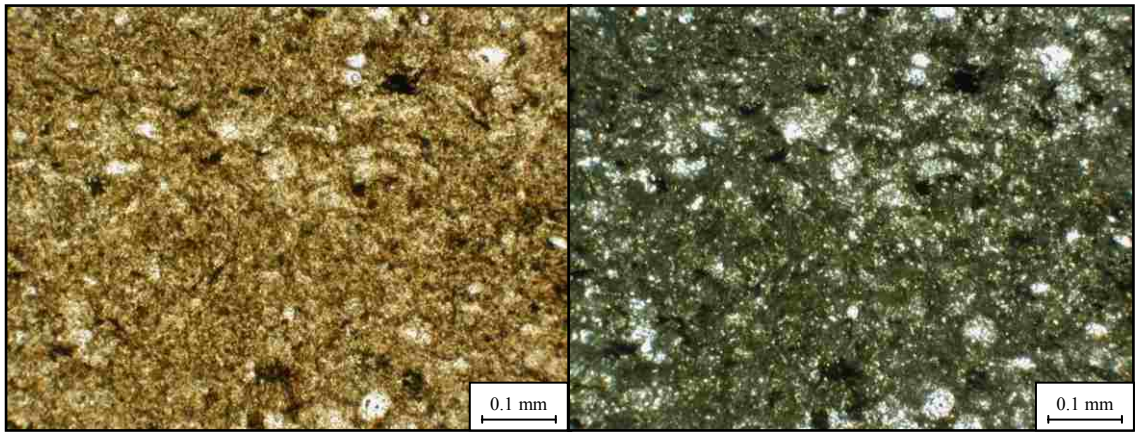

10CW40 Woodruff Fm

Radiolarian mudstone, more massive; disseminated OM observed.

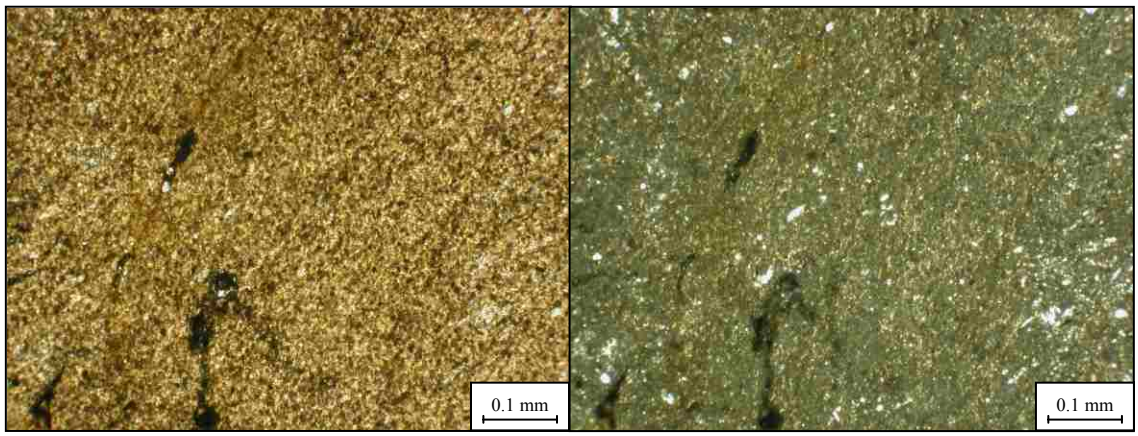

10CW41 Woodruff Fm

Radiolarian mudstone, laminated; fractures filled with quartz, disseminated OM observed.

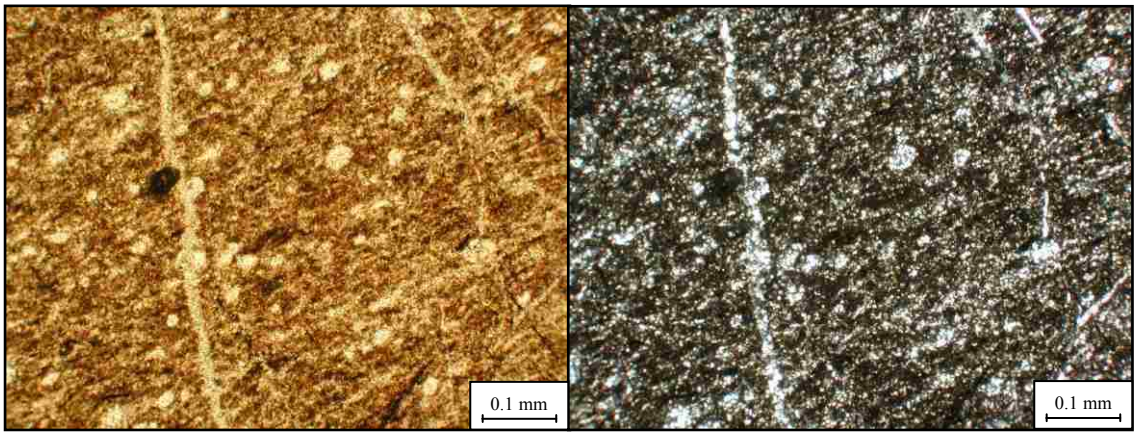

10CW80 Woodruff Fm

Mudstone with microfossils, disseminated OM silicified, silt sized pieces of detrital quartz present.

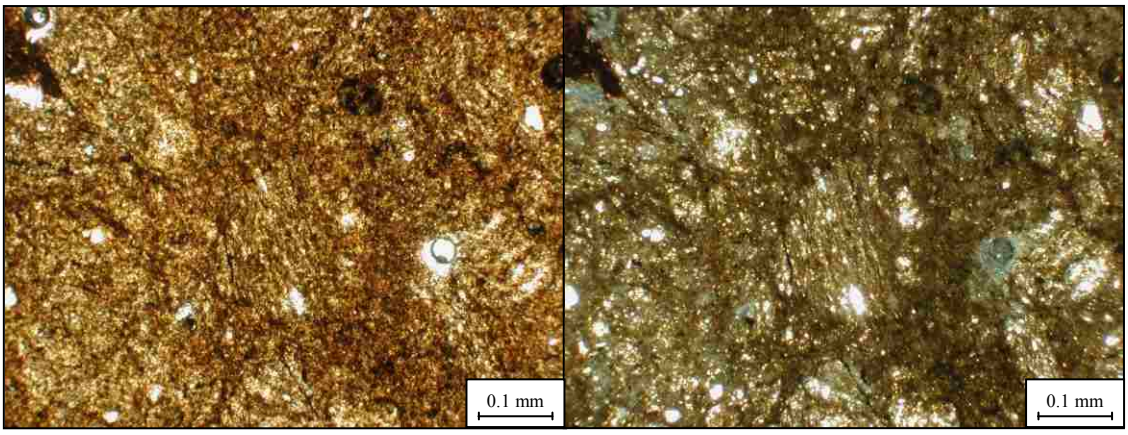

10CW84 Woodruff Fm

Breccia with silica cement; silicification.

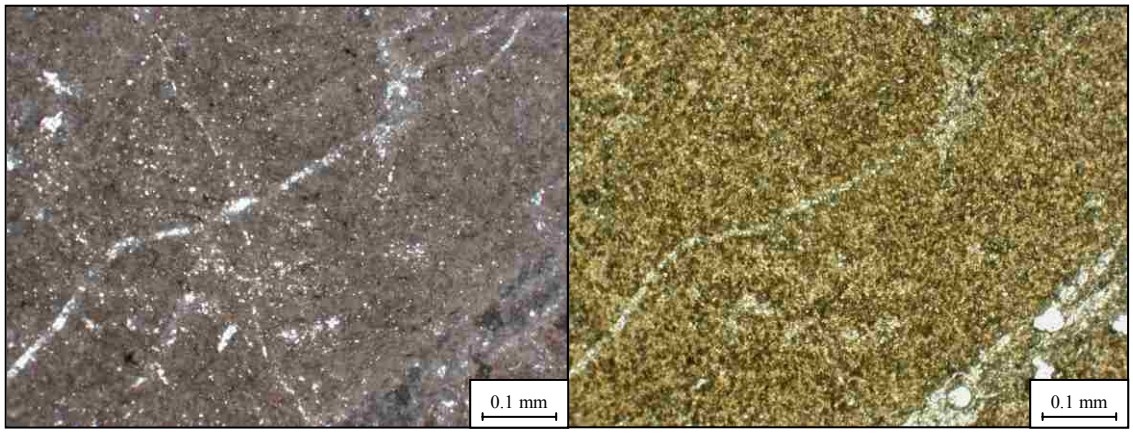

10CW85 Woodruff Fm

Mudstone, laminated, quartz crystals observed.

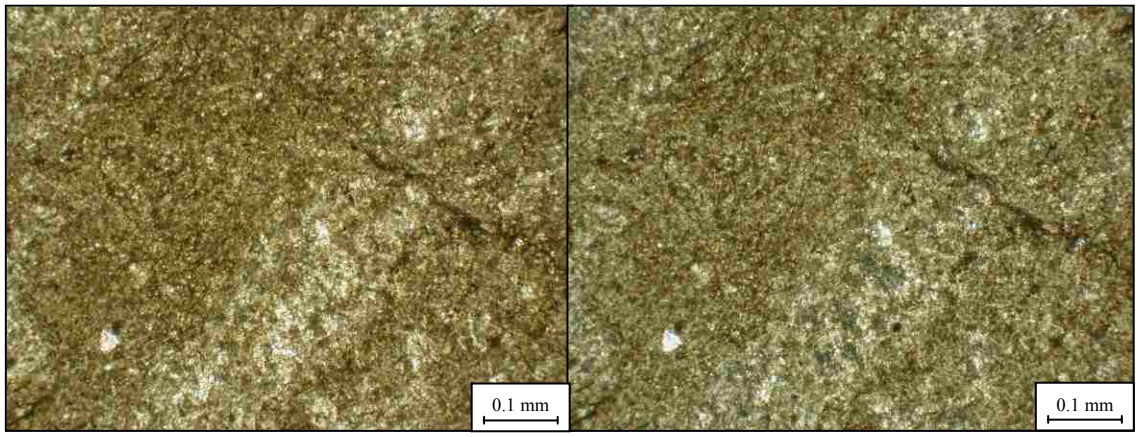

10CW86 Woodruff Fm
Mudstone, fractures filled with silica (recrystallized radiolaria)

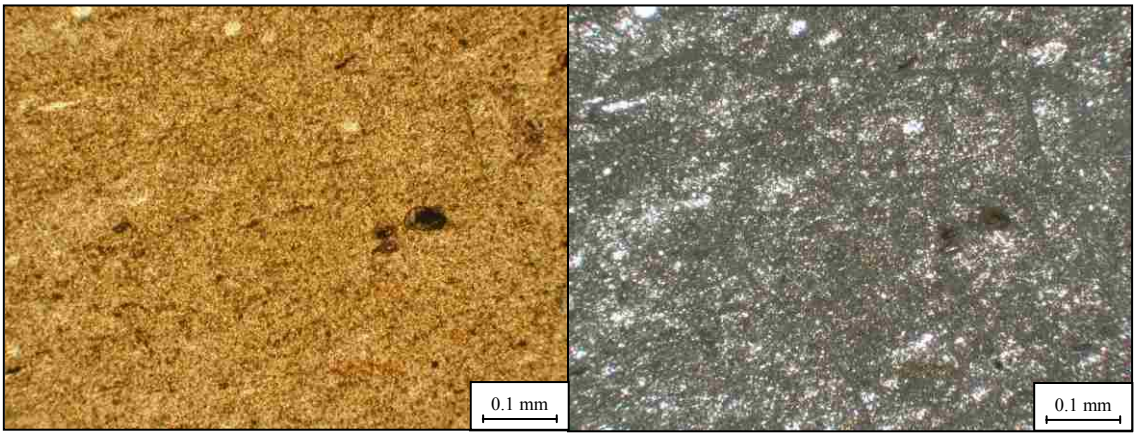

10CW91 Woodruff Fm
Mudstone, more fractures, quartz-rich.

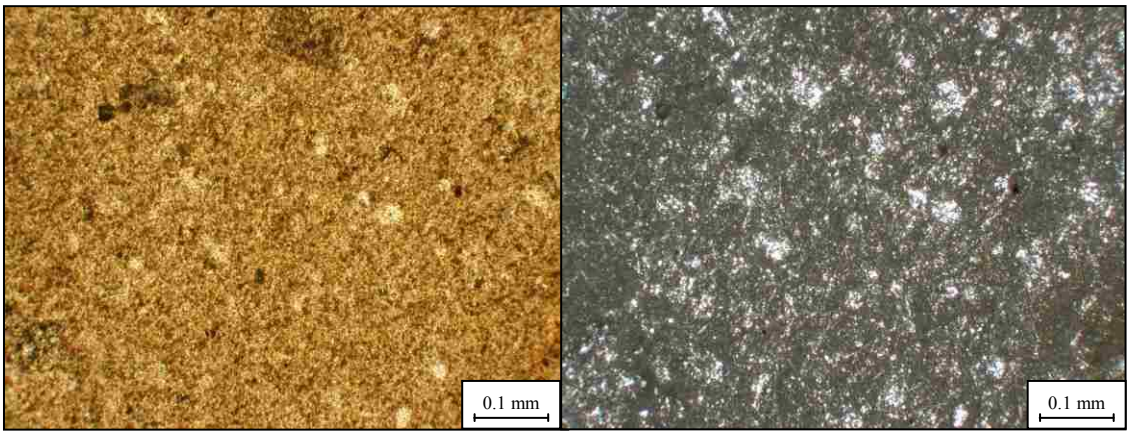

10CW92 Woodruff Fm
Mudstone, laminated, loaded with radiolaria, disseminated OM observed.

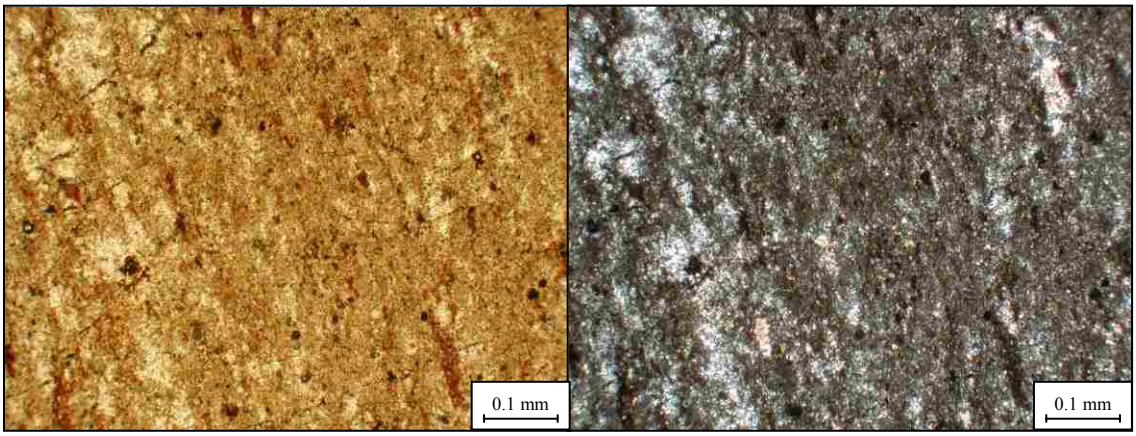

APPENDIX 8

LOCATION MAP OF WOODRUFF FORMATION SAMPLES

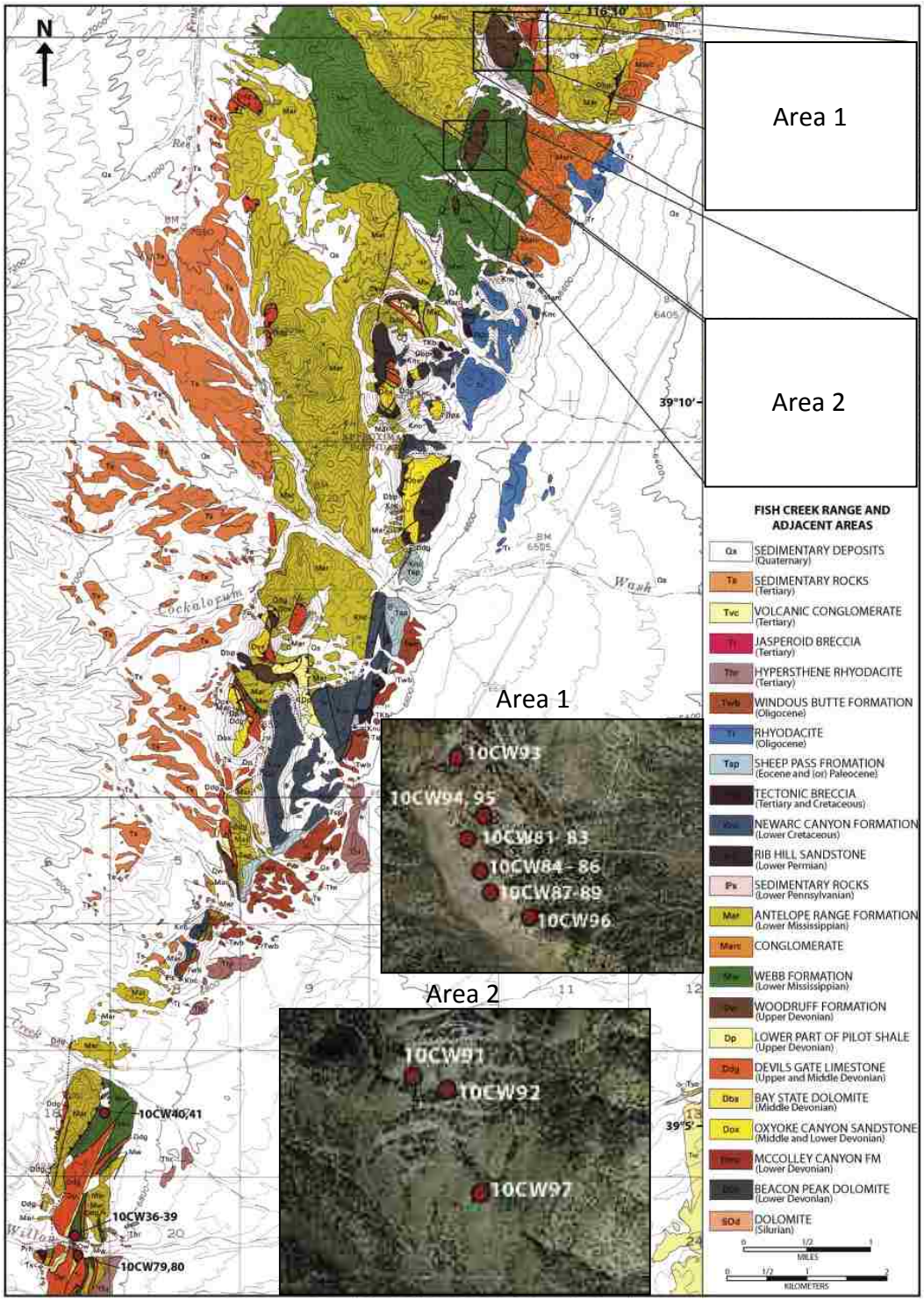

Base map is part of geologic map of the Cockalorum Wash Quadrangle by Hose (1983).

APPENDIX 9

GC CHROMATOGRAMS OF SOURCE ROCK EXTRACTS

GC traces for both samples have a sharp rising baseline forming a shape of a "hump", that consist of an unresolved complex mixture (UCM) of compounds. This shape and absence of n-alkanes are characteristic for biodegraded and low-maturity oils (Peters et al., 2007). Pristine (Pr) and phytane (Ph) are distinguished, however their relative abundance could have been lowered. Sample 10CW95 appeared to be less biodegraded and/or more mature than 10CW79, since its relative abundance of Pr and Ph is distinguishably higher.

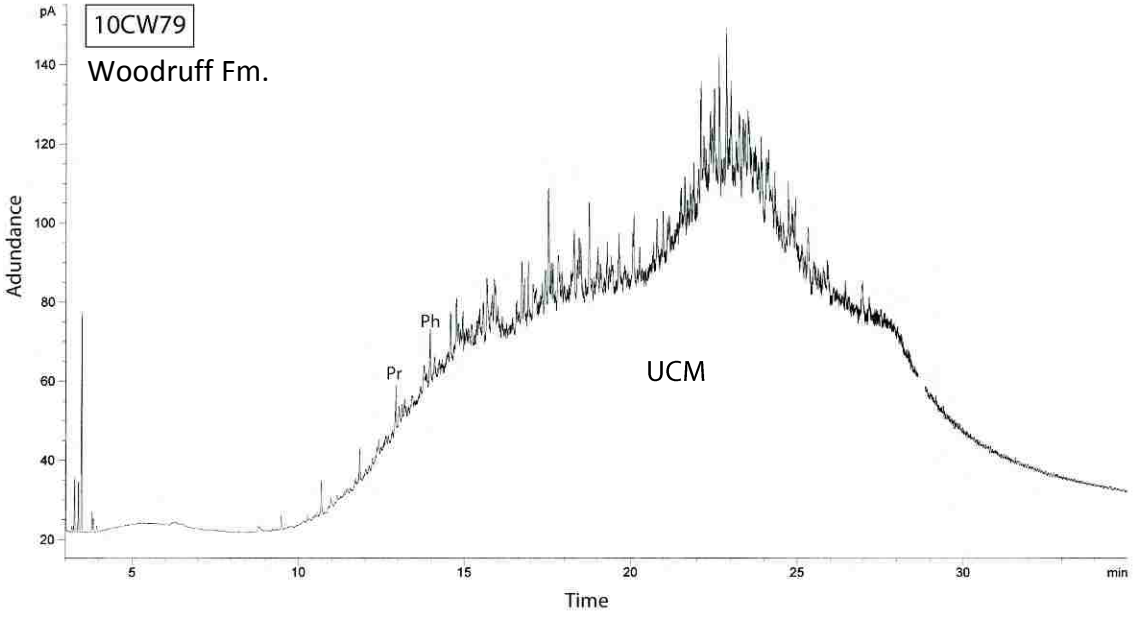

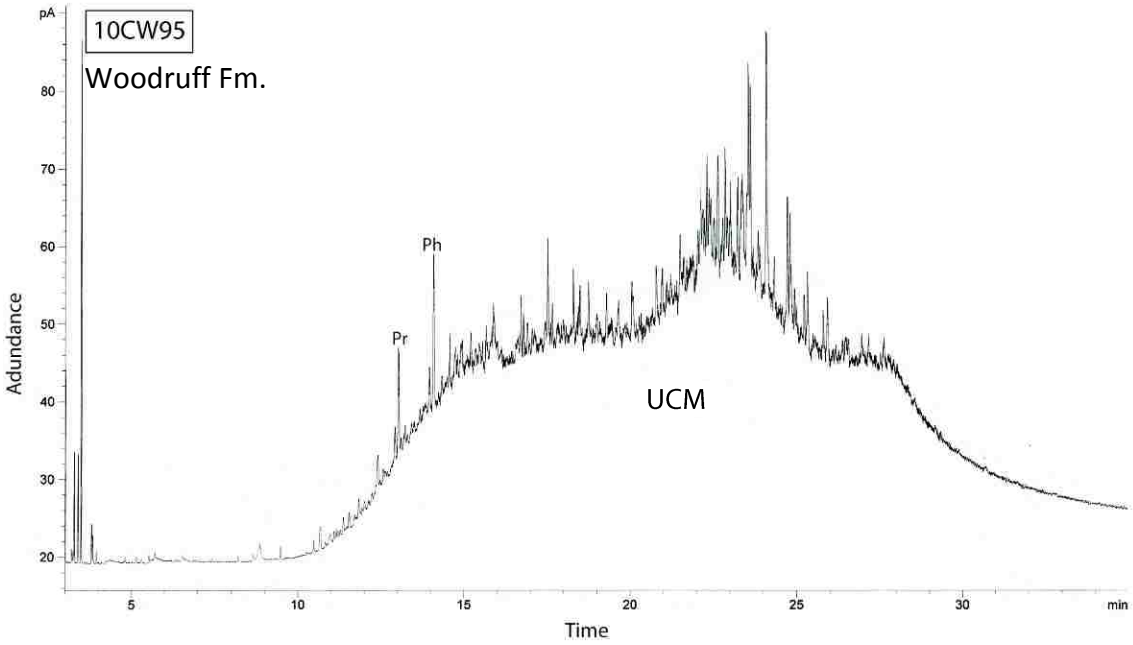

GC CHROMATOGRAMS OF SOURCE ROCK PYROLYZATES

(All numbered peaks correlate to different biomarker compounds as listed in Table 8)

Thermally immature samples 10CW79 and 10CW80 of Woodruff Fm. underwent hydrous pyrolysis experiment in order to generate products (10CW79p and 10CW95p) chemically and physically similar to natural crude oils (Peters et al., 2007; Ruble et al., 2001).

Both pyrolyzates have common geochemical features, such as similar distribution of *n*-alkanes ($nC_{12} - nC_{34}$) with predominance of odd versus even *n*-alkanes, particularly in the nC_{12}–nC_{34} range, and they show *n*-alkanes profiles that are fairly typical of mature oil.

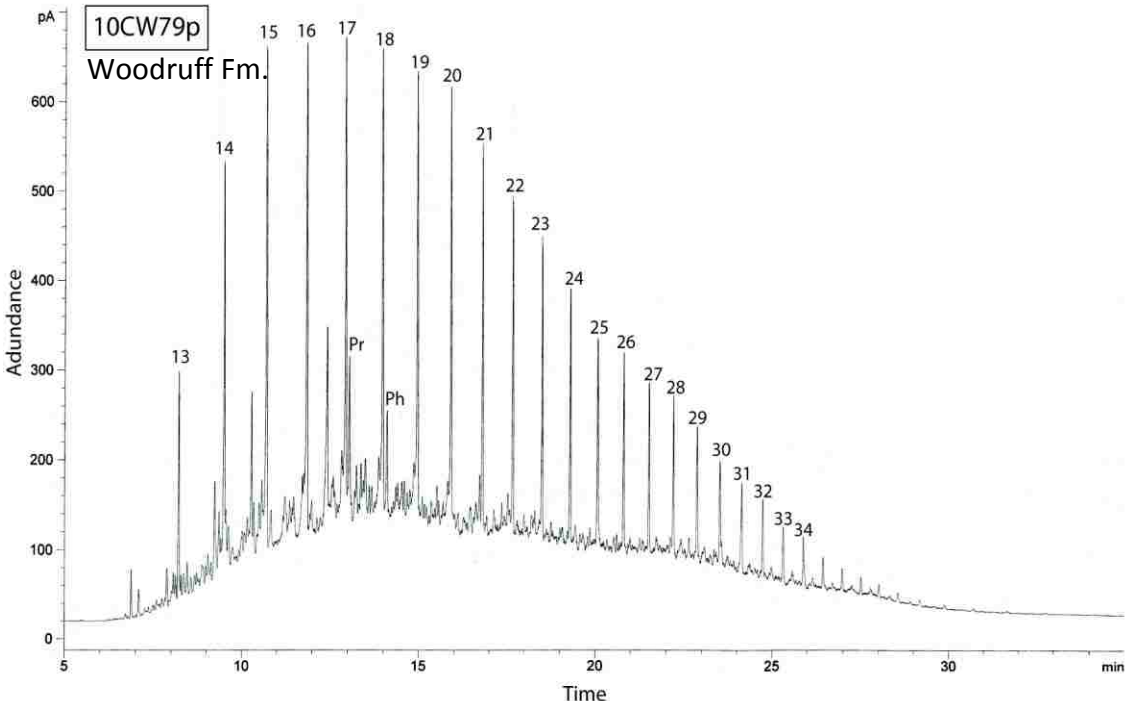

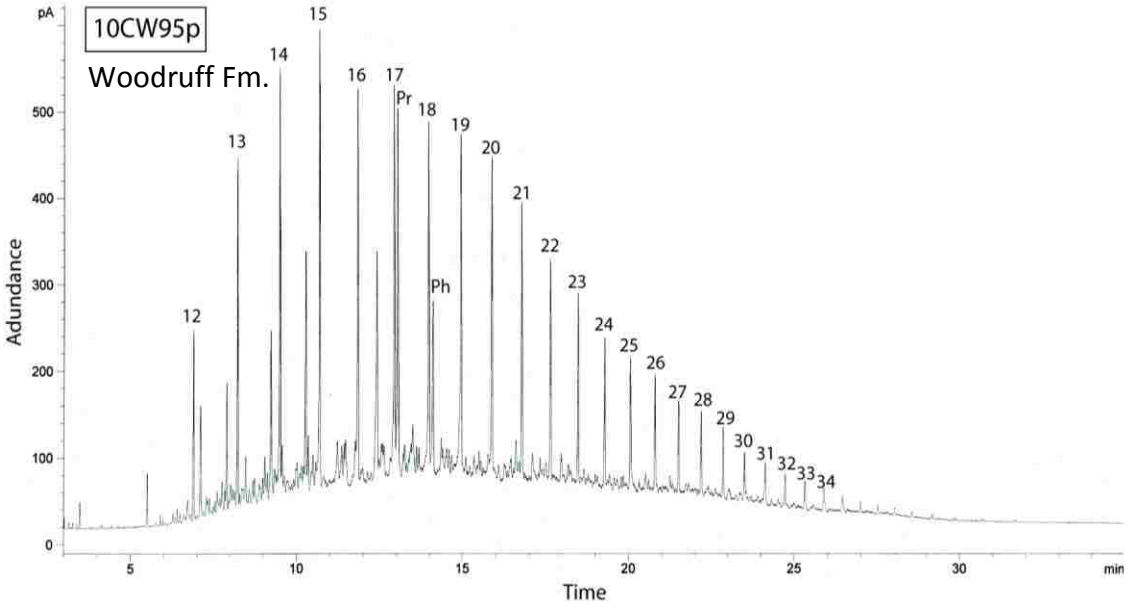

APPENDIX 10

GC-MSD CHROMATOGRAMS OF SOURCE ROCK EXTRACTS

(All numbered peaks correlate to different biomarker compounds as listed in Table 9)
For detailed explanation see text on p. 30 - 31.

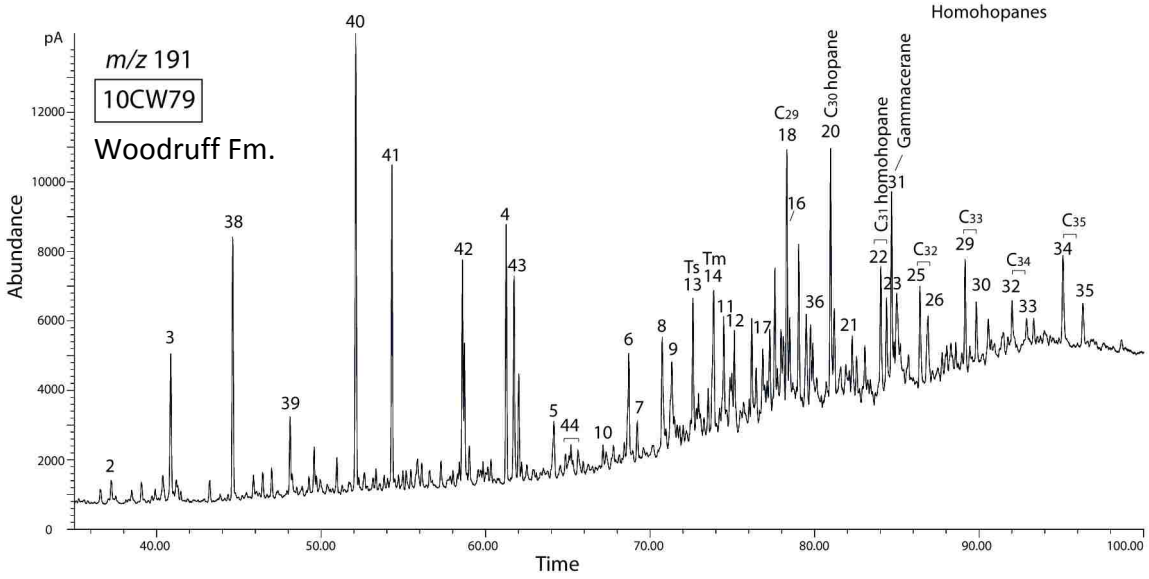

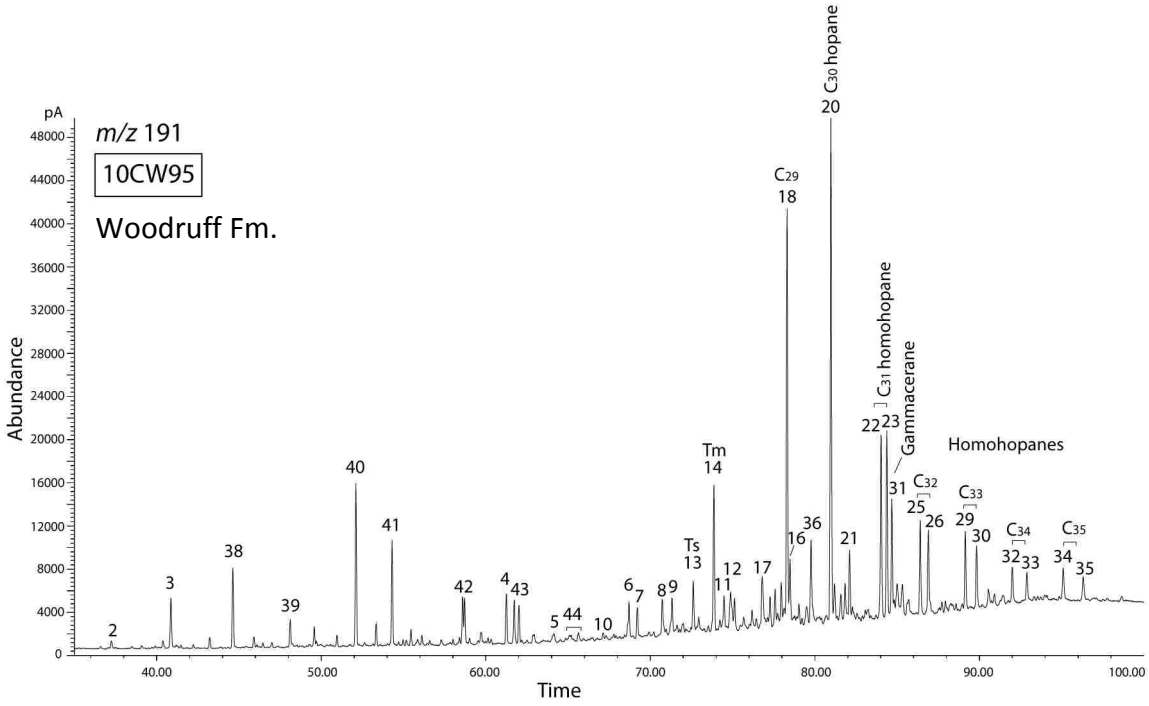

GC-MSD CHROMATOGRAMS OF SOURCE ROCK PYROLYZATES

(All numbered peaks correlate to different biomarker compounds as listed in Table 9)

For detailed explanation see text on p. 30 - 31.

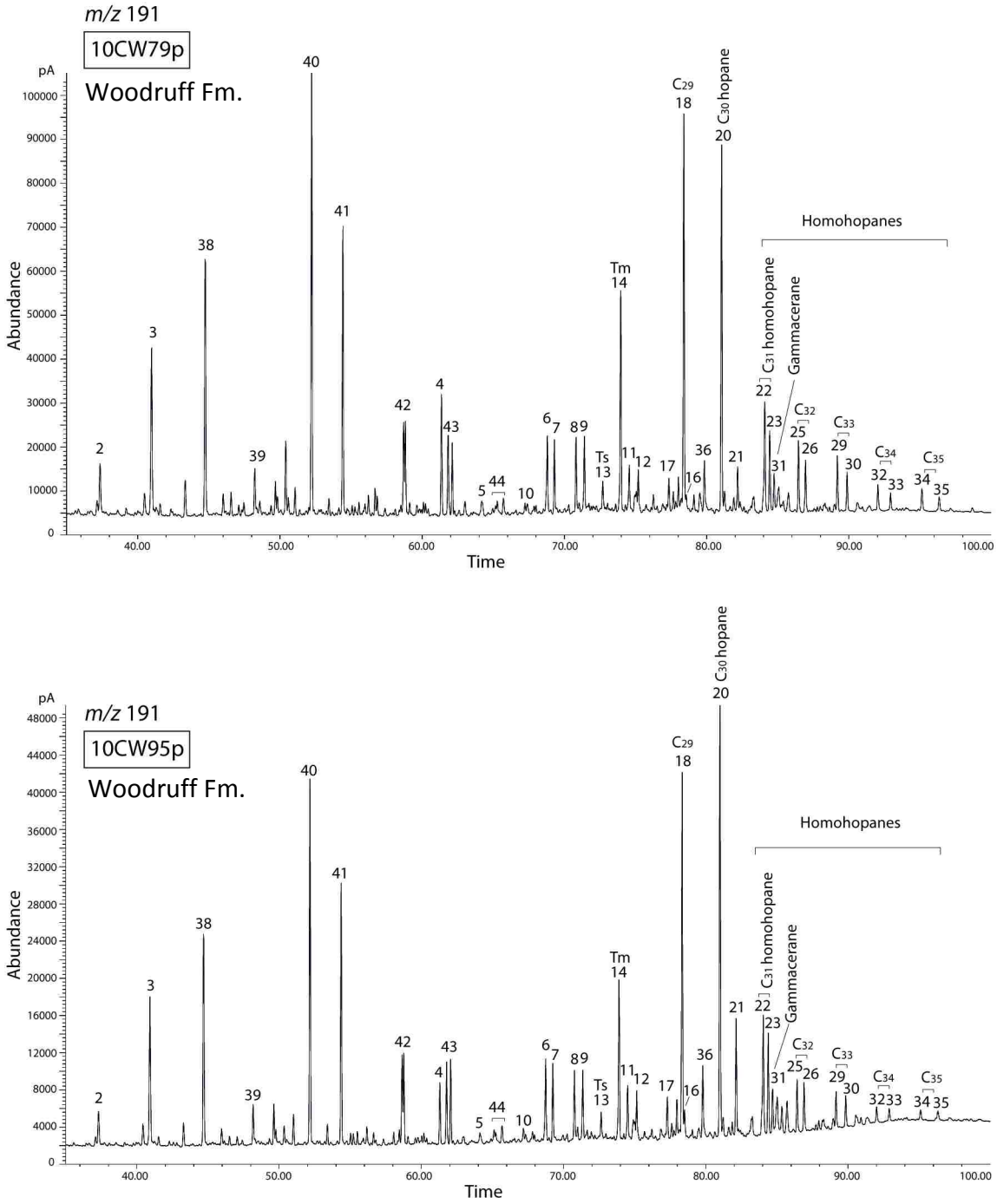

APPENDIX 11

GC-MSD CHROMATOGRAMS OF SOURCE ROCK EXTRACTS

FOR DIAMONOID ANALYSIS

(All numbered peaks correlate to different biomarker compounds as listed in Table 9)

For detailed explanation see text on p. 30 - 31.

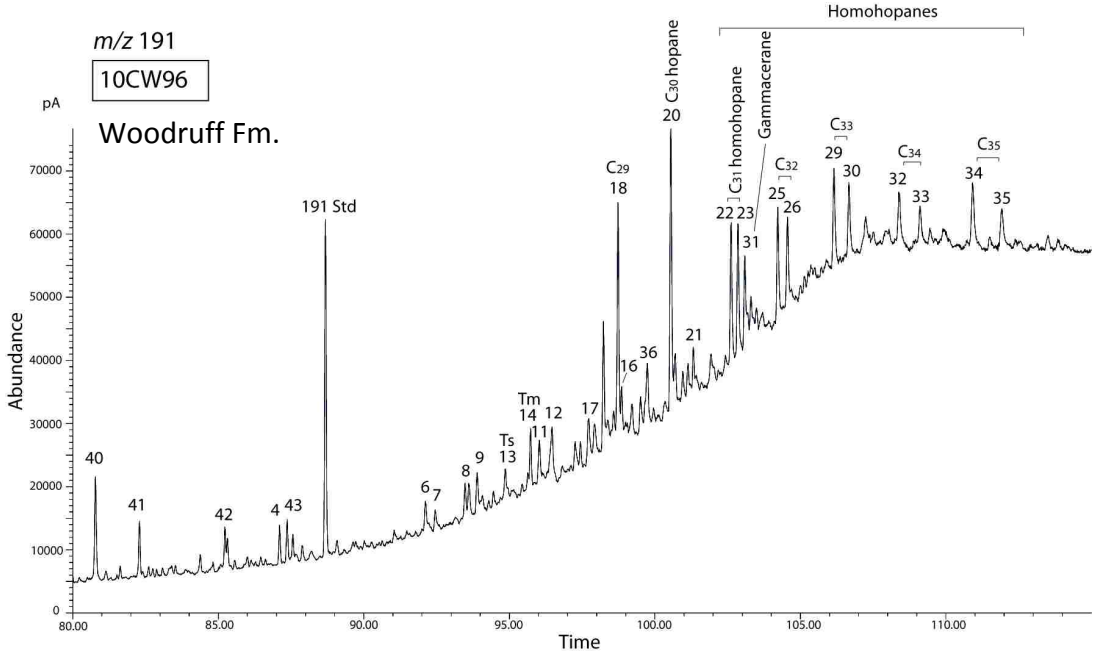

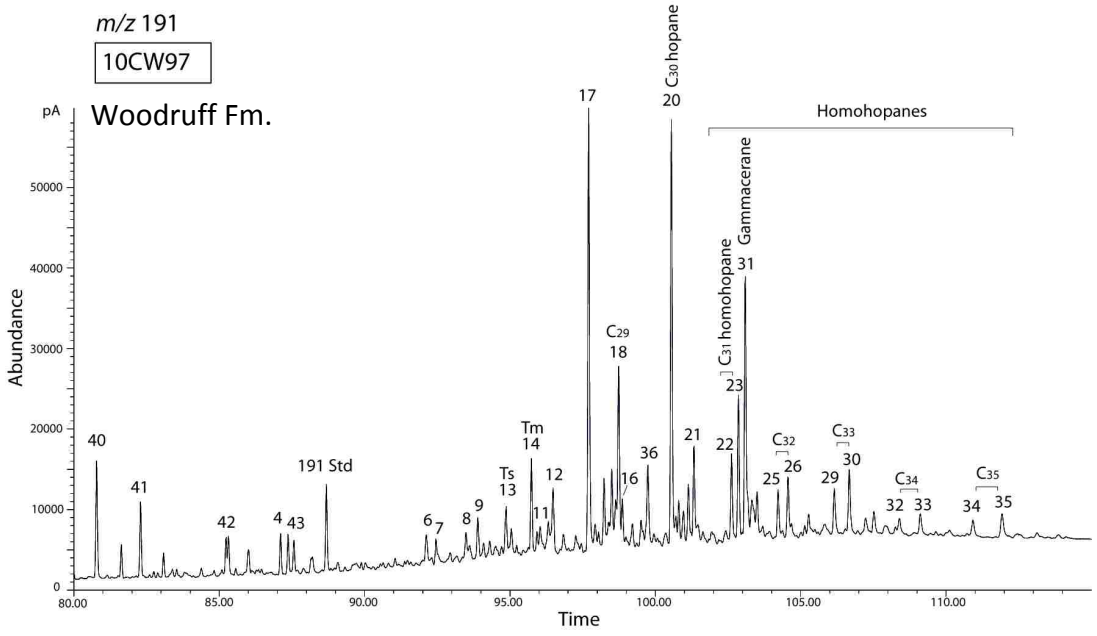

APPENDIX 12

GCMS-MRM CHROMATOGRAMS OF 10CW79 SOURCE ROCK EXTRACT

(All numbered peaks correlate to different biomarker compounds as listed in Table 10)

For detailed explanation see text on p. 31 - 32.

10CW79 Woodruff

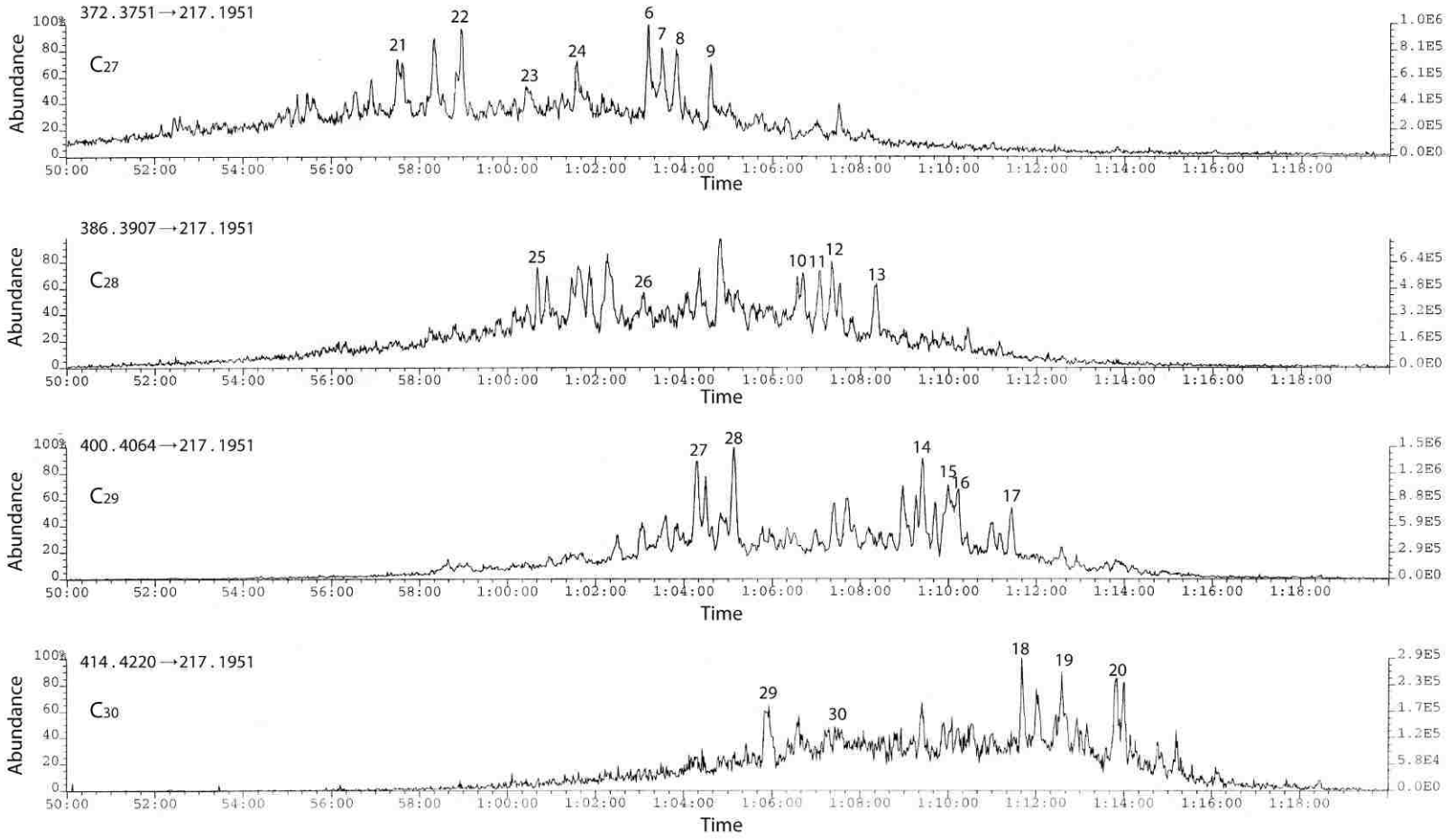

GCMS-MRM CHROMATOGRAM OF 10CW95 SOURCE ROCK EXTRACT

(All numbered peaks correlate to different biomarker compounds as listed in Table 10)

For detailed explanation see text on p. 31 - 32.

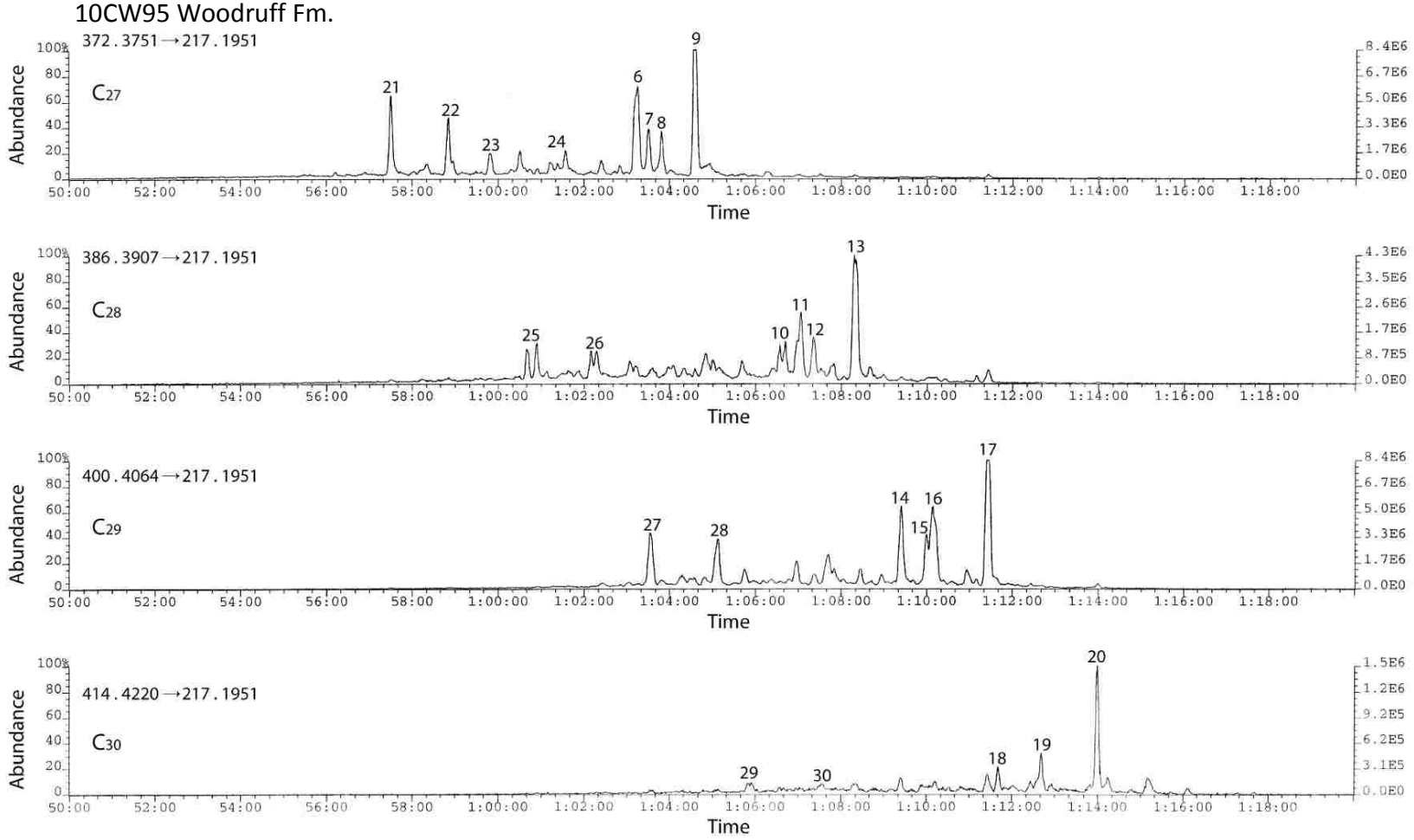

GCMS-MRM CHROMATOGRAM OF 10CW79P SOURCE ROCK PYROLYZATE

(All numbered peaks correlate to different biomarker compounds as listed in Table 10)

For detailed explanation see text on p. 31 - 32

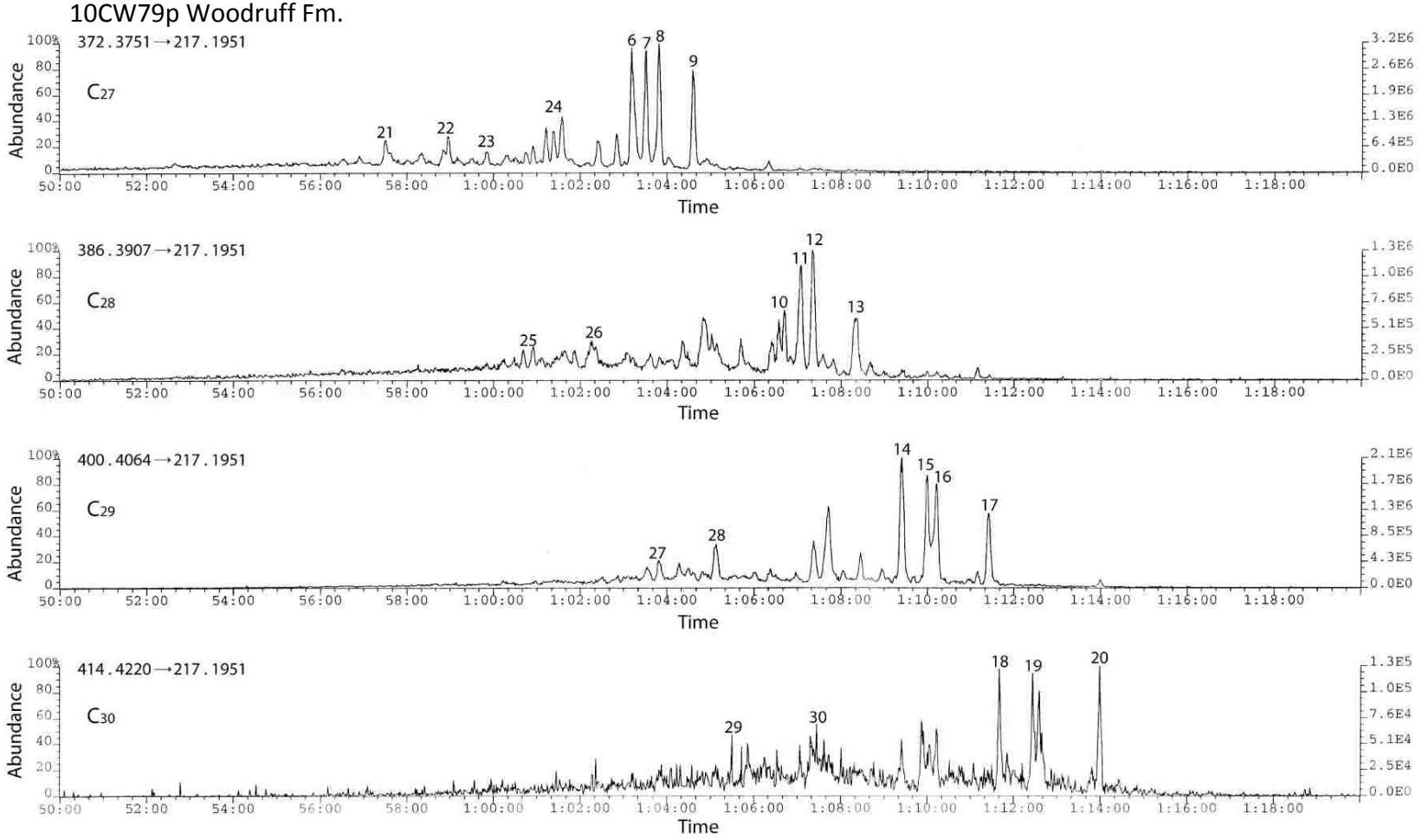

GCMS-MRM CHROMATOGRAM OF 10CW95P SOURCE ROCK PYROLYZATE

(All numbered peaks correlate to different biomarker compounds as listed in Table 10)

For detailed explanation see text on p. 31 – 32.

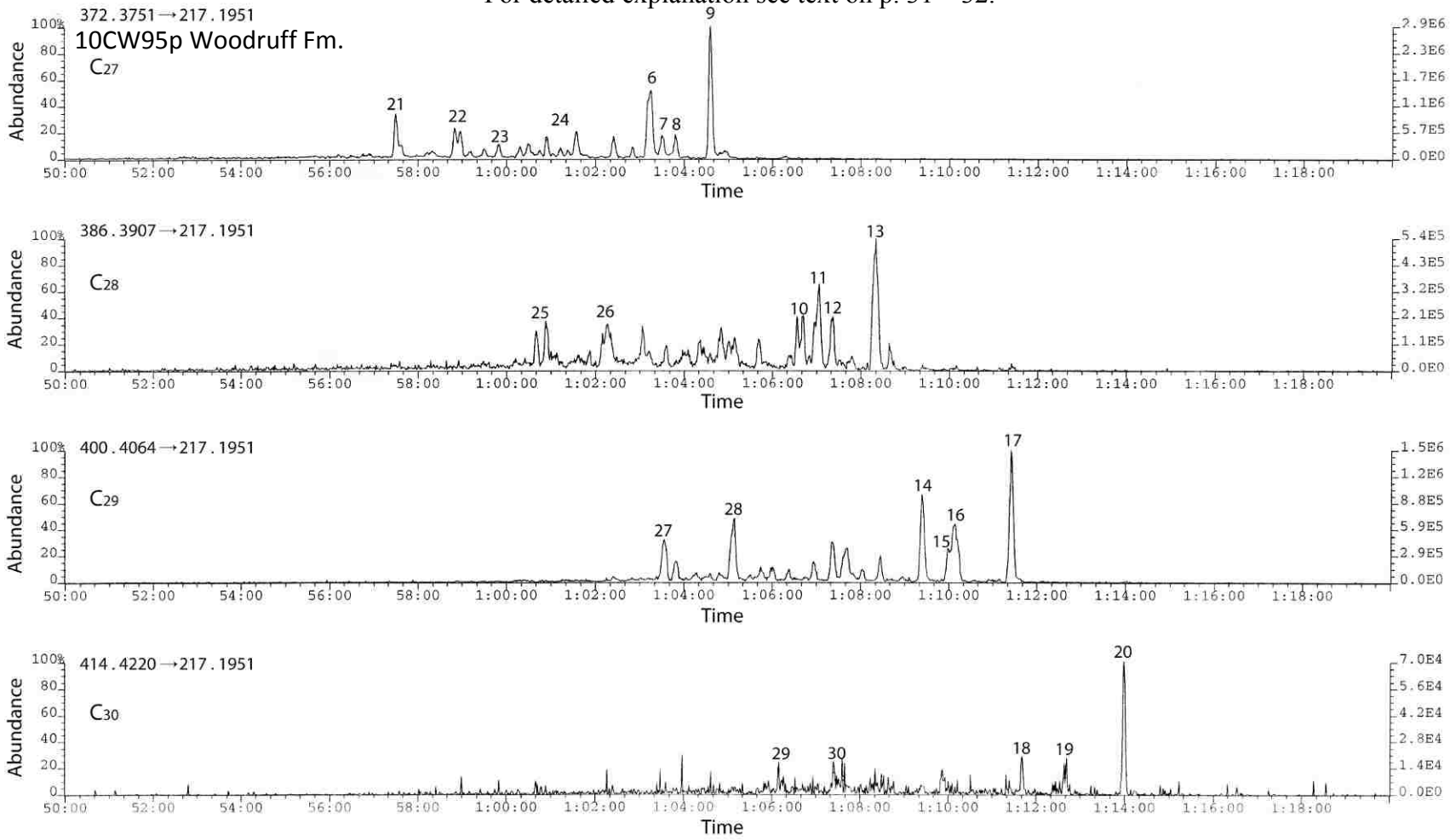

APPENDIX 13

GC-MSD CHROMATOGRAMS OF SOURCE ROCK EXTRACTS

(All numbered peaks correlate to different biomarker compounds as listed in Table 11)

For detailed explanation see text on p. 32.

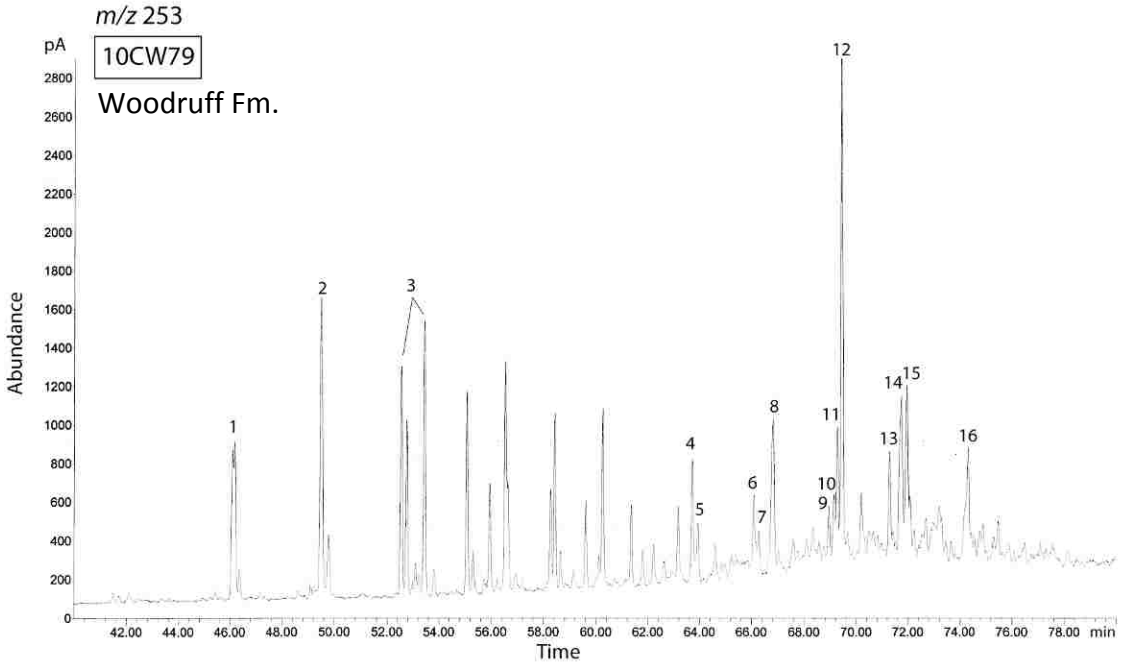

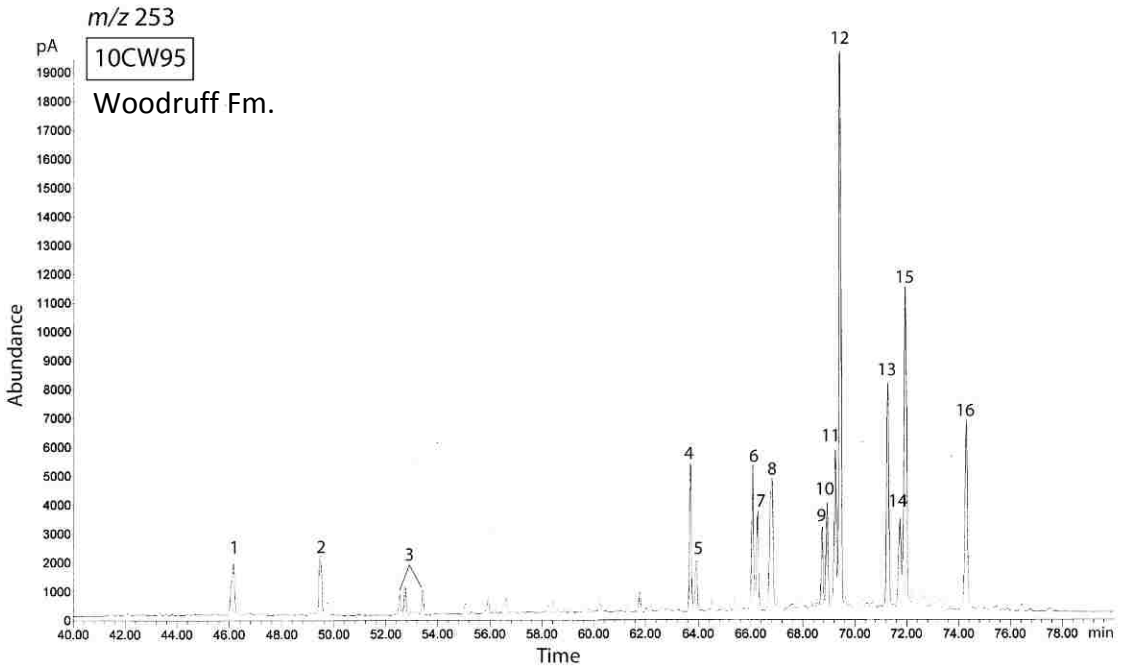

GC-MSD CHROMATOGRAMS OF SOURCE ROCK PYROLYZATES

(All numbered peaks correlate to different biomarker compounds as listed in Table 11)

For detailed explanation see text on p. 32.

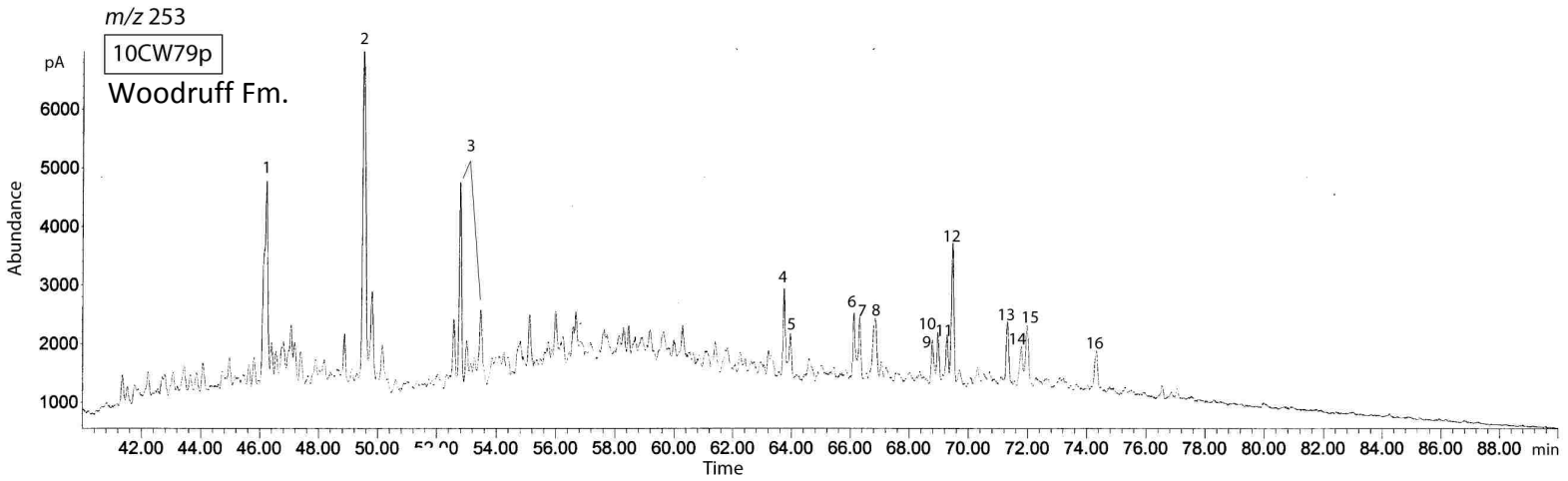

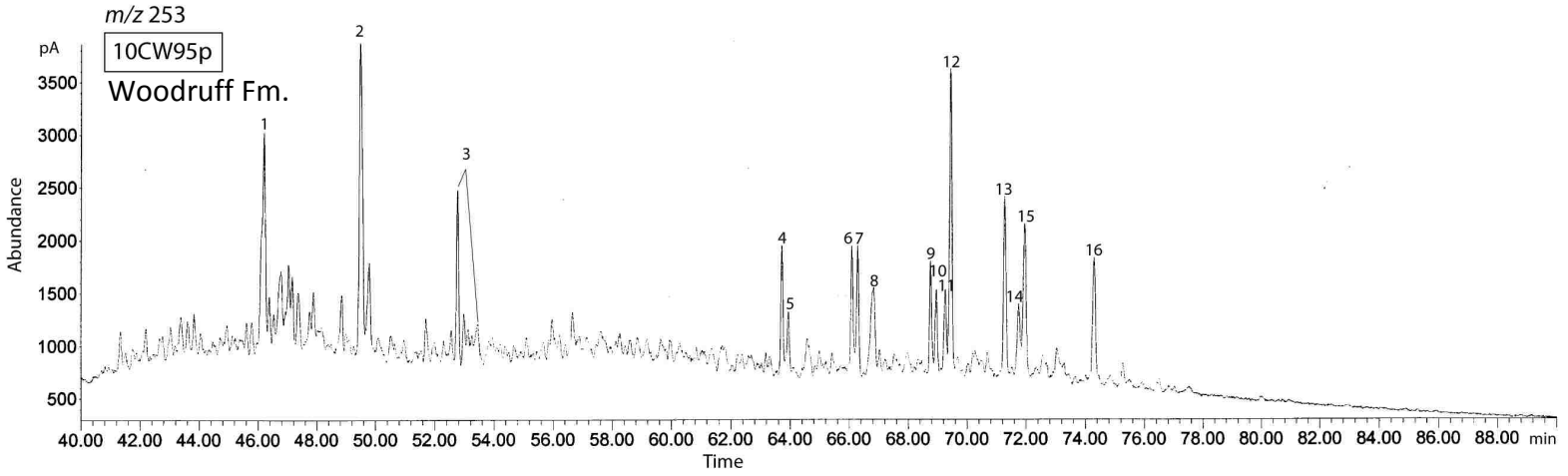

APPENDIX 15

GC-MSD CHROMATOGRAMS OF SOURCE ROCK EXTRACTS

(All numbered peaks correlate to different biomarker compounds as listed in Table 12)

For detailed explanation see text on p. 32 – 33.

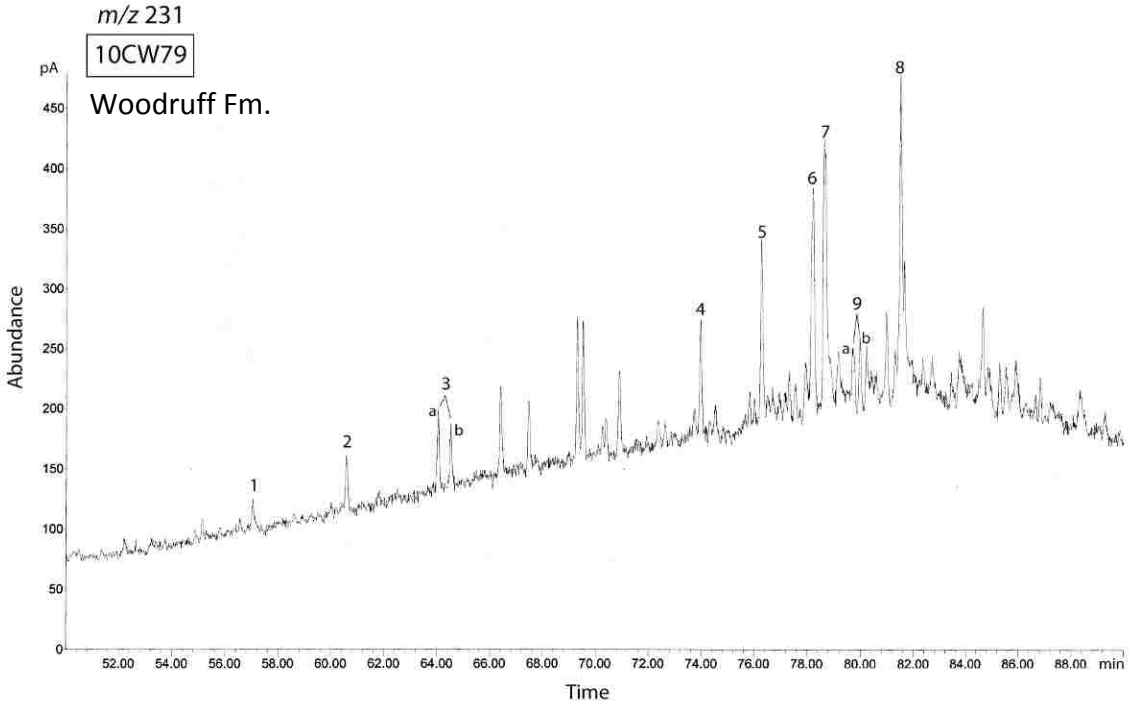

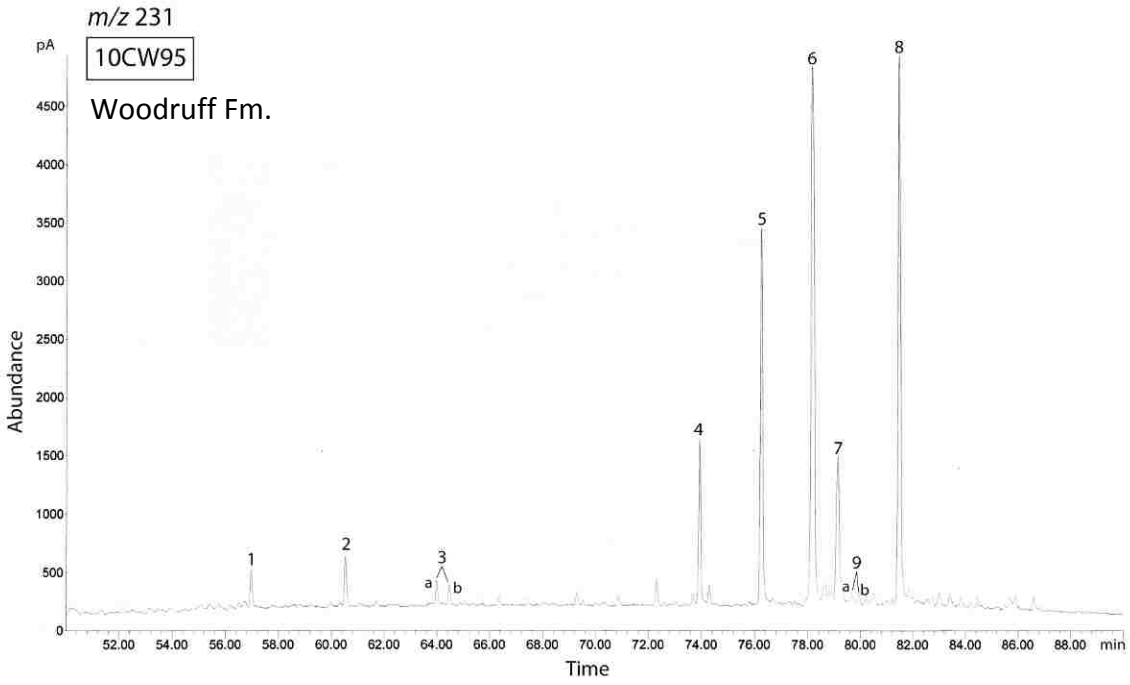

GC-MSD CHROMATOGRAMS OF SOURCE ROCK PYROLYZATES

(All numbered peaks correlate to different biomarker compounds as listed in Table 12)

For detailed explanation see text on p. 32 – 33.

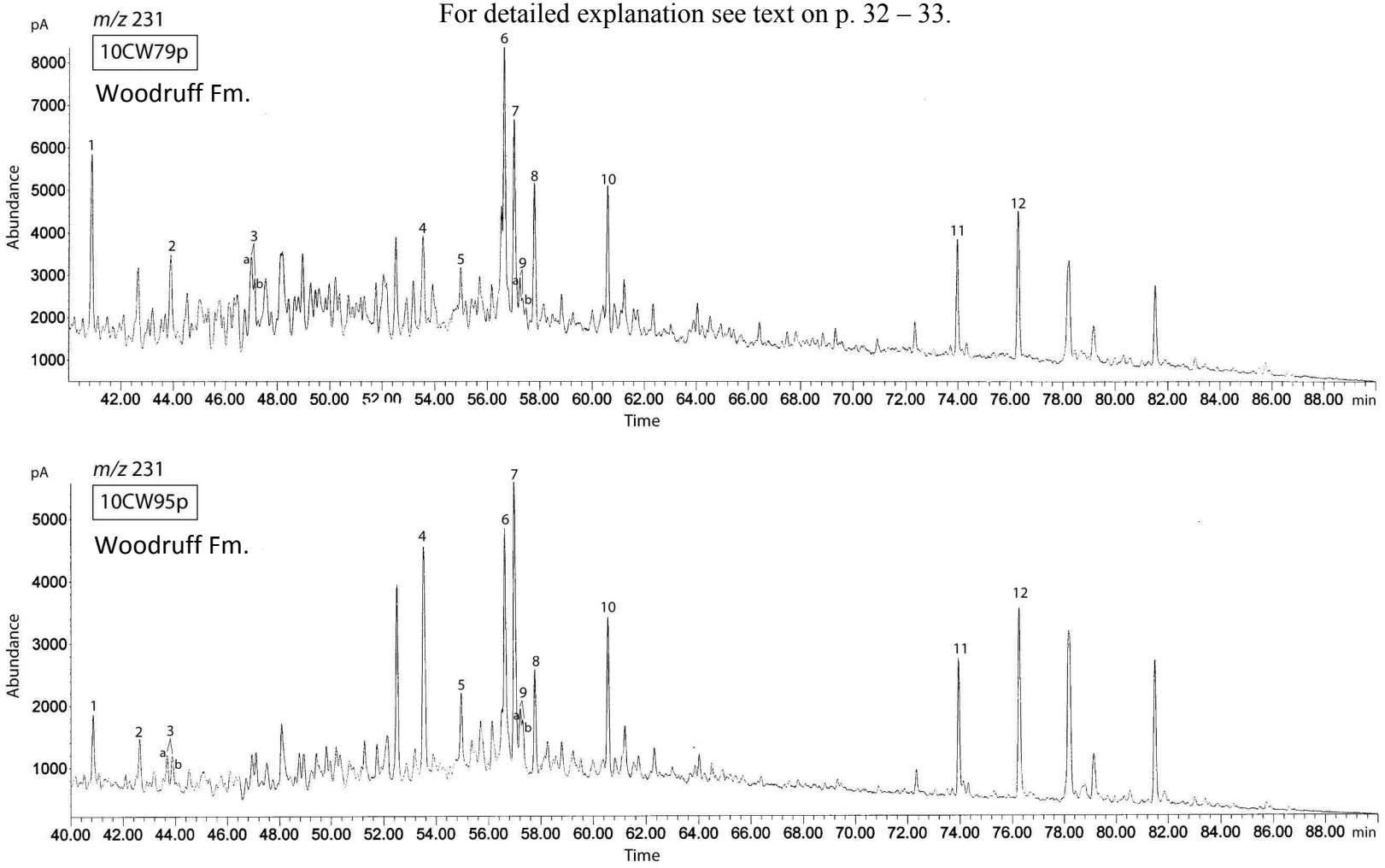

APPENDIX 15

KEY FOR CALCULATED RATIOS

1. **OEP** (1) = $(C_{21} + 6C_{23} + C_{25})/(4C_{22} + 4C_{24})$

2. **OEP** (2) = $(C_{25} + 6C_{27} + C_{29})/(4C_{26} + 4C_{28})$

3. **OEP** (3) = $(C_{29} + 6C_{31} + C_{33})/(4C_{30} + 4C_{32})$

4. **TAR**=$(C_{27} + C_{29} + C_{31})/(C_{15} + C_{17} + C_{19})$

5. **CPI** = $[(C_{25} + C_{27} + C_{29} + C_{31} + C_{33})/(C_{24} + C_{26} + C_{28} + C_{30} + C_{32}) + (C_{25} + C_{27} + C_{29} + C_{31} + C_{33})/(C_{26} + C_{28} + C_{30} + C_{32} + C_{34})]/2$

6. **CPI** (1) = $2(C_{23} + C_{25} + C_{27} + C_{29})/(C_{22} + 2(C_{24} + C_{26} + C_{28}) + C_{30}$

7. **Tricyclic/ Hopane =** $[C_{28} + C_{29}\,(22S+22R)]/\,[C_{29} + C_{30} + (C_{31} + C_{32} + C_{33}\,(22S+22R)]$

8. **Gammacerane Index** = Gammacerane / (Gammacerane + C_{30} hopane)

9. **C_{35} homohopane index** = (C_{35} homohopane (22S+22R))/(C_{31} + C_{32} + C_{33} + C_{34} + C_{35} homohopanes (22S+22R)

10. **% C_{31} homohopane** = [(C_{31} homohopane (22S+22R))/(C_{31} + C_{32} + C_{33} + C_{34} + C_{35} homohopanes (22S+22R)]*100%

11. **% C_{27} Steranes** = (Total C_{27} steranes)/(Total C_{27}+C_{28}+C_{29} steranes)*100

11. **% C_{27} Diasteranes** = (Total C_{27} diasteranes)/(Total C_{27}+C_{28}+C_{29} diasteranes)*100

12. **C_{27} diasterane/(Dia+Reg) steranes**= C_{27} diasteranes / (C_{27} diasteranes + (C_{27} + C_{28} + C_{29}) steranes

13. **C_{30}/(C_{27} - C_{30}) steranes** = C_{30} / (C_{27}+C_{28}+C_{29}+C_{30}) Steranes

14. **Diasterane / sterane** = C_{27} diasteranes / C_{27} Steranes

APPENDIX 16

INPUT PARAMETERS FOR CLUSTER ANALYSIS

1. C_{24} tetracyclic / (C_{24} tetracyclic + C_{26} tricyclic)

2. Diahopane / (diahopane + C_{30})

3. Diahopane / (diahopane + C_{29})

4. C_{29} Ts / (C_{29}Ts + C_{29} hopane)

5. Gammacerane index

6. Homohopane index

7. Oleanane

8. Diasteranes / steranes

9. C_{27} steranes %

10. C_{29} steranes %

BIBLIOGRAPHY

Ahdyar, L., 2011, Molecular Organic Geochemistry of the Oil and Source Rocks in Railroad Valley, Eastern Great Basin, Nevada, United States [M.S. thesis]: University of Nevada, Las Vegas, Las Vegas, Nevada, 109 p.

Anna, L. O., Roberts, L. N., and Potter, C. J., 2007, Geologic assessment of undiscovered oil and gas in the Paleozoic-Tertiary composite total petroleum system of the Eastern Great Basin, Nevada and Utah: U.S. Geological Survey Digital Data Series DDS-69-L, v. 2, 50 p.

Barker, C.E., and Peterson, J.A., 1991, Burial history of the Mississippian Chainman Shale and the Eocene Sheep Pass Formation, Railroad and White River valleys, eastern Nevada, *in* Flanigan, M.J., Hansen, J., and Flanigan, T.E., eds., Geology of White River Valley, the Grant Range, eastern Railroad Valley and western Egan Range, Nevada: Nevada Petroleum Society 1991 Fieldtrip Guidebook, p. 37–46.

Best, M. G., Scott, R. B., Rowley, P. D., Swadley, W. C., Anderson, R. E., Gromme, C. S., Harding, A. E., Deino, A. L., Christensen, E. H., Tingey, D. G., and Sullivan, K. R., 1993, Oligocene-Miocene caldera complexes, ash-flow sheets, and tectonism in the central and southeastern Great Basin, *in* Lahren, M. M., et al., eds., Crustal Evolution of the Great Basin and Sierra Nevada: Reno, Nevada, University of Nevada-Reno, Guidebook, p. 285-311.

Burchfiel, B.C., Cowan, D.S. and Davis, G.A., 1992, Tectonic overview of the Cordilleran orogen in the western United States, in Burchfiel, B. C., Lipman, P. W., and Zoback, M. L., eds., The Cordilleran orogen-Conterminous U.S. Geological Society of America, Geology of North America, v. G-3, p. 407-479.

Cashman, P., Trexler, J., Snyder, W., Davydov, V., and Taylor, W., 2008, Late Paleozoic deformation in central and southern Nevada, *in* Duebendorfer, E. M., and Smith, E. I., eds., Field Guide to plutons, volcanoes, faults, reefs, dinosaurs, and possible

glaciation in selected areas of Arizona, California, and Nevada: Geological Society of America Field Guide 11, p. 21-42.

Cashman, P., Villa, D., Taylor, W., Davydov, V., and Trexler, J., 2011, Late Paleozoic contractional and extensional deformation at Edna Mountain, Nevada: Geological Society of America Bulletin, v. 123, p. 651-668.

Compton, R.R., 1985, Geology in the field: New York, New York, John Wiley and Sons, 398 p.

Cook, H.E., 1988, Overview—Geologic history and carbonate petroleum reservoirs of the Basin and Range Province, western United States, *in* Goolsby, S.M., and Longman, M.W., eds., Occurrence and petrophysical properties of carbonate reservoirs in the Rocky Mountain region: Rocky Mountain Association of Geologists Carbonate Symposium, p. 213–227.

Cook, H.E., and Corboy, J.J., 2004, Great Basin Paleozoic carbonate platform—Facies, facies transitions, depositional models, platform architecture, sequence stratigraphy and predictive mineral host models: U.S. Geological Survey Open-File Report 2004–1078, 129 p.

Dahl, J.E., Moldowan, J.M., Peters, K.E., Claypool, G.E., Rooney, M.A., Michael, G.E., Mello, M.R., and Kohnen, M.L., 1999, Diamondoid hydrocarbons as indicators of natural oil cracking: Nature, v. 399, p. 54-57, doi: 10.1038/19953.

Davis, D.A., 2007, Oil and gas, in The Nevada Mineral Industry 2006:Nevada Bureau of Mines and Geology Special Publication MI-2006, p. 78-86.

Demaison, G. J., Holck, A.J.J., Jones, R.W., and Moore, G.T., 1983, Predictive source bed stratigraphy; a guide to regional petroleum occurrence: Proceedings of the 11th World Petroleum Congress, London, v. 2, p. 17-29.

Dickinson, W.R., 2006, Geotectonic evolution of the Great Basin: Geosphere, v. 2, p. 353-368; doi: 10.1130/GES00054.

Espitalié, J., Marquis, F., and Barsony, I., 1984, Geochemical logging *in* Voorhees, K.J. ed., Analytical pyrolysis - techniques and applications: Boston, Butterworth, p. 276-304.

Garside, L. J., Hess, R. H., Fleming, K. L., and Weimer, B. S., 1988, Oil and gas development in Nevada: Nevada Bureau of Mines and Geology Bulletin 104, 136 p.

Hansen, J. B., Ransom, K. L., and Schaftenaar, C. H., 1994, North Willow Creek oil field, Eureka, Nevada, in Schalla, R. A., and Johnson, E. H., eds., Oil Fields of the Great Basin: Reno, Nevada Petroleum Society, p. 327-332.Hose, R.K., 1983, Geologic map of the Cockalorum Wash Quadrangle, Eureka and Nye Counties, Nevada: Miscellaneous Investigations Series Map I-1410, scale 1:31,680.

Inan, S., and Davis, A., 1994, The history of oil generation in Pine and Railroad Valleys, eastern Nevada, *in* Schalla, R.A., and Johnson, E.H., eds, Oil fields of the Great Basin: Nevada Petroleum Society Special Publication, Reno, Nevada, p. 57–84.

Kleinhampl, F.J., and Ziony, J.I., 1984, Geologic map of northern Nye County, Nevada: Nevada Bureau of Mines and Geology Bulletin 99A, scale 1:250 000.

LaPointe, D.D., Price, J.G., and Hess, R.H., 2007, Assessment of the Potential for Carbon Dioxide Sequestration with Enhanced Oil Recovery in Nevada: Nevada Bureau of Mines and Geology Open-File Report 07-7, 24 p.

Maughan, E.K., 1984, Geological setting and some geochemistry of petroleum source rocks in the Permian Phosphoria Formation, *in* Woodward, J., Meissner, F.F., and Clayton, J.L., eds., Hydrocarbon source rocks of the Greater Rocky Mountain Region, Rocky Mountain Association of Geologists, Denver, Colorado, p. 281–294.

Morrow, J. R., and Sandberg, C. A., 2008, Evolution of Devonian carbonate-shelf margin, Nevada: Geosphere, v. 4, p. 445-458, doi:10.1130/GES00134.1.

Mullarkey, J.C., Wendlandt, R.F., Clayton, J.L., and Daws, T.A., 1991, Petroleum source rock evaluations of the Cretaceous Newark Canyon Formation in north-central Nevada: American Association of Petroleum Geologists Bulletin, v. 75, no. 3, 642 p.

Nevada Bureau of Mines and Geology, 2004, Nevada oil and gas source rock database: Nevada Bureau of Mines and Geology Open-File Report, OF 92–5, 27 p.

Nevada Division of Minerals, Nevada Oil Patch Newsletter, 2009, published monthly, available online at: http://minerals.state.nv.us/formspubs_ogg.htm#Nevada_Oil_Patch.

Palmer, S.E., 1984, Hydrocarbon source potential of organic facies of the lacustrine Elko Formation (Eocene/Oligocene), northeast Nevada, *in* Woodward, J., Meissner, F.F., and Clayton, J.L., eds., Hydrocarbon source rocks of the Greater Rocky Mountain region: Rocky Mountain Association of Geologists, Denver, Colorado, p. 497–511.

Peters, K. E., and Simoneit, B.R.T., 1982, Rock-Eval pyrolysis of Quaternary sediments from Leg 64, Sites 479 and 480, Gulf of California: Initial Reports of the Deep Sea Driling Project, v. 64, p. 925-931.

Peters, K.E., 1986, Guidlines for evaluating petroleum source rock using programmed pyrolysis: American Association of Petroleum Geologists Bulletin, v. 70, p. 318-329.

Peters, K.E., and Casa, M.R., 1994, Applied Source Rock Geochemistry, *in* Magoon, L.B., and Dow, W.G., 1994, The petroleum system - from source to trap: AAPG Memoir 60.

Peters, K. E., Walters. C. C., and Moldowan. J. M., 2007, The biomarker Guide 2nd edition volume 2. Biomarker and isotopes in petroleum exploration and earth history: New York, Cambridge University Press, 1155 p.

Peterson, J. A., 1994, Regional geology of the Eastern Great Basin and paleotectonic history of the Railroad Valley Area, Eastern Nevada: U.S. Geological Survey and University of Montana, Missoula, Montana, p. 15-40.

Poole, F. G., and Sandberg, C.A., 1977, Mississippian paleogeography and tectonics of the western United States, *in* Stewart, J.H., Stevens, C.H., and Fritsche, A.E., eds., Paleozoic paleogeography of the Western United States, Pacific Coast Paleogeography Symposium 1: SEPM (Society for Sedimentary Geology), Pacific Section, p. 67–85.

Poole, F. G., Claypool, G. E., and Fouch, T. D., 1983, Major episodes of petroleum generation in part of the northern Great Basin: Geothermal Resource Council Special Report 13, p. 207-213.

Poole, F.G., and Claypool, G. E., 1984, Petroleum source-rock potential and crude-oil correlation in the Great Basin, in Woodward, J., Meissner, F. F., and Clayton, J. L., ed., Hydrocarbon source rock of the greater Rocky Mountain region: Denver, Rocky Mountain Association of Geologists, p. 179-231.

Price, J.G., and Meeuwig, R.O., 2007, Overview, in The Nevada Mineral Industry 2006: Nevada Bureau of Mines and Geology Special Publication MI-2006, p. 3-13.

Ransom, K. L., and Hansen, J. B., 1990, Devonian Woodruff Formation at Cole Creek Canyon: A world class Devonian source rock, *in* Flanigan, D.M.H., Garside, L.J., and Hansen, M., eds., Oil fields and geology of the Pine Valley, Eureka County area, Nevada: Nevada Petroleum Society 1990 Fieldtrip Guidebook, p. 13.

Rullkötter, J., and Philp, P., 1981, Extended hopanes up to C_{40} in Thornton bitumen: Nature, v. 292, p. 616–618.

Ruble, T.E., Lewan, M.D., and Philip, R.P., 2001, New insights on the Green River petroleum system in the Unita Basin from hydrous pyrolysis experiments: American Association of Petroleum Geologists Bulletin, v. 85, p. 1333-71.

Sandberg, C.A., and Poole, F.G., 1975, Petroleum source beds in Pilot Shale of eastern Great Basin—Oil and gas session I: Rocky Mountain section meeting, American Association of Petroleum Geologists, Albuquerque, New Mexico, June 2, 1975, U.S. Geological Survey Open-File Report, 75–371, 11 p.

Sandberg, C.A., Morrow, J.R., Poole, F.G., and Ziegler, W., 2003, Middle Devonian to Early Carboniferous event stratigraphy of Devils Gate and northern Antelope Range sections, Nevada, USA: Courier Forschungsinstitut Senckenberg, v. 242, p. 187–207.

Seifert, W.K., and Moldowan, J.K., 1978, Applications of steranes, terpanes and monoaromatics to the maturation, migration and source of crude oils: Geochimica et Cosmochimica Acta, v. 42, p. 77–95.

Siebenaler, S. A., 2010, Late Paleozoic deformation in the Osgood Mountains and Dry Hills, northern Nevada States [M.S. thesis]: University of Nevada, Las Vegas, Las Vegas, Nevada, 188 p.

Speed, R. C., Elison, M. W., and Heck, F. R., 1988, Phanerozoic tectonic evolution of the Great Basin, in Ernst, W. G., ed., Metamorphism and crustal evolution of the western United States, Rubey Volume 7: Englewood Cliffs, New Jersey, Prentice-Hall, p. 572-605.

Taylor, W. J., Bartley, J. M., Martin, M. W., Geissman, J. W., Walker, J. D., Armstrong, P. A., and Fryxell, J. E., 2000, Relations between hinterland and foreland shortening: Sevier orogeny, central North American Cordillera: Tectonics, v. 19, p. 1124-1143.

Taylor, W. J., 2001, Mesozoic thrusting in the hinterland of Sevier orogenic belt - The central Nevada thrust belt: Geological Society of Nevada, 2001 annual meeting abstracts.

Tissot, B.P., Durand, B., Espitalie, J., and Combaz, A., 1974, Influence of the nature and diagenesis of organic matter in formation of petroleum: American Association of Petroleum Geologists Bulletin, v. 58, p. 499-506.

Tissot, B.P., and Welte, D.H., 1984, Petroleum formation and occurrence: New York, Springer-Verlag, 699 p.

Williams, J.A., Bjorøy, M., Dolcater, D.L., and Winters, J.C., 1986, Biodegradation in South Texas Eocene oils - effects on aromatics and biomarker: Organic Geochemistry, v. 10, p. 451-461.

VITA

Graduate College
University of Nevada, Las Vegas

Inessa Yurchenko

Degrees:

Bachelor of Science, Geology, 2009
Moscow State University, Russia

Special Honors and Awards:

Bernard French Scholarship, UNLV, 2011
ExxonMobil Geosciences Scholarship, 2010/present,
Schlumberger Scholarship Award, 2009/2010
AAPG Imperial Barrel Award Competition (European Region Finals), 2010

Thesis Title: Evaluation of Possible Source Rocks in Northern Nye County, Nevada: Implications for Hydrocarbon Exploration

Thesis Examination Committee:

Chairperson, Andrew D. Hanson, Ph. D.
Committee Member, Ganqing Jiang, Ph. D.
Committee Member, Wanda J. Taylor, Ph. D.
Graduate Faculty Representative, Sean Clark, M.S.